UNIVERSITÄT
DES
SAARLANDES

Microfluidic Platform to Study the Model Cell Membranes: Biophysical Properties and Organelle Interactions of Lipid Droplets

Dissertation

zur
Erlangung des Grades
des Doktors der Naturwissenschaften
der Naturwissenschaftlich-Technischen Fakultät
der Universität des Saarlandes

VON

SHIMA ASFIA

SAARBRÜCKEN

2025

Declaration

I hereby declare that the dissertation entitled "**Microfluidic Platform to Study the Model Cell Membranes: Biophysical Properties and Organelle Interactions of Lipid Droplets**" which I have submitted for the degree of Doctor of Natural Science at Saarland University is a record of work carried out by me under the supervision of Prof. Dr. Seemann. I further declare that the work reported in this dissertation has not been submitted and will not be submitted, either in part or in full, for the award of any other degree or diploma in this institute or any other institute or university. This is to certify that the printed version is equivalent to the submitted electronic one. I am aware of the fact that a misstatement may have serious legal consequences. I also agree that my thesis can be sent and stored anonymously for plagiarism purposes. I know that my thesis may not be corrected if the declaration is not issued.

Place: Saarbrücken **Shima Asfia**

Date: 24.11.2025

Tag des Kolloquiums: 06.02.2026

Dekan: Prof. Dr.-Ing. Dirk Bähre

Mitglieder des Prufungsausschusses

Berichterstatter:

Prof. Dr. Ralf Seemann

Prof. Dr. Albrecht Ott

Vorsitzender:

Prof. Dr. Jochen Hub

Akademischer Mitarbeiter:

Dr. Yazdan Rashidi

Kurzzusammenfassung

Diese Dissertation präsentiert mikrofluidische In-vitro-Studien zu Modellzellmembranen, mit einem Schwerpunkt auf den biophysikalischen Eigenschaften von Lipidtröpfchen (LDs) und deren proteinvermittelten Interaktionen. Mittels fluoreszenzbasierter optischer Methoden und Messungen der Grenzflächenspannung wurde untersucht, wie die Lipidzusammensetzung einer LD-Membran die Diffusionsraten und die Membranspannung beeinflusst. Außerdem wurde der Einfluß von Perilipin-2 (PLIN2) auf die in eine Lipid-Doppelschicht inserierte LDs untersucht. Diese LDs nahmen eine charakteristisch abgeflachte Form an, was auf eine lokal veränderte Grenzflächenspannung hinweist, während die Lipidmobilität weitgehend unverändert blieb. Dennoch erleichterte PLIN2 den Lipidaustausch über die Grenze zwischen LD. Zusätzlich wurde die Ausbildung von Kontaktstellen zwischen LDs und Modellorganellen mithilfe großer unilamellarer Vesikel (LUVs) untersucht. Es zeigte sich, dass Perilipin-5 (PLIN5) die stabile Bildung von Protein Tether fördert und von lipidischen Brücken erschwert und damit LD-Organellen-Interaktionen nachbildet. Insgesamt demonstriert diese Arbeit, wie mikrofluidische Systeme genutzt werden können, um die Struktur und Funktion von LDs unter kontrollierten Bedingungen nachzubilden und zu analysieren und eröffnet damit neue Möglichkeiten zur Untersuchung der Lipidbiologie und der Organellenkommunikation.

Abstract

This thesis presents an in vitro study to investigate model cell membranes, with a focus on biophysical properties of lipid droplets (LDs) and their protein-mediated interactions using a microfluidic platform. Using fluorescence-based optical techniques and interfacial tension measurements, it has been investigated how lipid composition affects LD surface behavior. Variations in lipid geometry and packing were found to influence diffusion rates and membrane tension, revealing how LD surface properties can be tuned by composition. The role of perilipin-2 (PLIN2) was examined by embedding PLIN2-decorated LDs into free-standing bilayers. These LDs adopted a characteristic flattened shape, indicating locally altered interfacial tension, while lipid mobility remained largely unchanged. Nevertheless, PLIN2 facilitated lipid exchange across the LD-bilayer boundary, suggesting a functional role in regulating interfacial permeability. Additionally, contact formation between LDs and model organelles was investigated using large unilamellar vesicles (LUVs). It was found that perilipin-5 (PLIN5) promotes stable protein tethering and reduces lipid exchange at these interfaces, mimicking LD-organelle interactions. Altogether, this work demonstrates how microfluidic systems can be used to reconstitute and analyze the LD structure and function under controlled conditions, thereby offering new possibilities for studying lipid biology and organelle communication.

Acknowledgment

I would like to express my deepest gratitude to my advisor, Prof. Dr. Ralf Seemann, for giving me the opportunity to pursue my PhD under his guidance. His continuous support, invaluable insights, and encouragement have shaped my academic journey in ways I could not have imagined. I am also sincerely grateful to Dr. Jean-Baptiste Fleury for his constructive feedback, enriching discussions, and guidance throughout this project.

I would like to extend my heartfelt appreciation to my colleague and friend, Mahsa Mohammadian, for her precious collaborations, and for being my side for all these years just like a family member. Also I would like to thank my wonderful colleagues Navid, Khalil, Martin and Karthik who made this journey not only intellectually stimulating but also enjoyable. The shared challenges, conversations, and laughter have been an integral part of this experience.

Most importantly, I am profoundly grateful to my family. Mom and Dad, your unwavering love and support have been the foundation of everything I have achieved. No words can express how much I appreciate your sacrifices and encouragement. The best sister one could ever have, Mona, thank you for always believing in me. Thank you all for always encouraging me to follow my dreams and for giving me the confidence that everything can be achieved with the right amount of effort. Even though I am far away from you, my heart beats for you, and I am so proud and grateful to have you.

And last but not the least, to Stefan, the love of my life and my greatest supporter, thank you for your patience, understanding, and for always being there, even from afar. The past years have been full of challenges but knowing that you were by my side made all the difference.

This work is dedicated to all my loved ones.

Table of Contents

1. Introduction

Lipid droplets (LDs) are dynamic cellular organelles consisting of a hydrophobic core of neutral lipids enclosed by a phospholipid monolayer decorated with proteins. Beyond their classical role as lipid storage depots, LDs participate in lipid trafficking, energy homeostasis, protein turnover, and interactions with other organelles, making them critical for cellular health [1]. Indeed, disrupted LD dynamics and contact-site formation with mitochondria, the endoplasmic reticulum, and other compartments have been implicated in metabolic and degenerative diseases, including obesity, fatty liver, cardiovascular disorders, and neurodegeneration. Understanding the biophysical properties of the LD interface and the molecular mechanisms that regulate LD behavior and contacts is thus key for unravelling their cellular functions and disease relevance [2].

Despite significant advances in lipid droplet research, there are still fundamental gaps in our knowledge of how lipid composition and surface protein association influence lipid packing, mobility, surface tension, and interactions with other cellular membranes [1]. To tackle these questions quantitatively and under well-controlled conditions, model systems must be developed that mimic key features of native LDs while allowing high-resolution, real-time measurements. Microfluidic devices offer a unique advantage for this purpose by enabling the formation of stable, highly tunable model LDs and facilitating the controlled apposition of different membranes, all at micrometer scale and observable under optical microscopy [3].

In this thesis, we have applied microfluidics to build a platform for generating model LDs and studying their biophysical properties, protein-modulated behavior, and contact-site formation with organelle-mimicking membranes.

In the first part of this work, we focused on characterizing the biophysical properties of LD surfaces by creating planar triolein-buffer interfaces decorated with defined phospholipid monolayers inside a microfluidic chip. To assess these properties, we employed fluorescence recovery after photobleaching (FRAP) and interfacial tension measurements. The lateral mobility and packing density of phospholipid monolayers were systematically examined as a function of the molecular geometry, such as cylindrical or conical shapes, and degree of saturation. Specifically, we investigated how these molecular characteristics influence LD membrane behavior under controlled experimental conditions.

Building on this biophysical foundation, we then investigated how lipid droplet-associated proteins modulate these properties by incorporating recombinant perilipin-2 (PLIN2), an abundant surface protein of LDs, into model LD membranes. In these experiments, we formed freestanding bilayer-embedded droplets and measured lipid mobility and exchange rates across the LD-bilayer interface. In this approach, freestanding bilayer-embedded droplets were

formed, and quantitative measurements of lipid mobility and exchange rates across the LD-bilayer interface were performed to assess protein regulation mechanisms.

Furthermore, to explore how protein-decorated lipid droplets interact physically and functionally with other organelles, we employed large unilamellar vesicles (LUVs) as model organelle membranes. By bringing LUVs into contact with model LDs within microfluidic channels and labeling components with distinct fluorescent markers, we established a framework for analyzing protein-mediated interactions at membrane contact sites. Perilipin-5 (PLIN5), known for its role in organelle tethering, was introduced to probe its effect on contact formation and lipid transfer processes.

Taken together, these investigations establish a systematic framework for analyzing lipid droplet interfaces and their protein-mediated interactions under microfluidic control. The approaches presented here show how lipid composition, protein association, and membrane contacts can be studied quantitatively in well-defined model systems. Beyond the individual studies, the methodology developed provides a adaptable foundation for future research into LD dynamics, organelle communication, and their roles in metabolic health and disease.

This thesis is presented in a cumulative format, encompassing three publications. While each study contributes independently to the central theme, their combination highlights how lipid composition and LD-associated proteins jointly shape droplet surface properties, morphology, and inter-organelle communication.

2. Overview and Connectivity

This cumulative dissertation is based on three original publications, two published in peer-reviewed scientific journals and one under review at the time of submission. Together, these studies investigate the dynamics of model cell membranes using a microfluidic platform, with a particular focus on lipid droplet (LD) membranes, including phospholipid diffusion, LD structure, and protein-mediated interactions with other organelles.

The first publication, **Asfia et al. (BBA - Biomembranes, 2023)** ***Phospholipids Diffusion on the Surface of Model Lipid Droplets***, explores the mobility of phospholipids on the LD surface using a microfluidic platform. By performing fluorescence recovery after photobleaching (FRAP) experiments using different phospholipids with various lipid packing features, this study demonstrates how monolayer packing influences lipid mobility, providing insights into the biophysical properties of LD surfaces. Together, these findings establish the biophysical foundation for this thesis, showing how lipid composition dictates LD surface dynamics, a crucial step in understanding how LD behavior can be systematically analyzed under microfluidic control.

Building on this foundation, the second publication, **Puza, Asfia, et al. (International Journal of Molecular Sciences, 2023)** ***Bilayer-Embedded Lipid Droplets Coated with Perilipin-2 Display a Pancake Shape***, to understand the impact of perilipin-2 (PLIN2) on LD morphology and phospholipid diffusion. This study shows that PLIN2 alters the three-dimensional shape of bilayer-embedded LDs, while its effect on phospholipid mobility remains minimal. By employing two different microfluidic setups, one mimicking a bilayer-embedded LD and the other representing an isolated LD surface, the work provides a comprehensive view of the role of perilipin proteins in LD organization. By showing how PLIN2 modifies LD morphology and lipid exchange, this study extends the central theme of the thesis, highlighting that LD-associated proteins introduce an additional regulatory layer that shapes LD function beyond lipid composition alone.

The third study, **Mohammadian, Asfia et al. (submitted, 2025)** ***Role of Perilipin 5 Protein in Lipid Droplet Contact Sites***, shifts the focus from LD structure and surface dynamics to LD interactions with other organelles, particularly through contact sites with large unilamellar vesicles (LUVs). Using fluorescence labeling techniques, the study provides evidence that perilipin-5 (PLIN5) promotes both contact formation and lipid exchange between LDs and LUVs. It further investigates the role of PLIN5 in mediating these contacts, distinguishing between protein tethering and lipid bridging as mechanisms of LD-organelle communication. This study completes the progression from surface biophysics to protein-driven interactions by showing how PLIN5 mediates LD-organelle contacts. It directly addresses the main question

of the thesis: how lipid composition and protein decoration together govern LD communication within the cellular environment.

Together, these three studies form a coherent progression from fundamental lipid diffusion on LD surfaces to protein-mediated structural changes, and to the role of LDs in cellular interactions. This work thus contributes to a deeper understanding of LD dynamics, offering new perspectives on how these organelles function within the complex cellular environment.

The structure of this thesis is as follows:

In the Chapter: *Background*, general information on lipid droplets (LDs) is provided, including their structure, biogenesis, size regulation, and growth. The diverse functions of LDs in the cell are discussed, along with their dynamic interactions with other organelles and their role in cellular homeostasis. At the end, techniques used to model lipid droplets in vitro are introduced to have a view of how to study the LDs in the lab.

In the Chapter: *Materials and Methods*, follows a detailed description of the specific materials used in the subsequent projects. This chapter also outlines the methods for μChip and microfluidic device fabrication, lipid droplet formation and their interaction with large unilamellar vesicles (LUVs), and also the techniques employed for fluorescence recovery after photobleaching (FRAP) and interfacial tension measurements.

In the Chapter: *Results and Discussion*, the key findings from the attached publications are presented and analyzed in the context of lipid droplet dynamics, membrane interactions, and microfluidic applications.

In the Chapter: *Summary and Outlook*, a summary of the research conducted is provided, highlighting the main conclusions and their implications. Finally, potential future research directions are proposed.

3. Background

Cells are the basic structural and functional units of living organisms. They are the smallest entities that can perform the necessary functions for life. All living organisms are composed of cells. Whether a single-celled organism or a complex multicellular organism, the cell is the basic structural and functional unit of life. Cells are complex structures with various components that work together to maintain life [4]. The major components of a cell include the cell membrane, which forms the outer boundary and regulates the passage of substances in and out of the cell. The cytoplasm is the site where most cellular activities take place. The nucleus contains the cell's genetic material, such as DNA or RNA. Additionally, the cell contains various organelles, each performing specific functions [5]. Since new energy sources are not consistently available, storing lipids in cells and tissues is often essential for survival. Additionally, cells need to buffer and store excess lipids in an inert form. Therefore, nearly all cells can store lipids in compartmentalized reservoirs. To efficiently package lipids, cells convert them into neutral lipids such as triacylglycerols (TG) and sterol esters (SE), which repel water. These neutral lipids are then stored within lipid droplets, specialized organelles that serve as energy reservoirs and play an important role in maintaining cellular homeostasis [6, 7].

3.1 Lipid Droplets Biology

Lipid droplets (LDs), also known as adiposomes, lipid bodies, or oil bodies, are essential cellular organelles that serve primarily as storage units for neutral lipids. They are a defining feature of fat cells (adipocytes), where they can occupy up to 95% of the cell's volume [2, 7]. LD properties, including size, number, and composition, vary depending on the cell type, nutrient availability, and metabolic state. Structurally, LDs consist of a neutral lipid core surrounded by a single phospholipid monolayer, which is decorated with various proteins that contribute to LD stability and function [2, 8].

Due to their leading role in lipid storage and metabolism, LDs are closely linked to various physiological and pathological processes. They are implicated in diseases related to lipid accumulation, such as obesity, diabetes, and atherosclerosis, and their dysfunction or mutation has been associated with lipodystrophy, non-alcoholic fatty liver disease (NAFLD), pancreatic steatosis, neurodegeneration, infection, cancer, and cardiovascular disease [7, 9].

In obesity, proteins including CIDEA, CIDEB, CIDEC, and perilipin-1 (PLIN1) regulate LD growth and adipocyte function, whereas mutations in LD-related genes (e.g., PLIN1, CIDEC) can cause lipodystrophy, characterized by loss of adipose tissue [10-12]. Excessive LD accumulation in organs can lead to diseases such as NAFLD (which may

progress to severe liver damage) and pancreatic steatosis, linked to type 2 diabetes and pancreatic cancer [13-16]. Protective LD formation in glial cells is promoted by proteins like ApoE4 and seipin in neurodegeneration [13]. During infections, LDs modulate pathogen interactions, restricting bacterial growth while facilitating viral replication, with proteins such as PLIN2 and DGAT1 playing key [17]. Cancer cells exploit LDs for growth and survival, with DGAT1 and PLIN2 playing key roles in LD biogenesis [18]. In cardiovascular disease, LDs in macrophages and cardiomyocytes help reduce lipotoxicity, regulated by proteins including PLIN5, PNPLA2, and DGAT1 [13, 19].

Thus, understanding LD biology not only expands fundamental cellular knowledge but also offers potential clinical insights for metabolic, cardiovascular, and neurodegenerative disorders.

3.2 Mechanisms of Lipid Droplet Biogenesis and Growth

As neutral lipid synthesis is essential for LD formation, it is important to examine this process in detail. Neutral lipids are produced by enzymes from the membrane-bound O-acyltransferase (MBOAT) family, such as ACAT1, ACAT2, and DGAT1, along with enzymes from the DGAT2 gene family. These enzymes are located at the endoplasmic reticulum (ER), where they face their substrates. One common substrate is fatty acyl-CoA, produced by acyl-CoA synthetase (ACSL) enzymes, which activate fatty acids for metabolic pathways. Fatty acyl-CoAs combine with lipid alcohols to form neutral lipids [20]. Researchers have shown that yeast can survive without these enzymes, but the resulting LDs are poorly detectable [21]. Knockout mouse studies demonstrated that ACAT1, ACAT2, and DGAT1 are not essential for life, although a lack of DGAT2 results in insufficient energy stores and skin defects associated with essential fatty acid deficiency, leading to death shortly after birth [22].

When free fatty acid (FA) levels inside cells rise, they trigger LD biogenesis. This process prevents lipotoxicity by converting excess free FAs into neutral lipids, which are then sequestered into cytosolic LDs. LDs can also appear in other compartments such as the nucleus, where ‘nuclear LDs’ resemble cytoplasmic LDs but their formation and functions in nuclear lipid balance and signaling remain under investigation [23, 24]. Unlike most self-replicating organelles, LDs can arise de novo or by fission of pre-existing LDs [25].

By accumulating neutral lipids such as triglycerides (TGs) between the leaflets of the ER bilayer, lens-like structures begin to form, occasionally described as pancake-shaped lipid lenses. These lenses may nucleate at pre-existing sites on the ER membrane that correspond to locations of previously budded LDs [26, 27]. Moreover, enzymes that catalyze triglyceride synthesis, including DGAT1 and DGAT2, concentrate around these

sites to promote lipid deposition and drive LD biogenesis [28]. As these lenses enlarge, they become unstable and eventually bud off into the cytoplasm. Although this process remains debated, it most likely occurs via a dewetting mechanism driven by thermal fluctuations [7]. Whether this budding is entirely spontaneous or protein-mediated is not fully understood, but specific proteins appear to facilitate the process [29].

Although newly formed LDs are small compared to the overall cell volume, they can grow significantly. Many cells contain larger LDs that either arise by fusion of smaller LDs or by continuous local synthesis of triglycerides at the surface of existing LDs [30]. Droplet growth requires trafficking pathways that deliver enzymes essential for triglyceride synthesis to LDs, with both newly formed and mature LDs obtaining these enzymes directly from the ER [31]. LD sizes vary substantially among cell types, ranging from nanoscale droplets (~100 nm) to macro-scale droplets (~100 μm). LD size can dynamically grow or shrink in response to cellular signals [30]. For instance, in yeast, LDs typically measure less than a micron, whereas adipocytes commonly contain a single LD that is tens to hundreds of microns across [7]. Once synthesized, LDs generally continue to grow due to excess intracellular fatty acids until they reach a stable final size. Proteins such as Fsp27, seipin, FITM2, and PLIN1, as well as lipid species such as phosphatidylcholine (PC) and phosphatidic acid, help regulate this growth process [9]. Moreover, even within the same cell, LD sizes may vary dramatically under different pathophysiological conditions, reflecting their highly dynamic nature [23]. Understanding how LDs grow sets the stage for examining their structural and molecular architecture, which underpins their dynamic functions in cells.

3.3 Structural and Molecular Architecture of Lipid Droplets

Unlike other membrane-enclosed organelles, LDs possess a distinctive structure characterized by a hydrophobic core of neutral lipids encased in a monolayer phospholipid membrane. This membrane serves to isolate the hydrophobic neutral lipids from the aqueous cytoplasmic environment [32]. Within the hydrophobic core of lipid droplets (LDs), neutral lipids, primarily triglycerides (TG) and sterol esters (SE), are stored in varying ratios, (see fig. 1). In white adipocytes, TGs are predominantly stored in LDs as lipid esters, whereas in steroidogenic cells, SEs are the main components [33]. Additionally, depending on the cell type, various other endogenous neutral lipids such as retinyl esters, ether lipids, and free cholesterol are stored within LD cores [34-36]. Interestingly, in some cell types, electron microscopy has revealed membrane-like structures containing ribosomal units extending into the core of LDs [37, 38]. In mammalian cells, the major constituent of lipid droplet (LD) monolayer membranes is

phosphatidylcholine (PC), comprising up to 60% of the membrane composition. This is followed in abundance by phosphatidylethanolamine (PE), phosphatidylinositol (PI), phosphatidylserine (PS), sphingomyelin (SM), and lyso forms of PC and PE [39-41]. Additionally, minor amounts of phosphatidic acid and free cholesterol are present on the surfaces of LDs [32, 42].

While the phospholipid structural composition of LD monolayers is well described, less is known about how different lipid species shape their biophysical properties. In particular, lateral lipid mobility and interfacial (surface) tension are strongly dependent on lipid type and composition, yet systematic quantitative insights into these dependencies remain limited. Since these parameters are central to LD stability, dynamics, and interactions with other organelles, understanding their molecular basis is essential. Addressing these questions is critical for clarifying how LD surface properties influence their biological behavior. In this thesis, these aspects were investigated experimentally by reconstituting model LD monolayers in vitro, quantifying lipid diffusion and interfacial tension, and examining how lipid type and composition modulate these properties.

Additionally, the LD membrane is decorated with various proteins, which can influence the subsequent function and fate of LDs. These proteins can already exist in the ER membrane and remain in the LD membrane after growth and budding or the proteins in the cytosol can add and localize into the LD membrane [7].

While it is believed that LD formation occurs between the leaflets of the endoplasmic reticulum (ER), the phospholipid composition of the LD monolayer membrane may differ from that of the ER and other organelles [32]. This unique phospholipid composition significantly influences LD synthesis, maturation (size), and degradation via lipophagy mechanisms [43-47]. Variations in the phospholipid composition of a LD monolayer membrane under different physiological conditions across various cell types suggest that the regulation of phospholipid composition is critical for maintaining the homeostasis of these organelles [23]. The surface composition is crucial in controlling LD size and their capacity to interact with other LDs or organelles, such as the ER and mitochondria [48].

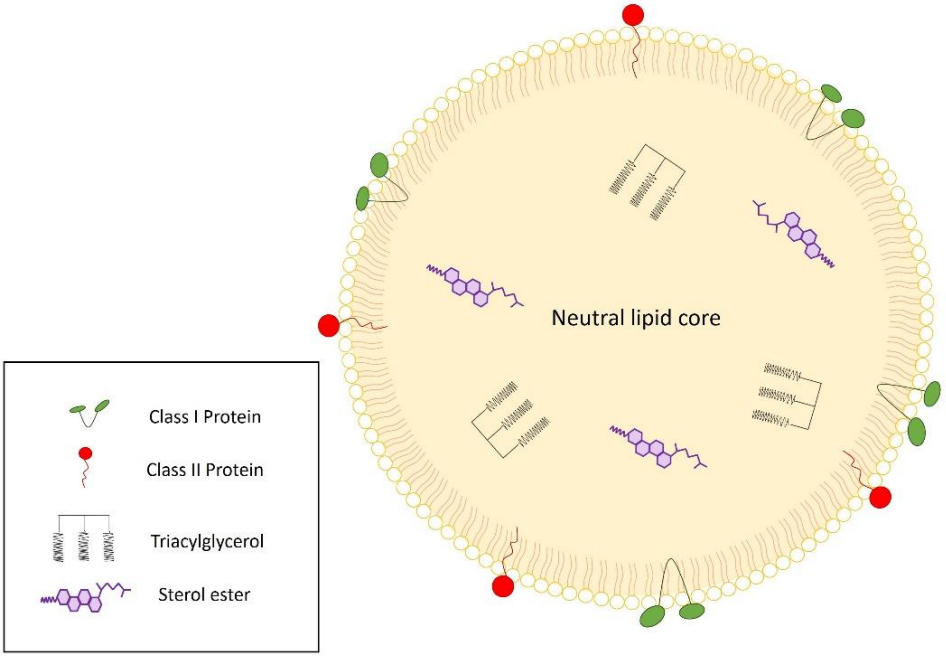

Fig.1. Schematic image of LD structure

In addition to the phospholipid composition of LD membranes, the surface proteins contained in the monolayer surrounding LD play a crucial role in regulating their homeostasis and intracellular interactions. The LD membrane is decorated with various structural and functional proteins that contribute to regulatory processes, and their composition can vary among LDs of different sizes or lipid compositions within the same cell [30, 49]. Several dozen proteins have been identified as LD proteins, which occur in bacteria, plants, yeasts, insects, and mammals, each contributing to a variety of cellular functions [23]. Many of these proteins are involved in lipid metabolism, including the synthesis and trafficking of phosphatidylcholine (PC), sterols, and triglycerides (TG). Additionally, certain proteins that do not directly participate in lipid metabolism play a role in regulating the surface properties of LDs [49, 50].

In mammalian lipid droplets (LDs), the most prominent group of proteins belongs to the PAT family, also known as the perilipin (PLIN) protein family. This family includes perilipin (PLIN1), adipocyte differentiation-related protein (ADRP), also known as adipophilin or PLIN2, tail-interacting protein of 47 kDa (TIP47) or PLIN3, as well as PLIN4 and PLIN5 [51]. These proteins share sequence similarity and have the capacity to bind intracellular LDs, indicating a common ancestral gene origin [52]. PLIN proteins are primarily expressed in adipose tissue and play key roles in regulating lipid homeostasis by controlling access of lipases to the neutral lipid core of LDs [53]. For example, PLINs have been proposed to protect LDs from lipolysis by shielding the triacylglycerol (TG) core

from lipase activity, and adipocytes from PLIN knockout mouse models exhibit elevated basal lipolysis levels [54, 55].

Although the general role of PLIN2 in LDs is well established, it remains unclear how this protein affects the mobility of phospholipids at the LD surface and their exchange with surrounding membranes. LD dynamics and contact site formation depend not only on lipid composition but also on protein-mediated modulation of surface properties. Therefore, clarifying the influence of PLIN2 on lipid diffusion is essential. In this thesis, these aspects were investigated experimentally by reconstituting bilayer-embedded LDs in a microfluidic setup and quantifying phospholipid diffusion and lipid exchange in the presence of PLIN2.

Each PLIN family member has a distinct function. PLIN1 acts as a gatekeeper for lipolysis, regulating access of lipases to LDs. PLIN2 and PLIN3 are widely expressed across different tissues and are associated with smaller LDs. The PLIN2 protein plays a permissive role in lipolysis. PLIN4 is mostly expressed in white adipose tissue and is involved in LD formation [56, 57]. PLIN5, the most extensively studied and last member of the family, is highly expressed in tissues with elevated energy demands (including liver, heart, and skeletal muscle) and its amino acid sequence, which is conserved across species, underscores its crucial role in mediating contacts between LDs and other organelles [56, 58]. PLIN5 also supports intramyocellular lipid (IMCL) accumulation and oxidation, making it important in the adaptation of skeletal muscle to physical activity [59]. Moreover, PLIN5 promotes LD-mitochondria interactions, facilitating fatty acid trafficking from LDs to mitochondria for β-oxidation [60]. In the heart, overexpression of PLIN5 can cause cardiac steatosis and mild mitochondrial dysfunction and hypertrophy, while PLIN5 knockout mice exhibit cardiac dysfunction [56], emphasizing the protein's essential role in energy metabolism. Understanding PLIN5’s roles at LD contact sites may offer therapeutic targets for metabolic diseases characterized by disrupted lipid homeostasis [61].

Beyond the PLIN family, lipid droplets also host other classes of proteins that contribute to lipid homeostasis, including those involved in lipid biogenesis, intracellular lipid metabolism, and lipid degradation [62]. In addition, several “refugee proteins,” not directly linked to traditional LD functions, have also been identified on LDs. These include signaling proteins such as mitogen-activated protein kinase (MAPK), phosphatidylinositol 3-kinase (PI3K), and Lyn kinase, as well as membrane trafficking proteins and chaperones [63-65].

Caveolins constitute another class of LD-associated proteins. Caveolin-1 and caveolin-2 localize to the surface of LDs and help form caveolae, characteristic membrane invaginations that regulate endocytosis, cholesterol transport, signal transduction, and

cellular growth [44, 66-68]. In addition, a diverse group of membrane trafficking proteins, such as small GTPases, motor proteins (e.g. kinesin, myosin), SNAREs, and vesicular trafficking proteins (e.g. ADP-ribosylation factors and COPs), also mediate dynamic interactions between LDs and other cellular compartments [69].

Finally, seipin (Berardinelli-Seip congenital lipodystrophy type 2 protein, BSCL2) is an integral ER protein that plays a central role in lipid droplet biogenesis and maintenance. This highly conserved protein is enriched at LD-endoplasmic reticulum contact sites and is critical for lipid droplet formation. Mutations in seipin cause severe lipodystrophies and other disorders such as distal hereditary motor neuropathy and Silver syndrome [2, 70, 71]. In yeast, seipin proteins localize to LD-ER junctions, marking sites where new LDs emerge, while enzymes that catalyze triglyceride synthesis, such as diacylglycerol acyltransferases 1 and 2 (DGAT1 and DGAT2), also accumulate at these junctions to drive droplet formation [28, 72].

3.4 Lipid Droplets Function in the Cell

LDs are dynamic cellular organelles that act as important lipid reservoirs. The lipids they store not only provide energy but also serve as building blocks for membrane synthesis, making LDs central hubs of cellular metabolism [30]. Many enzymes involved in the synthesis of phospholipids (PLs), triacylglycerols (TGs), and their intermediates, along with lipases and lipolytic regulators, are localized on the surfaces of LDs. Beyond their well-established role in lipid metabolism, growing evidence indicates that LDs also participate in protein degradation, the response to endoplasmic reticulum (ER) stress, protein glycosylation, and defense against pathogen infections [73-76].

In many cell types, including adipocytes and hepatocytes, lipids accumulate within lipid droplets so they can provide energy when the cell requires it. Lipid droplets play an important role in maintaining homeostasis and energy balance during periods of nutrient stress. Moreover, LDs are recognized as major phospholipid precursors and thus contribute significantly to cell growth and proliferation [6, 77]. Several studies have shown that the lipid core of LDs can also store fat-soluble vitamins (A, D, E, and K) [6]. For example, in liver cells, vitamin A (retinol) can be esterified and stored in the core of LDs to buffer periods of dietary insufficiency [78]. Likewise, excess vitamin D can accumulate in LDs in an inactive form and, when needed, is mobilized, activated, and released into the bloodstream to help maintain adequate circulating levels and support physiological functions [79].

The number of LDs increases in various diseases characterized by altered or dysfunctional lipid metabolism, such as non-alcoholic fatty liver disease and cancer. A common factor

driving the accumulation of LDs in non-adipose tissues is cellular stress, which can be triggered by an excess of free fatty acids, nutrient deprivation, or redox imbalances. Under these conditions, LDs appear to contribute to stress reduction by sequestering potentially harmful or excess lipids and preserving lipid homeostasis within cellular membranes [6, 80].

In addition to these metabolic and protective functions, LDs are increasingly recognized as hubs of protein quality control. They can transiently sequester aggregation-prone or misfolded proteins. This prevents cytotoxic accumulation and facilitates their degradation via proteasomal or autophagic pathways [1,6]. Furthermore, LDs act as signaling platforms by supporting the synthesis of bioactive lipids such as eicosanoids, which are key mediators of inflammation and immunity [6, 81]. These additional functions underscore the multifaceted roles of LDs as both metabolic and regulatory organelles.

3.5 Lipid Droplets Communication in the Cell

LDs must establish connections with other organelles to fulfill their diverse functions such as their significant role in regulating cellular metabolism. Furthermore, LDs also supply essential lipids for membrane biogenesis in response to cellular demands, making their contact and communication with other organelles critical [82].

To form a contact site between two organelles within a cell, they must be closely apposed, typically at a distance of about 10-70 nm (with many researchers emphasizing 30 nm). This nanoscale spacing is critical, as it enables direct protein-protein or protein-lipid interactions across organelles without fusion, allowing regulated communication while preserving compartmental identity [83]. The main structures that bring organelles into contact are called molecular tethers Like other tethering proteins, these tethering proteins play a central role in mediating lipid droplet interactions with other organelles [2]. These protein tethers promote close organelle apposition and include well-characterized examples such as perilipins and seipin, which regulate lipid droplet contacts with mitochondria and the ER, respectively [84, 85]. Specifically, PLIN5 anchors mitochondria to lipid droplets to facilitate fatty acid trafficking during metabolic demand, thereby supporting energy production under nutrient-limited conditions [61, 86] (see Fig. 2). Figure 2 illustrates three possible scenarios: (A) a free LD positioned near a membrane without direct connection, (B) a protein-mediated tether, where proteins such as perilipins or seipin bridge the LD to another organelle membrane, and (C) a lipid-mediated contact, where the LD monolayer connects directly with the bilayer of another organelle through a hemifusion-like structure**.** These different modes of communication highlight how LDs

can either remain independent, establish transient interactions, or form more intimate structural connections.

Some studies have shown that these modes of communication are not mutually exclusive, and in some cases, protein-mediated tethering and lipid-mediated connections may occur simultaneously, providing both stability and direct lipid exchange capacity [2].

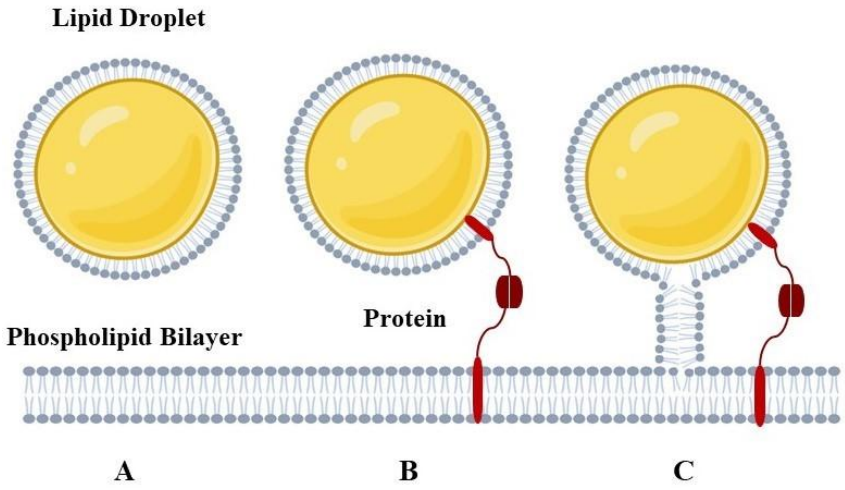

Fig. 2. (A. B & C) Schematic image of possible ways of LD contact sides with and without protein connection

Beyond these established protein tethers, lipid droplet contact sites are highly dynamic and adapt to the cell's metabolic state. Proteins such as Mdm1 in yeast and its human homolog Snx14 can bridge lipid droplets with multiple organelles at once, for instance, linking lipid droplets with the ER and vacuoles or the plasma membrane [87, 88]. These multitether proteins not only position organelles together but also concentrate lipid-synthesizing or lipid-remodeling enzymes at these junctions, creating specialized microenvironments that optimize lipid metabolism [88].

Interestingly, although protein tethers are the primary focus in the field of contact-site research, lipidic structures forming connections between LDs and the endoplasmic reticulum (ER), and in some cases other organelles, have also been frequently observed [88, 89]. These findings have drawn attention to the possible involvement of lipidic bridges in facilitating the formation of LD contact sites. Due to the unique structure of lipid droplets, which possess a monolayer rather than a bilayer like most other organelles, specialized physical interactions can occur (especially at ER contact sites) via hemifusion intermediates known as lipidic bridges. These bridges connect the phospholipid monolayer of the LD to the outer leaflet of the bilayer membrane of the neighboring organelle. It is still uncertain whether these lipidic connections are rigid and stable, or whether they exist

only transiently alongside protein tethers [90-93]. In addition to ER-LD contact sites, where these connections can arise through biogenesis or de novo reconnection, similar lipidic bridges have also been observed between LDs and peroxisomes [94]. Lipidic bridges enable the exchange of materials, including lipids and proteins between organelles [2]. Both hemifusion and full fusion of these lipidic bridges incur energetic costs, and the stability of these bridges depends largely on the surface tension of the lipid droplet. Unlike bilayer membranes, which generally have low surface tension, the surface tension of the LD monolayer is highly dependent on its phospholipid composition, a factor that may also influence the formation of tethering complexes [7].

Together, these findings highlight that lipid droplets do not exist in isolation but instead integrate into the cellular landscape through a combination of protein- and lipid-mediated connections that are essential for their biological functions. Despite these insights, the nature of lipidic bridges at LD contact sites remains poorly understood. It is still unclear whether such connections are inherently stable or predominantly transient, how their formation is influenced by the lipid composition of the LD monolayer, and how they coexist or compete with protein tethers such as PLIN5. Furthermore, the energetic and structural factors determining whether lipidic bridges persist long enough to facilitate substantial lipid transfer have yet to be clarified.

Addressing these questions is critical for understanding the balance between lipid- and protein-mediated organelle interactions. In this thesis, I investigated these aspects experimentally by reconstituting LD contact sites in vitro, quantifying lipid transfer via lipidic bridges, and examining how surface tension and tether proteins like PLIN5 modulate their formation and stability.

3.6 Experimental Approaches to Model Lipid Droplets

Studies of LDs have been greatly advanced by a range of both in vivo and in vitro approaches. In vivo models enable the study of LDs under physiologically relevant conditions and across tissues and developmental stages. Transparent vertebrate models like transgenic zebrafish expressing fluorescently tagged LD proteins, e.g. PLIN2-tdTomato, allow real-time imaging of LD formation and turnover in response to dietary, pharmacological, or genetic perturbations. These models have revealed tissue-specific regulation of LD dynamics for example, rapid LD expansion under high-fat diets and shrinkage under fasting and have been critical for testing small-molecule regulators of lipid storage [95]. Mouse models and cell-type-specific knockouts of key LD proteins such as PLINs, enzymes of neutral lipid metabolism, have further linked LDs to systemic processes including lipid homeostasis, ER stress, and inflammatory responses [81].

In parallel, in vitro methods provide precise experimental control, enabling detailed mechanistic studies that are difficult to achieve in vivo [96, 97]. These approaches allow the manipulation of lipid composition, protein decoration, and physical environment, facilitating investigations into LD formation, growth, membrane curvature, surface tension, and protein binding dynamics. In vitro systems have revealed how the interplay between proteins and lipids affects LD stability, asymmetry, and interaction with other organelles, linking LD behavior to cellular metabolic states, diet, or pathological conditions [98]. For instance, studies using surface-adhered TAG droplets, droplet interface bilayers, or microfluidic-generated lipid droplet models have demonstrated that phospholipid composition and associated proteins strongly influence droplet morphology and interfacial dynamics [99].

Below, we describe common in vitro techniques reported in the literature to generate model lipid droplets for in vitro studies, some of which were specifically adapted or developed for this dissertation. These methods allow systematic manipulation of LD composition, size, and protein decoration, providing a well-controlled platform for studying lipid-protein interactions, interfacial dynamics, and LD contact sites under controlled conditions. Several in vitro strategies have been developed to generate model LDs, each with unique advantages and limitations depending on the experimental question.

3.6.1 Spherical Model LDs

A commonly reported technique for producing model lipid droplets involves generating spherical oil-in-water or water-in-oil droplets by dispersing neutral lipids and phospholipids in an aqueous buffer through sonication or vigorous vortexing [96, 100-102]. These emulsified droplets, although artificial, mimic the fundamental biophysical principles of cellular LD formation, where neutral lipids phase-separate and become stabilized by a surrounding phospholipid monolayer. This phospholipid coating acts as a surfactant, lowering interfacial tension and preventing the droplets from fusing immediately after formation. Sonication typically produces more uniform and stable droplets than vortexing, but experimental conditions must be carefully optimized to prevent either coalescence due to over-sonication or incomplete droplet formation when insufficient energy is applied [96, 101]. The produced droplet size depends strongly on the lipid composition and mixing method. Increasing the neutral lipid content yields larger droplets with less surface area per unit volume of lipid, while increasing the phospholipid content promotes smaller droplets with greater surface coverage. Thus, by tuning lipid ratios and mixing intensity, researchers can reproducibly

generate droplet populations suited to different experimental needs, from single-droplet imaging to bulk biophysical assays. The relative volumes of buffer and oil also determine whether water-in-oil or oil-in-water droplets form: when the buffer volume exceeds the oil volume, oil-in-water droplets predominate; the opposite volume ratio favors water-in-oil droplets, which are less amenable to fluorescence imaging and further surface modifications due to restricted exchange between the encapsulated aqueous core and the external aqueous environment. To facilitate microscopy observation of oil-in-water droplets, droplets can be trapped between a glass slide and a coverslip separated by microspheres, which restricts vertical movement and stabilizes them against buoyancy effects so that their equatorial monolayer plane can be imaged with minimal distortion. However, protein-induced aggregation can complicate cytometric measurements of droplet shape and protein binding [96].

3.6.2 Droplet-Embedded Vesicles (DEVs)

In the literature-reported technique of Droplet-Embedded Vesicles, triacylglycerol (TAG) is introduced into giant unilamellar vesicles (GUVs) to produce droplets embedded within GUV bilayer [103, 104]. These droplet-embedded vesicles (DEVs) feature two types of lipid environments, the phospholipid monolayer surrounding the oil droplet and the phospholipid bilayer of the enclosing GUV, making them a useful model for mimicking the contact interface between lipid droplets and the endoplasmic reticulum. Bright-field microscopy readily distinguishes the refractive index contrast between the GUV and the embedded lipid droplet, and confocal microscopy enables selective imaging of different focal planes. Typically, the buoyant oil droplet rises toward the top of the GUV lumen, allowing clear optical sections through the monolayer and bilayer surfaces. The density of the surrounding buffer and of the GUV interior can be tuned to control droplet buoyancy, for example, GUVs filled with high-molecular-weight solutes (e.g. sucrose) will sink when placed into a physiological buffer.

Electroformation is often used to produce GUVs. However, the resulting vesicle population can be heterogeneous, with some vesicles nesting inside others [96, 103]. This nesting can complicate fluorescence quantification because overlapping bilayers contribute additive intensity signals. Imaging also depends on the orientation of the membrane relative to the focal plane: a perpendicular bilayer appears bright, while a bilayer parallel to the focal plane (e.g. at the top or bottom of the GUV) yields a much dimmer signal.

Overall, droplet-embedded vesicles provide a versatile and well-characterized platform for studying lipid droplet-membrane interactions under controlled conditions. However, issues such as GUV heterogeneity, complex 3D imaging requirements, and overlapping bilayers require careful attention during quantitative analyses [103].

3.6.3 Surface-adhered LD caps

Surface-adhered lipid droplet caps provide a simple and stable model for studying lipid droplets under controlled buffer conditions [96]. It is another literature-reported method that triacylglycerol (TAG) is first deposited as small droplets on a glass coverslip, and then a phospholipid-containing buffer is added to mimic physiological conditions. This setup allows high-resolution imaging of LD surfaces and simplifies buffer exchange and long-duration observations, see fig. 3. To prepare surface-adhered caps, approximately 3 mL of TAG, which is thoroughly vortexed or sonicated, is pipetted onto the center of a cleaned glass-bottom Petri dish. The oil is dispersed across the coverslip by directing a focused stream of nitrogen gas onto the surface, producing a uniform array of microdroplets. Successful formation of small droplets can be verified by visual inspection of the coverslip prior to buffer addition. Once the TAG droplets are deposited, buffer is gently added to the dish. This exchange does not disturb the shape of droplets smaller than approximately 80 μm in diameter. In the absence of phospholipids or surfactants, buffer exchange has negligible effect on the droplet morphology. In the presence of surfactants and under static buffer conditions, droplets larger than 40 μm in diameter may detach and float away over a period of hours. Smaller droplets ($\leq$ 40 μm) remain firmly attached to the glass, are not displaced during buffer exchanges, and can be readily imaged or analyzed by optical and scanning probe microscopy for extended timescales.

The contact angle and long-term stability of these caps depend on the cleanliness of the glass surface. Excessively hydrophilic surfaces (e.g. achieved by aggressive plasma or piranha cleaning) prevent stable adherence of TAG. In contrast, insufficiently cleaned surfaces can make the glass too hydrophobic, causing the TAG to spread excessively without forming discrete caps. Phospholipid monolayer formation on the caps can be achieved by adding fluorescently labeled large unilamellar vesicles (LUVs) to the buffer and monitoring the increase in monolayer fluorescence over time. Within as little as 5 minutes of exposure to Cy5-labeled LUVs, the monolayer fluorescence on the oil-water interface saturated, indicating

rapid adsorption of phospholipids from the vesicles. Importantly, the rate and extent of exchange depended on the lipid species present; for example, mixtures containing phosphatidylethanolamine (PE) or phosphatidylinositol (PI) led to faster LUV binding and exchange rates than phosphatidylcholine (PC)-only vesicles. This surface-adhered lipid droplet caps method requires careful calibration of sonication or vortexing to achieve uniform droplet sizes and complete phospholipid monolayer coverage. Other disadvantages of this method are droplet stability and imaging that can be limited by the coverslip's surface properties and by potential fluorescence bleaching or labeling artifacts during long-duration measurements [96].

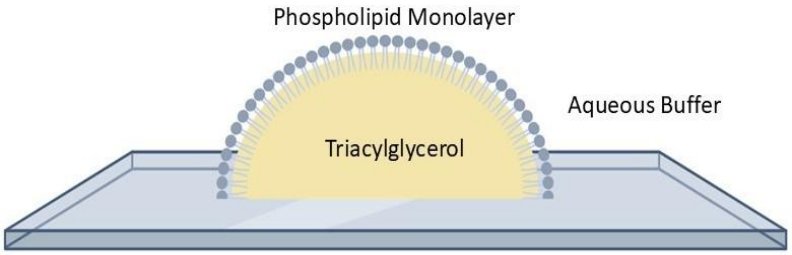

Fig. 3. Schematic image of coverslip bounded LD which provides optical accessibility by inverted microscopy

3.6.4 LD Formation using Microfluidic Devices

Although surface-adhered caps offer optical simplicity, microfluidic systems provide higher control over droplet size, composition, and dynamic manipulation, making them particularly suited for mechanistic studies. Microfluidics is a multidisciplinary field focused on the manipulation of fluids at the microscale, typically within channels measuring tens to hundreds of micrometers. This scale-specific regime exhibits characteristics such as laminar flow, high surface-to-volume ratios, and diffusion-dominated mixing, all of which enable the precise handling of small volumes. These unique properties have made microfluidic platforms invaluable across physics, chemistry, engineering, and life sciences, especially for applications requiring high-throughput, minimal reagent use, and finely controlled microenvironments [105].

In this thesis, microfluidic approaches were employed to generate model lipid droplet systems, making it useful to provide a more detailed description of the technique. In the context of biological and biophysical research, microfluidic devices, often referred to as "lab-on-a-chip" systems, are frequently fabricated using soft lithography. This process involves photolithographic patterning of a

master mold followed by casting elastomeric materials such as polydimethylsiloxane (PDMS). The resulting chips are optically transparent, biocompatible, and capable of forming microchannels and chambers with precise geometries. Microfluidics has become particularly important for studying model biomembranes due to its ability to generate stable droplets, emulsions, and interfaces under controlled conditions [106]. The predictable flow behavior and compartmentalization achievable in microfluidic systems have enabled significant advances in mimicking cell membranes, including the formation of lipid vesicles, bilayer networks, and monolayer-coated droplets. These systems serve as platforms to study membrane protein dynamics, interfacial tension, lipid diffusion, and compartmentalized biochemical reactions. Among these applications, the modeling of LDs has emerged as a growing area of interest [107].Among various strategies in the literature, microfluidic generation of lipid monolayer-coated water-in-oil (w/o) droplets has been proposed as a simplified model for cellular LDs, which consist of a neutral lipid core enclosed by a phospholipid monolayer. These systems are typically realized using flow-focusing or T-junction geometries within microfluidic chips, where aqueous droplets are formed in a lipid-containing oil phase. Phospholipids spontaneously assemble at the oil-water interface during droplet formation, creating monolayer-coated structures. While these droplets often contain aqueous cores, they effectively replicate the surface organization of LDs. In modified versions, neutral lipids such as triolein are incorporated into the droplet core, producing hydrophobic interiors that closely resemble endogenous lipid droplets. These microfluidic models offer high reproducibility, monodispersity, and compatibility with fluorescence and interfacial tension studies [108]. However, microfluidic LD models also present certain limitations, including droplet stability compromised by evaporation-driven shrinkage (especially in PDMS devices), which can limit lifetimes for micrometer-sized droplets [109]. Also, handling and optimization of fluidic circuits can be intricate, requiring precise control over flow rates and device geometry, this complexity makes the technique less feasible for industrial scale-up and routine lab use [110].Another related literature-reported technique involves the creation of nanoliter-scale lipid-coated droplets via microfluidic devices and their deposition onto open substrates patterned with microcavities. In this method, droplets are generated in a lipid-rich oil phase (such as a hexadecane-squalane mixture) and spotted on SU-8 patterned glass substrates with micrometer precision. As the droplets come into contact, their lipid monolayers can form droplet interface bilayers (DIBs) [111]. While originally used to mimic inter-compartmental communication, this system can also be adapted for

LD modeling by using oil-phase droplets containing neutral lipids surrounded by phospholipids. Such a configuration enables label-free detection (e.g., via matrix-assisted laser desorption/ionization mass spectrometry or so called MALDI-MS) and long-term monitoring of membrane permeability and diffusion. While both microfluidics-related strategies offer versatile platforms for artificial cell and LD research, they are not employed within the experimental framework of this thesis but are included here to provide a broader perspective on state-of-the-art microfluidic approaches for LD mimicry [112]. Later in the method section, the adapted techniques that were used in this dissertation to form the model LDs will be described thoroughly.

4. Materials and Methods

4.1 Materials

A variety of phospholipids and related molecules were used in this study to model lipid monolayers and lipid droplet (LD) interfaces. These molecules were selected to reproduce the compositional and physicochemical diversity found in biological LDs and cellular membranes. Phospholipids are amphiphilic molecules consisting of a hydrophilic headgroup and two hydrophobic fatty acid tails. Their dual nature enables them to spontaneously orient at oil-water interfaces, forming stable monolayers where the headgroups face the aqueous phase and the tails extend into the oil phase. These monolayers are fluid and dynamic, in contrast to crystalline self-assembled monolayers, and their molecular packing is influenced by both chemical composition and molecular geometry [113].

In the current study, the LD monolayer was mainly composed of 2-dioleoyl-sn-glycero-3-phosphocholine (DOPC) and 1,2-dioleoyl-sn-glycero-3-phosphoethanolamine (DOPE), chosen to closely mimic the composition of cellular membranes. To tune monolayer motility and packing, additional unsaturated phospholipids such as N-methylated DOPE (N-DOPE), 1-palmitoyl-2-oleoyl-sn-glycero-3-phosphocholine (POPC), and lysophosphatidylcholine (LPC) were used. Saturated phospholipids, including 1,2-dipalmitoyl-sn-glycero-3-phosphocholine (DPPC) and 1,2-distearoyl-sn-glycero-3-phosphate (DSPA), were introduced to explore the effects of tighter molecular packing. These lipids typically form more rigid, ordered films, although DSPA, with its negatively charged headgroup, can exhibit looser packing due to electrostatic repulsion. Sphingomyelin (SM), a saturated sphingolipid with a cylindrical geometry, was also tested because it contributes to the formation of rigid domains in membranes.

Sterols were further included to probe how non-phospholipid species modulate LD interfaces. Cholesterol, which intercalates between phospholipids and disrupts tight packing, increases surface tension and lipid mobility when mixed into monolayers [113, 114]. In contrast, cholesteryl ester, which resides mainly in the neutral lipid core, has little effect on monolayer properties [114, 115]. Together, these components allowed exploration of how both interfacial and core composition contribute to LD stability and dynamics. Triglyceride-based oil, glyceryl trioleate (triolein), was used to create the LD core, reproducing the neutral lipid environment found in natural LDs [116]. For comparative experiments, squalene served as an alternative oil phase. The chemical structures of all lipid species, cholesterol, and oil phases used are summarized in Fig. 4.

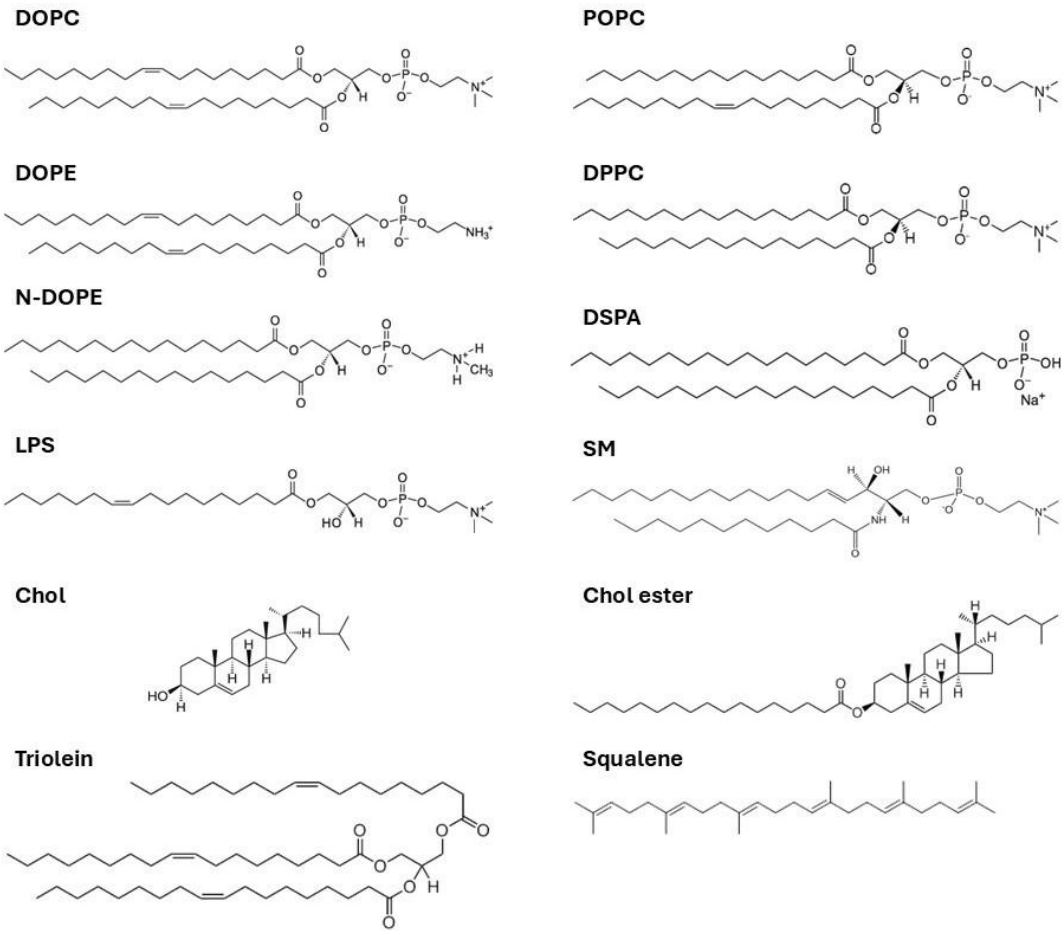

Fig. 4. Chemical Structures of Lipids, Cholesterol and Squalene oil used in the experiments [117].

After establishing the molecular compositions, the behavior of phospholipids at interfaces can be better understood through their geometry and packing characteristics. The geometry of a phospholipid molecule, defined by the relative size of its hydrophilic headgroup and hydrophobic tails, determines its packing parameter, which governs how molecules arrange themselves at an interface [113]. Depending on these proportions, phospholipids can be cylindrical, conical, or inverted-conical in shape (Fig. 5). Cylindrical lipids such as phosphatidylcholine (PC) pack tightly and form flat interfaces. Inverted-conical lipids such as phosphatidylethanolamine (PE) promote negative curvature and higher fluidity, whereas conical lipids such as lysophosphatidylcholine (LPC) induce positive curvature and disrupt ordered packing.

These shape-dependent variations control packing density, curvature, and lateral mobility within the monolayer, parameters crucial for LD stability and lipid-protein interactions. Cylindrical lipids maximize van der Waals attractions between their hydrocarbon chains, forming relatively ordered films, while conical or inverted-conical lipids introduce steric

hindrance and electrostatic repulsion, reducing packing density and increasing fluidity. Consequently, lipid geometry determines interfacial properties such as curvature elasticity, surface pressure, and molecular diffusion, all of which influence LD behavior [113].

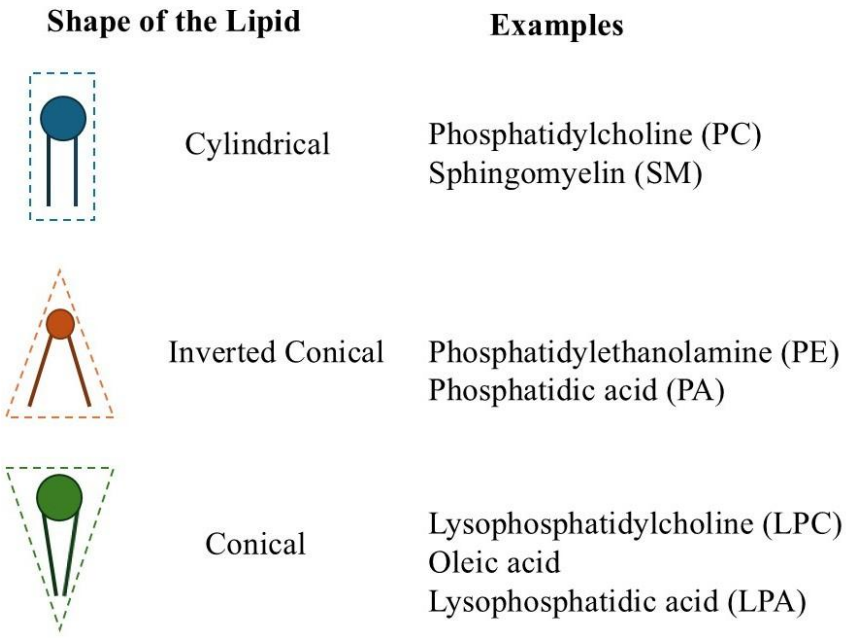

Fig. 5. Schematic representation of lipids with different shapes and their examples

Unsaturation further contributes to interfacial dynamics. In unsaturated lipids, the cis-double bonds introduce kinks in the acyl chains that hinder tight packing. This reduces van der Waals interactions, increases the effective cross-sectional area, and shifts the molecular geometry toward more conical shapes. As a result, unsaturated chains remain disordered and fluid under physiological conditions, whereas saturated chains readily align into tightly packed, gel-like states [113].

Fluorescently labeled lipids were employed for visualization and fluorescence recovery after photobleaching (FRAP) studies. These included 1,2-dioleoyl-sn-glycero-3-phosphoethanolamine labeled with fluorescein (FITC-DOPE), rhodamine (Rhod-PE), Atto647N (Atto647N-DOPE), and DOPE-Cy5.5. The fluorescent lipid concentration was typically 1-2 mol% of total lipid content. In some experiments, BODIPY 493/503 labeled the LD core, and Cy5-labeled dextran served as a water-soluble dye to assess molecular transport. These probes were selected for their compatibility with the imaging system, as described later [118].

Recombinant proteins used for lipid-protein interaction studies included human perilipin-2 (PLIN2) and bovine perilipin-5 (PLIN5), both well-established LD-associated proteins

[56]. PLIN2 and PLIN5 were purchased from Abcam and Cusabio Technology LLC, respectively, and purified according to supplier protocols.

Unless otherwise stated, all experiments were performed in buffer solution containing 150 mM KCl prepared with ultrapure Milli-Q water. All phospholipids and lipid-related molecules were obtained from Avanti Polar Lipids (Alabaster, AL, USA) unless otherwise noted. Triolein (T7140) and squalene (S3626) were from Sigma-Aldrich, FITC-DOPE from Santa Cruz Biotechnology (ChemCruz), and Cy5-dextran from Creative Biolabs.

4.2 Methods

4.2.1 µChip and Microfluidic Platforms for Lipid Droplet Studies

To investigate the properties and interactions of lipid droplets (LDs), this thesis employed a series of custom-designed microfluidic platforms developed in our laboratory. Unlike more complex systems reported in the literature, our method aims to mimic the native architecture of lipid droplets and their properties [119]. To differentiate between them, the term "µChip" refers to experiments with free-standing LD membranes (artificial LD monolayers), whereas "microfluidic device" refers to those used for LD contact site experiments. A third setup, the free-standing bilayer device, allowed studies of LD-bilayer interactions and lipid exchange.

The devices were fabricated using soft lithography, a replica-molding technique in which an elastomer (typically polydimethylsiloxane, PDMS) is cast against a master mold to generate micro- and nanoscale features. This method is widely applied in microfluidics because it is inexpensive, rapid, and enables highly accurate replication of channel geometries [119]. The main steps include mold preparation (via 3D printing or photolithography), PDMS casting and curing, demolding, and finally bonding the PDMS structure to glass substrates. Regardless of the final application, all structures were designed in AutoCAD and fabricated using the silicone elastomer kit Sylgard 184 (Dow Corning) to produce PDMS microfluidic devices and the final bonding was strengthened by baking at 90-95°C for 1 h.

For the µChip device, which was used for planar monolayer studies, a 3D-printed cylindrical well (3 mm diameter) was placed at the center of a glass Petri dish, and a degassed PDMS mixture was poured to a thickness of ~3 mm, partially embedding the cylinder, cf. Fig. 6. The mold was fabricated using UltiMaker tough

PLA (polylactic acid), a modified PLA-based 3D printing filament designed to provide enhanced mechanical performance while retaining the ease of use of standard PLA. Compared to conventional PLA, tough PLA offers higher impact strength and improved resistance to deformation, making it particularly suitable for functional prototyping and structural applications requiring durability. The PDMS was cured for 6-7 hours at 60 °C, a temperature well below the softening point of UltiMaker tough PLA (150-160 °C), which ensured that the PLA mold maintained its structural integrity during curing and enabled precise replication of the microchannel geometry. After curing, the PLA mold was carefully removed. Then, a square PDMS blocks containing the cylindrical cavity were cut, removed and bonded to PDMS-coated glass coverslips (spin-coated at 3000 rpm for 5 min) using oxygen plasma treatment (Diener Electronics), followed by incubation at 90-95 °C for 1 hour to enhance sealing (see Fig. 6 for production steps). The resulting shallow wells provide a stable and optically, accessible oil-water interface for planar monolayer formation.

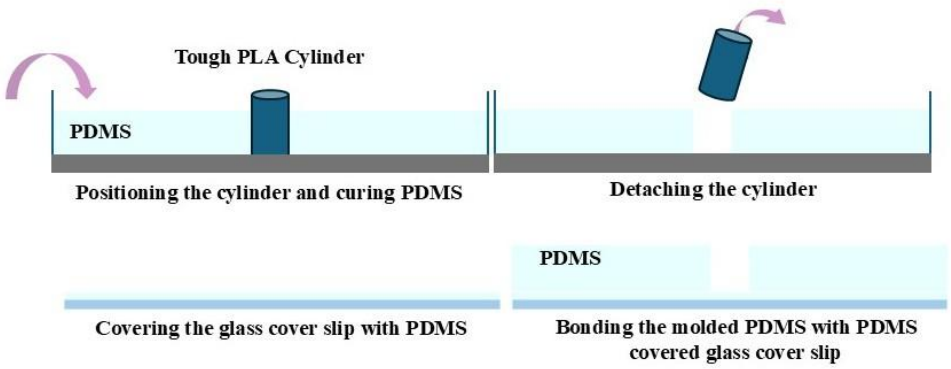

Fig. 6. Schematic representation of steps for μChip production

For lipid droplet model assembly, phospholipids (DOPC, DOPE, or a 1:1 mixture) were dissolved in ethanol, dried under vacuum, and rehydrated with triolein. The mixture was ultrasonicated to a final concentration of 2% w/w phospholipid in triolein, supplemented with 2 mol% FITC-DOPE for fluorescence visualization [120]. This concentration is slightly above the critical threshold required to form stable droplet interface bilayers. In order to model LD's monolayer membrane, 6 μL of the lipid-in-oil phase was pipetted into the PDMS well, followed by the gentle addition of 20 μL of 150 mM KCl buffer. This lipid-in-oil phase mimics the lipid composition of the LD core (DOPC and DOPE), providing a realistic oil environment for monolayer formation at the oil-water interface. Upon addition of

the aqueous buffer, a phospholipid monolayer spontaneously assembles within seconds at the interface between the two immiscible phases, see fig. 7. The order of layering, placing the denser aqueous phase above the less dense oil phase, was deliberately chosen to ensure a stable and well-defined oil-water interface. In this configuration, the higher-density buffer remains positioned above the lighter triolein phase, while the cylindrical well confines both liquids within a controlled geometry. The small dimensions of the well (3 mm in diameter, millimeter-scale depth) are critical to maintaining interfacial stability and preventing phase inversion, in which the less dense oil could otherwise rise and spread over the buffer. This design not only preserves a stationary and optically accessible interface but also provides the practical advantage of allowing subsequent addition of buffer-dispersed vesicles or proteins without disturbing the underlying oil phase. Such geometric and compositional considerations were essential to achieving reproducible and stable monolayer formation in the µChip. This minimal system is reproducible, optically accessible, and well-suited for studying protein-lipid interactions, lipid diffusion dynamics (e.g., via FRAP), and the influence of lipid composition [123, 124].

This µChip system was used to study both the biophysical properties of lipid monolayers and the effects of PLIN2 (ADRP) on phospholipid diffusion. Incorporating fluorescently labeled lipids allows quantitative analysis of lateral mobility, providing insights into diffusion dynamics under various lipid compositions [121, 122].

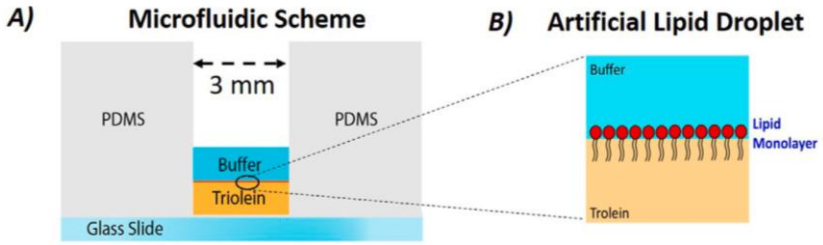

Fig. 7. (A) Sketch of the microfluidic device. (B) Schematic of the phospholipid decorated triolein-buffer interface.

In addition to the µChip, a 3D microfluidic device was fabricated to investigate interactions between lipid droplets (LDs) and large unilamellar vesicles (LUVs) (Fig. 8). The device consisted of a straight microchannel with dimensions of 15 mm × 1 mm × 100 µm. The master mold was produced using standard

photolithography: SU-8 photoresist was spin-coated onto a 2-inch silicon wafer to achieve the targeted 100 μm channel height. Spin-coating was performed under optimized conditions (500 rpm for 20 s with 100 rpm/s acceleration, followed by 1500 rpm for 60 s with 300 rpm/s acceleration), yielding a uniform resist layer. After soft-baking (65 °C for 15 min, 95 °C for 45 min), the wafer was exposed to UV light (400 nm, 15 mW/cm², 20 s) through a photomask and post-baked (65 °C, 1 min; 95 °C, 5 min). Development in acetone, ethanol, and distilled water produced a well-defined negative channel mold.

PDMS (Sylgard 184) was poured onto the SU-8 master, degassed for 30 min to remove air bubbles, and cured with the standard protocol. After demolding, inlet and outlet ports were punched, and the PDMS channel was plasma-bonded to a glass coverslip. The assembled device was baked at 90-95 °C for 1 h to strengthen the bond and partially restore PDMS hydrophobicity. This 3D microfluidic chip provides a controlled, optically accessible environment for studying droplet-vesicle interactions [121, 122].

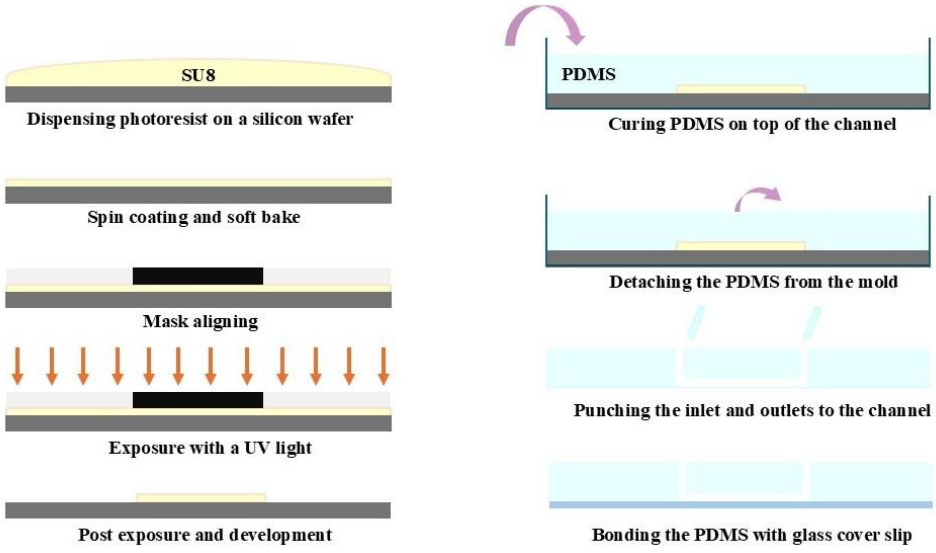

Fig. 8. Schematic representation of steps of photolithography (A) and soft-lithography (B)

The 3D microfluidic device was used to study LD-LUV contact-site formation under well-defined conditions. Lipid droplets of controlled size and composition were prepared using a spherical model droplet technique [96]. Specifically, phospholipids (DOPC or DOPE, 25 mg/mL in chloroform) were diluted to 2 wt% in chloroform, dried under vacuum for 60 min to remove the solvent completely, and rehydrated with 250 μL of triolein. When required, proteins such as PLIN5 were incorporated by adding 4 μL of a 0.1 mg/mL protein solution in reconstitution

buffer (Tris-HCl, EDTA, trehalose, 5% glycerol) at this stage. The lipid-oil mixture was dispersed into 8-10 mL of 150 mM KCl buffer by magnetic stirring at 250 rpm for 5 min. Stirring speed and duration were optimized to produce droplets with diameters of ~5-20 μm, suitable for fluorescence microscopy. Large unilamellar vesicles (LUVs) were prepared from DOPC:DOPE (60:40 molar ratio), containing 2 mol% Rhod-PE and Dextran-Cy5 to label the vesicle surface and core, respectively. Lipids and dyes (1 mg/mL in chloroform) were vacuum dried for 1 h and rehydrated in 150 mM KCl buffer by pipetting and vortexing. The suspension was extruded 10 times through a 1 μm polycarbonate filter at 50 °C. A 1:100 dilution yielded optimal visibility and minimal background, corresponding to a final vesicle concentration of 8.67×10^8 vesicles/mL. For contact-site assays, 10 μL of LUV suspension was incubated with 60 μL of LD dispersion for 1 h at room temperature before loading into the microfluidic observation chamber. Time-lapse fluorescence microscopy allowed visualization of LD-LUV interactions and enabled quantitative analysis of protein-mediated tethering, lipid exchange, and dynamic remodeling at the monolayer interface.

In addition to the μChip and 3D microfluidic platforms, a dedicated device for free-standing bilayer formation was employed to investigate lipid droplet (LD)-bilayer interactions and lipid/protein exchange (Appendix II, Puza, Asfia et al., IJMS 2023). The device consisted of a PDMS block containing a narrow rectangular aperture (200-300 μm wide) in the middle of a channel, fabricated using the same soft lithography techniques described for the other platforms. The PDMS block was plasma-bonded onto a glass coverslip to create a stable, optically accessible chamber for bilayer formation and microscopy. The geometry of the aperture enabled reproducible formation of free-standing bilayers, with stability ranging from 10 min to several hours depending on lipid-oil composition, providing a platform for quantitative measurements such as FRAP and protein-lipid interaction assays.

Bilayers were assembled by sequential deposition of a phospholipid-oil mixture (DOPC:DOPE, 3:1 in squalene) and buffer. Opposing monolayers gradually zipped together to form a stable bilayer across the aperture. ADRP-coated LDs could then be deposited onto the bilayer, where they spontaneously docked and inserted, enabling studies of lipid and protein exchange at the LD-bilayer interface. The approach, developed and optimized in collaboration with S. Puza, allowed quantitative comparison of lipid diffusion with and without protein decoration.

The main application of this device is to provide a controlled platform to examine diffusion and partitioning of lipids and proteins between a bilayer and bilayer-

embedded LDs. This design ensures high optical accessibility for microscopy, and compatibility with quantitative assays such as FRAP, making it suitable for studies of LD-bilayer interactions under well-defined conditions.

Together, the μChip and 3D microfluidic device constitute robust, reproducible platforms for modeling lipid droplets, enabling both simplified monolayer studies and dynamic contact site experiments under well-defined conditions.

Together, the μChip, the 3D microfluidic device, and the free-standing bilayer platform provide a robust and reproducible suite of tools for investigating lipid droplet (LD) biology under well-defined conditions. Collectively, these devices bridge the gap between minimal and more complex in vitro systems, offering versatile platforms for mechanistic studies of LD properties, interactions, and protein-mediated dynamics.

4.2.2 Interfacial Tension Measurement

The pendant drop method is a standard technique for measuring interfacial tension, and in this work it was applied at the triolein-buffer interface decorated with phospholipids, using a contact angle measurement system (OCA 20, DataPhysics, Germany), cf. Fig. 9 as an example. In this method, a transparent cuvette with optical grade surfaces is first filled with the lighter phase, in our experiments the phospholipid-containing triolein solution (density: 0.91 g/cm³). Subsequently, a pendant droplet of the denser aqueous buffer (density: 0.998 g/cm³) is formed at the tip of a hollow needle submerged in the oil phase [125, 126].

Once the pendant droplet is formed, its shape is governed by the balance of gravitational, buoyancy, and interfacial (surface) forces. The effective weight of the droplet causes it to elongate due to gravity, while the interfacial tension acts to minimize its surface area and maintain a rounded shape. The final equilibrium shape reflects this balance:

$$p(z) = p_{apex} - \Delta\rho g z = \gamma(\kappa_1 + \kappa_2) = \gamma\left(\frac{1}{R_1} + \frac{1}{R_2}\right) = \Delta P$$

Here in this balance, p(z) is the local pressure at height z (the vertical distance measured downward from the droplet apex), p_{apex} is the pressure at the droplet apex, $\Delta\rho = \rho_{buffer} - \rho_{oil}$ is the density difference between the aqueous and oil phases, and g is the gravitational acceleration. The term γ denotes the interfacial tension, and R_1 and R_2 are the principal radii of curvature at a given point on the droplet surface. The local curvatures $\kappa_1 = 1/R_1$ and $\kappa_2 = 1/R_2$ together define the total curvature κ =

$\kappa_1 + \kappa_2$ of the interface [127]. While the classical Young-Laplace equation describes only the mean curvature of a free interface in the absence of gravity and buoyancy, for pendant droplets under gravity, the droplet profile is determined by an extended version of the Young-Laplace equation that also accounts for hydrostatic pressure resulting from gravitational and buoyancy forces. This results in a description where both pressure and curvature vary along the rotationally symmetric interface as a function of height, and the shape can be calculated numerically by solving the modified Young-Laplace equation for the specific system [128].

In the pendant drop method, this equation is applied by fitting the observed droplet profile to a theoretical shape derived from the Young-Laplace equation. The measurement software (SCA 20) captures high-resolution images of the droplet and analyzes its contour. From this analysis, the radii of curvature and volume are extracted, and the interfacial tension is calculated by solving the extended Young-Laplace equation for γ.

To ensure precise and reproducible measurements, the droplet volume was maintained at (2.0 ± 0.5) µL. Volumes outside this range may lead to inaccuracies: droplets that are too small exhibit minimal deformation, as the surface forces dominate over gravitational forces, limiting the sensitivity of the analysis, while overly large droplets are prone to detachment or instability and may even fall off during the measurement, which can distort the shape and reduce the precision of the interfacial tension fitting [129, 130].

All measurements were carried out at room temperature (23 ± 1) °C, with each droplet allowed to equilibrate until its shape stabilized at a plateau, giving sufficient time for phospholipids or other surfactants to diffuse and fully decorate the liquid/liquid interface before acquisition. For each experimental condition, at least three independent droplets were analyzed, and the reported interfacial tension values represent averaged results. Calibration of the system was verified against pure water-air measurements (72 mN/m at 23 °C) to confirm accuracy.

Fig. 9. Pendant drop image as it used for interfacial tension measurement

4.2.3 Optical Microscopy

Optical microscopy was employed to observe lipid droplet (LD) membrane models, characterize LD and large unilamellar vesicle (LUV) dispersions, and monitor LD-LUV interactions in microfluidic devices. Prior to incubation, LD and LUV samples were imaged separately to confirm size distribution, fluorescence labeling, and dispersion stability. For interaction experiments, 10 µL of LUV suspension was incubated with 60 µL of LD dispersion for 1 h at room temperature before being introduced into the microfluidic observation chamber.

Most experiments were performed using widefield fluorescence microscopy on an inverted Axio Observer 7 (Carl Zeiss Microscopy GmbH) equipped with a Colibri7 LED light source and a CMOS camera (Axiocam 712). Images were acquired with a 40× objective (NA 0.95), and 14-bit depth. Fluorescent phospholipids (FITC-DOPE, Rho-DOPE, Atto647-DOPE) were visualized with the appropriate filter cubes. FITC fluorescence was excited with filter sets in the range of 390-530 nm and emitted between 460-605 nm. Fluorescence from Rhodamine and Cy5 was collected using filter sets with excitation at 538-562 nm and 614-647 nm, and emission at 570-640 nm and 659-759 nm, respectively. This system was used mainly for LD monolayer imaging, z-stack acquisitions, and FRAP experiments.

To achieve higher spatial resolution and optical sectioning, spinning disk confocal microscopy was employed using an inverted Nikon Ti-Eclipse microscope equipped with a LU-NV laser unit and a Yokogawa CSU-W1 spinning disk head. Excitation lasers at 481 nm, 561 nm, and 643 nm, combined with emission filters

at 417-477, 515-540, 589-625, and 665-705 nm, enabled simultaneous detection of bilayer regions, LDs, and fluorescently tagged proteins. A 40× oil-immersion objective (working distance 220 μm) was used.

Diffusion Investigation based on the Fluorescence Recovery After Photobleaching (FRAP) Technique

Fluorescence recovery after photobleaching (FRAP) was employed in this study both to investigate the lateral diffusion of different phospholipids at the LD surface and to examine how the LD-associated protein PLIN2 modulates lipid mobility. FRAP is a widely used biophysical technique that allows the quantification of molecular mobility within membranes and monolayers by monitoring the rate at which fluorescently labeled molecules move back into a photobleached region. This approach not only provides the diffusion coefficient (D) but also reveals dynamic heterogeneity, potential diffusion barriers, and the effects of protein binding or crowding at the interface. In the context of lipid droplets, FRAP is particularly informative for understanding how proteins such as PLIN2 influence lipid packing, monolayer fluidity, and lateral organization. FRAP experiments were conducted on the same widefield (Axio Observer 7) and confocal (Nikon Ti-Eclipse) systems described above, with bleaching and recovery protocols adapted to each optical configuration.

On the Axio Observer 7 widefield microscope, photobleaching was performed using the LED illumination system at maximum output (~25 mW at the sample plane, corresponding to ~8 mW/mm²). A circular bleaching region was defined by a 50 μm pinhole aperture projected onto the LD monolayer and illuminated for ~30 s until fluorescence was nearly abolished. Fluorescence recovery was then monitored at low LED intensity (<1 mW at the sample plane) to minimize secondary bleaching. Imaging was performed with 150 ms exposure time, and time-lapse acquisition continued until recovery reached a plateau.

On the Nikon Ti-Eclipse spinning disk confocal, bleaching was performed within software-defined circular ROIs ranging from 5-50 μm in diameter, depending on LD size. Each measurement began with a 20-second pre-bleach acquisition phase. Photobleaching was carried out by applying maximum laser power (70 mW for 481 and 561 nm; 125 mW for 647 nm) for 20 s, divided into 10 loops repeated three times. Recovery was then monitored for at least 5 minutes under reduced illumination to capture the complete dynamics.

All experiments were performed at room temperature (23 °C). Recovery curves were normalized by dividing intensity values by the maximum pre-bleach fluorescence, thereby setting the pre-bleach intensity to unity and allowing comparisons across experiments. The normalized curves were fitted to the Soumpasis equation [131] using Python:

$$D = 0.224\,.\ \frac{r^2}{\tau_{1/2}}$$

where D is the diffusion coefficient, r the radius of the bleached area, and $\tau_{1/2}$ the half-time of recovery. This model assumes negligible diffusion during the bleaching step and provides a robust estimate of lipid mobility within the monolayer [48].

The results consistently showed that FITC-DOPE, Rho-DOPE, and Atto647-DOPE displayed comparable recovery dynamics in pure DOPE monolayers, confirming the reproducibility of the approach. The bleaching region was carefully controlled to remain constant within each setup (50 µm pinhole for the Axio Observer, 5-50 µm ROIs for the Nikon system). Interestingly, Rho-DOPE exhibited markedly higher photostability compared with FITC-DOPE and Atto647-DOPE. Although this did not alter the diffusion coefficients calculated from the recovery data, it resulted in more stable fluorescence signals during repeated acquisitions. Therefore, Rho-DOPE was preferentially used as the fluorescent probe in subsequent imaging experiments whenever possible to ensure higher signal reliability and minimize photobleaching artifacts.

5. Results and Discussions

This chapter presents the results of three projects forming the core of this thesis. Two are published in peer-reviewed journals, and the third has been submitted at the time of thesis submission. Across these studies, microfluidic platforms (which are introduced already in the method part) were employed to investigate lipid droplet (LD) dynamics, phospholipid mobility, and protein-mediated interactions with organelles. All three publications are attached in Appendices I-III.

In the first project (Asfia et al., *BBA - Biomembranes, 2023*), a planar LD model was established to quantify lipid diffusion using FRAP. The results demonstrated that lipid mobility is strongly governed by molecular packing, with conical or charged lipids promoting higher diffusion and cylindrical or saturated lipids restricting it. In the second study (Puza, Asfia et al., *IJMS, 2023*), perilipin-2 (PLIN2) was shown to reshape the morphology of bilayer-embedded LDs while exerting minimal effects on lipid mobility, linking protein binding to interfacial mechanics. The third project (Mohammadian, Asfia et al., *Biochemistry and Biophysics Reports, 2025)* extended this framework to LD-organelle communication, showing that perilipin-5 (PLIN5) facilitates contact formation and lipid transfer between LDs and large unilamellar vesicles (LUVs).

The following sections provide a detailed discussion of these results in the context of LD biophysics and microfluidic modeling.

5.1 Biophysical Properties of Lipid Monolayers at the Lipid Droplet Interface: Influence of Lipid Type and Composition

Lipid droplets (LDs) originate in the endoplasmic reticulum (ER) and are covered by a phospholipid monolayer enriched with proteins and sterols [132, 133]. The composition and physical properties of this monolayer strongly influence LD behavior, including packing, interfacial tension, and lateral diffusion. To explore these effects, planar LD models were generated at a triolein-buffer interface, and lipid mobility was quantified using FRAP for the categorized saturated, unsaturated, and sterol lipids. The results are published in Asfia et al., Biochimica et Biophysica Acta - Biomembranes (2023) and summarized here. For further details on materials, methods, and results, refer to Appendix I.

Unsaturated phospholipids generally promote looser packing and higher lateral mobility, consistent with their molecular geometry. For example, cone-shaped DOPE reached diffusion coefficients of ~17 $\mu m^2/s$, while cylindrical DOPC displayed ~8 $\mu m^2/s$. Intermediate lipids, such as POPC and N-DOPE, showed diffusion values between these

extremes, illustrating how both molecular shape and resulting packing density influence monolayer dynamics. Surface tension measurements were consistent with these observations: monolayers containing more conical lipids exhibited higher surface tension, indicative of lower packing density (Fig. 10). LPC, a single-tailed inverted cone lipid, displayed similar diffusion to DOPC and POPC, further supporting the link between molecular shape and lateral mobility.

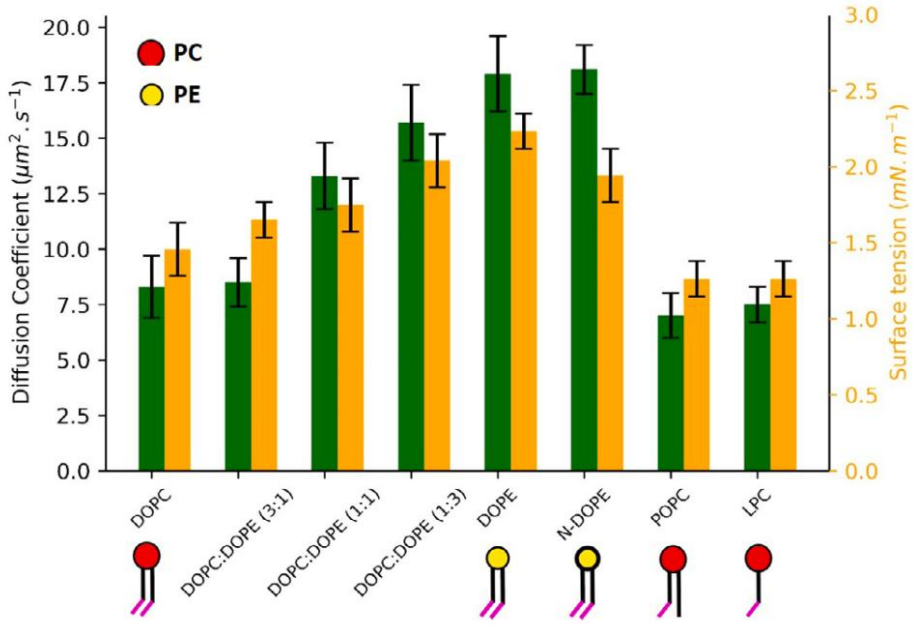

Fig. 10. FRAP-derived diffusion constants (green) and surface tension values (yellow) for selected unsaturated phospholipids at the triolein–buffer interface. Schematic representations illustrate lipid geometry (cone vs. cylinder).

Saturated phospholipids, such as DPPC and sphingomyelin (SM), formed densely packed monolayers with reduced mobility (~5-8 μm²/s), consistent with their cylindrical shapes and tighter packing. DSPA, a negatively charged saturated lipid, displayed higher diffusion (~20 μm²/s) primarily due to electrostatic repulsion between headgroups rather than packing. Mixtures of DOPC with DSPA, or of other saturated/cylindrical lipids with charged lipids, yielded intermediate mobility and surface tension, demonstrating how both geometric packing and electrostatic interactions jointly influence monolayer properties (Fig. 11). These findings highlight the central role of lipid type and composition in determining the biophysical landscape of the LD interface.

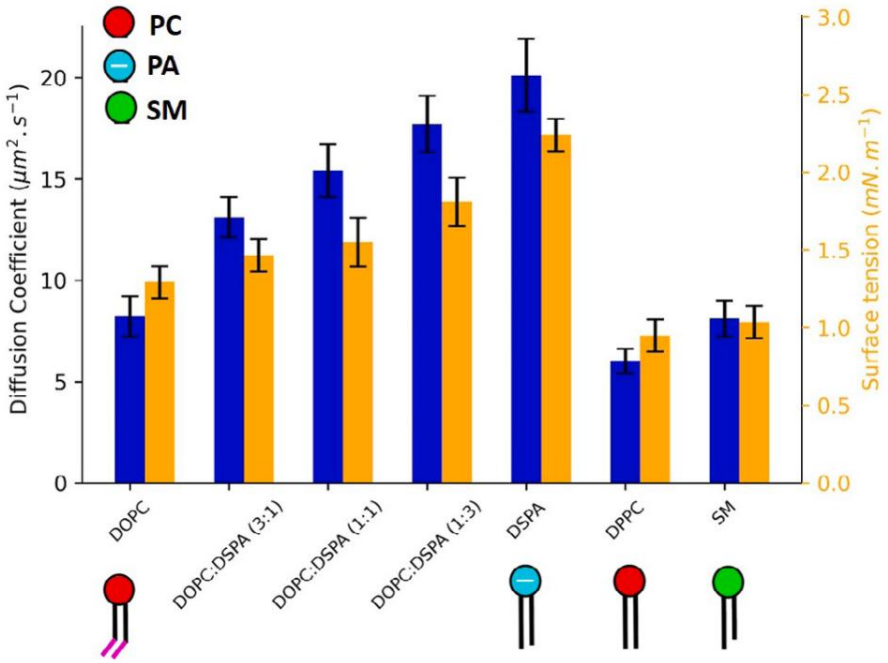

Fig. 11. FRAP-derived diffusion constants (green) and surface tension values (yellow) for saturated phospholipids and DOPC-DSPA mixtures. Schematic representations indicate the combined effects of molecular shape and charge on packing and lateral mobility.

Moreover, sterols were also explored to study their influence on LD monolayer biophysics. Cholesterol at 10% molar fraction increased both lipid diffusion and surface tension, consistent with its ability to disrupt packing and create free volume at the interface. In contrast, cholesteryl esters, which partition into the neutral lipid core, had minimal effect on monolayer properties. Monolayers containing up to 15% cholesteryl ester showed diffusion and surface tension values essentially identical to pure DOPC or DOPE monolayers. These results suggest that sterols can selectively modulate interfacial dynamics depending on their localization: membrane-inserting sterols affect packing and diffusion, while core-localized esters do not.

In summary, the lateral mobility and surface tension of lipid monolayers decorating LDs depend on lipid molecular shape, packing, charge, and mole fractions. Unsaturated, cone-shaped lipids favor looser packing and faster lateral diffusion, while saturated, cylindrical lipids pack more densely and diffuse more slowly. Sterols can further modulate these properties by changing the effective packing density at the interface, although cholesteryl esters, which localize in the neutral lipid core, do not affect the monolayer. This consistent reasoning clarifies how molecular structure, packing, and electrostatic interactions jointly

define LD monolayer biophysics, providing a foundation for interpreting LD-protein and LD-organelle interactions.

5.2 Effect of PLIN2 (ADRP) protein on the Phospholipid Diffusion Properties of an LD Embedded in a Bilayer

To investigate how ADRP (also known as PLIN2) influences the mobility of phospholipids on lipid droplets (LDs) and the exchange of lipids between LD monolayers and surrounding bilayers, we employed two complementary microfluidic approaches. The results presented in this section have been published in Puza, Asfia et al., International Journal of Molecular Sciences, 2023, and the complete experimental details can be found in Appendix II.

In the first approach, we used a simplified LD model by forming a phospholipid monolayer at the buffer-triolein interface inside a microfluidic chamber which is thoroughly described in the method section. The monolayer consisted of DOPC and DOPE in a 3:1 molar ratio with 2 mol% DOPE-Cy5 as a fluorescent probe. Using FRAP, we quantified lateral diffusion with and without the presence of ADPR protein. For total phospholipid concentrations in triolein at or above 1 wt% (defined as the weight percentage of phospholipids relative to the triolein phase), the monolayer exhibited a concentration-independent diffusion coefficient of ≈8 $\mu m^2/s$. At lower phospholipid concentrations, the diffusion coefficient increased, consistent with reduced monolayer packing and incomplete surface coverage. Upon addition of the fluorescently labelled protein ADRP-Alexa488 (1 μM), the protein decorated the interface and formed micrometer-scale clusters, corresponding to the patchy distribution observed in Fig. 12, A (bottom row). Because ADRP organizes into clusters rather than remaining uniformly distributed, its markedly lower diffusion coefficient is consistent with confined or collective motion of these assemblies. Interestingly, the presence of ADRP did not significantly alter the phospholipid diffusion, which remained within experimental error of the control condition. By contrast, ADRP itself exhibited much slower lateral motion, with a diffusion coefficient of ≈0.3 $\mu m^2/s$, over twenty times lower than that of the surrounding lipids. This constitutes the first direct quantification of ADRP mobility on a lipid monolayer and indicates that while the protein remains mobile, it diffuses in a fundamentally different regime compared with phospholipids (Fig. 12, B). These results show that ADRP decorates LD surfaces in a clustered yet partially dynamic manner, without creating a detectable steric barrier to lipid motion.

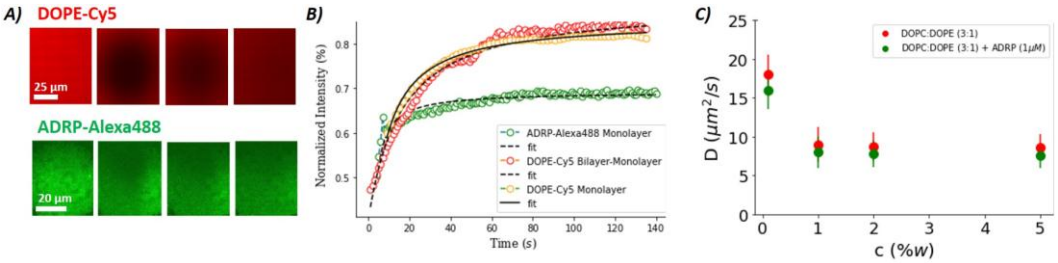

Fig. 12. (A) Fluorescence images of a DOPC:DOPE (3:1) monolayer at the buffer-triolein interface before and after bleaching (DOPE-Cy5, 2% mol; ADRP-Alexa488, 1 µM). (B) FRAP curves showing recovery for DOPE-Cy5 (red), ADRP-Alexa488 (green), and DOPE-Cy5 on bilayer-embedded LDs (yellow). (C) DOPE diffusion versus total lipid concentration, with and without ADRP; averages of ≈30 measurements with error bars.

Additionally, the lipid exchange between ADRP-coated LDs and a free-standing DOPC:DOPE (3:1) bilayer were examined. Upon deposition, LDs spontaneously inserted into the bilayer and remained stably positioned at the interface, allowing direct observation of lipid dynamics across the LD-bilayer contact. FRAP experiments were performed on DOPE-Cy5 within both the LD monolayer and the bilayer to quantify lateral diffusion and potential lipid transfer between them. DOPE-Cy5 fluorescence on ADRP-coated LDs recovered rapidly after photobleaching, with kinetics comparable to those of monolayers and bilayers in the absence of ADRP. This indicates that the LD-bilayer boundary remained permeable to lipid exchange. This behavior differs from observations in LDs lacking ADRP, where accumulation of cone-shaped lipids such as DOPE at regions of negative curvature has been hypothesized to form a stabilizing, curvature-supporting ring that may act as a partial diffusion barrier [121, 138, 139].

The morphology of ADRP-coated LDs further supports this interpretation. 3D confocal imaging revealed a characteristic “pancake-like” flattening of the LD at the bilayer interface. Because such morphology requires altered wetting behavior at the three-phase contact line, based on wetting theory and prior literature [140], we infer that ADRP protein accumulates there. Such enrichment would help explain the increased lipid exchange we observe, by localizing to regions of highest curvature and interfacial tension, ADRP likely disrupts any DOPE-enriched ring that could otherwise act as a barrier, allowing lipids to move more freely between the LD and the bilayer. Consistent with this interpretation, our measurements also confirm that while ADRP forms micrometer-scale clusters on LD surfaces, it remains mobile, even though with a diffusion coefficient significantly lower than that of phospholipids (~0.3 µm²/s versus ~8 µm²/s), highlighting a distinct dynamic regime for the protein.

In summary, our findings demonstrate that ADRP organizes into micrometer-scale clusters on LD surfaces that remain mobile, as quantified by FRAP, without restricting phospholipid diffusion. By accumulating at regions of high curvature at the LD-bilayer interface, ADRP promotes lipid exchange and supports the characteristic flattened, "pancake-like" LD morphology. These results provide a mechanistic link between ADRP's structural organization on LDs and its functional role in facilitating lipid redistribution, illustrating how the protein modulates both LD surface dynamics and LD-bilayer interactions to maintain lipid homeostasis.

5.3 Role of PLIN5 and lipid composition in LD's Contact Sites with LUVs as a model for organelle membranes

To investigate how lipid composition and the presence of PLIN5 influence interactions between lipid droplets (LDs) and organelle membranes, we modeled LDs coated with either DOPE or DOPC and incubated them with large unilamellar vesicles (LUVs) to mimic organelle bilayer membranes, observing their interactions in a microfluidic device. Details of the LD and LUV model systems, as well as the microfluidic setup, are provided in the Methods section. This study is described in the manuscript "Influence of PLIN5 and Lipid Composition on Lipid Droplet Contact Sites with Other Organelles" (under review in Biochemistry and Biophysics Reports), and additional information on lipid compositions, fluorescent labeling, and imaging protocols is available in Appendix III.

In the first series of experiments, LDs coated with either DOPE or DOPC were incubated with DOPC/DOPE LUVs. After the incubation time, many previously non-fluorescent LDs acquired a distinct orange signal, indicating the transfer of rhodamine-labeled phospholipids from the LUV membrane into the LD monolayer (Fig. 13). No fluorescence from the aqueous core dye of the LUVs was detected on LDs, confirming that these events did not result from full vesicle fusion. Instead, the data indicates the formation of transient lipidic bridges that allow phospholipid transfer while maintaining the integrity of both compartments. Although only transient lipidic bridges were observed regardless of whether LDs were coated with DOPE or DOPC, the type of phospholipid significantly influenced fusion efficiency. DOPE-coated LDs exhibited a high proportion of fusion events (≈95%), whereas DOPC-coated LDs showed substantially fewer fusions (≈35-40%) over the same incubation period. These statistics were obtained by analyzing at least 150 LDs in each set of experiments. This difference aligns with the distinct properties of the two monolayers. DOPE, being conical and less tightly packed, generates higher surface tension (~2.3 mN/m) and faster lipid mobility (~18 $\mu m^2/s$), which favor the initiation of lipid bridges. In contrast, the more cylindrical and tightly packed DOPC monolayers (~1.5

mN/m, ~8 μm²/s) present a less permissive interface. These observations emphasize that lipid packing geometry is a key determinant of LD contact behavior, with more loosely packed monolayers enabling efficient transient interactions. These findings are consistent with our earlier study on LD monolayer dynamics, which demonstrated that phospholipid geometry and packing strongly influence lateral mobility and the tendency for fusion.

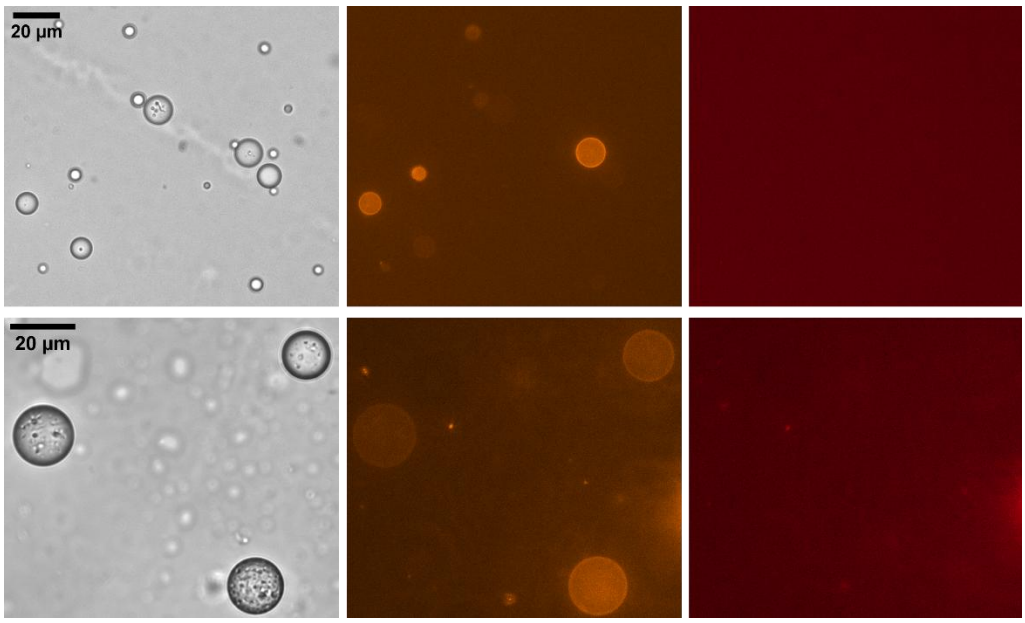

Fig. 13. Fusion behavior of LD's monolayer with LUVs after the incubation time. LD's monolayer consists of DOPC (top row) and DOPE (bottom row). The different columns show the same spot of one sample with different microscopy contrast methods, respectively fluorescent wavelengths. (left) Bright field micrographs, (middle) rhodamine dye channel and (right) Cy5 dye channel.

To investigate the contribution of perilipin-5 (PLIN5), a similar set of experiments was carried out with PLIN5 incorporated into the LD monolayer. The presence of PLIN5 reduced phospholipid transfer: the fusion rate of LDs showing rhodamine uptake decreased by ~1.3 times for DOPE-coated LDs and ~8 times for DOPC-coated LDs. Although lipid exchange was reduced, additional interaction behaviors were observed. LDs frequently displayed discrete, punctuate fluorescence signals corresponding to LUVs that remained stably attached for extended periods of time (Fig. 14). These puncta were showing the signals for both the membrane-associated dye (rhodamine) and the core dye (Cy5), indicating that intact LUVs had been attached to the LD surface. Unlike the transient lipidic bridges observed in the absence of PLIN5, these events represent protein-mediated tethering, where LUVs are anchored at the LD surface without undergoing fusion.

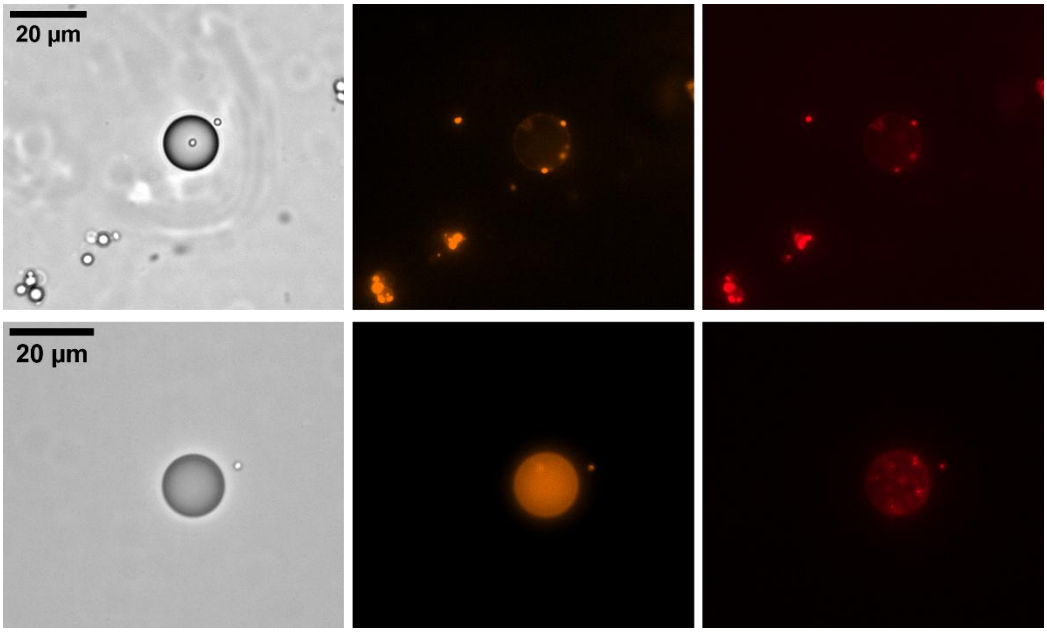

Fig.14. Fusion behavior of PLIN5-decorated LDs with LUVs after the incubation time. LD's monolayer consists of DOPC (top row) and DOPE (bottom row), plus PLIN5. Different columns show bright field images (left), rhodamine dye channel (middle) and Cy5 channel (right). The different columns show the same spot of one sample with different microscopy contrast methods, respectively fluorescent wavelengths.

Together, these experiments demonstrate that lipid composition and PLIN5 cooperatively regulate LD-membrane interactions. DOPE-coated LDs favor efficient lipid transfer through transient lipidic bridges, while DOPC-coated LDs show lower transfer efficiency due to tighter packing. PLIN5 limits lipid exchange, particularly on DOPC-coated LDs, and promotes the formation of stable, long-lived contacts via protein-mediated tethering. These findings highlight how both lipid geometry and protein decoration jointly determine the nature and efficiency of LD contact sites with organelle membranes, extending the mechanistic understanding of LD interactions established in our prior studies.

6. Summary and Outlook

This thesis presents a comprehensive investigation into the dynamics, biophysical properties, and inter-organelle interactions of lipid droplets (LDs) using microfluidic platforms. The motivation behind this research was to develop reproducible, optically accessible, and precisely controlled model systems that model the unique architecture and functional complexity of LDs in living cells. By systematically studying LD composition, protein association, and membrane contact behavior, this work contributes fundamental insights into lipid biology and organelle communication.

The first part of the research focused on establishing a well-controlled microfluidic model of the LD interface, where a triolein-buffer system formed a planar lipid monolayer mimicking the phospholipid-coated surface of intracellular LDs. By varying lipid composition, particularly between cylindrical (DOPC) and conical (DOPE, DSPA) molecules, it was demonstrated that lipid packing geometry plays a dominant role in controlling both diffusion dynamics and surface tension. These results, quantified using FRAP and pendant drop methods, revealed that unsaturated, conical lipids enhance molecular mobility and interfacial tension, while saturated or densely packed lipids restrict diffusion.

In the second part, the role of perilipin-2 (PLIN2/ADRP) in regulating the morphology and behavior of bilayer-embedded LDs was investigated. PLIN2-coated LDs consistently adopted a pancake-like morphology, in contrast to the spherical shape of protein-free droplets. This altered geometry was attributed to an inhomogeneous surface tension distribution caused by localized PLIN2 accumulation, particularly near the three-phase contact line. Importantly, while PLIN2 did not affect phospholipid diffusion on the LD surface, it disrupted the diffusion barrier between the LD monolayer and the surrounding bilayer, thereby facilitating lipid exchange across the interface.

The final part explored LD contact sites with model organelles, using large unilamellar vesicles (LUVs) as models for cellular organelles. Dual labeling revealed the formation of lipidic bridges that enabled phospholipid transfer and membrane fusion, suggesting transient hemifusion-like states as a mechanism of lipid communication. Furthermore, perilipin-5 (PLIN5) was found to stabilize these contact sites, supporting its known role in tethering LDs to mitochondria and other organelles.

Taken together, the three studies provide a stepwise and complementary view of LD dynamics: lipid composition defines baseline surface properties, PLIN2 introduces protein-mediated regulation of LD geometry and exchange, and PLIN5 promotes inter-organelle connectivity. Beyond these biological insights, the work demonstrates the adaptability of microfluidic platforms for dissecting LD biology under controlled conditions. By bridging molecular-scale mechanisms (lipid packing and protein decoration) with organelle-level interactions (tethering

and lipid transfer), this thesis establishes a cohesive framework that links the physicochemical principles of LD organization to their biological roles.

Looking ahead, the flexible design of the microfluidic systems developed here allows for future integration of complex organelle geometries, multi-organelle assemblies, or energy-coupled processes that better mimic cellular metabolism. Mutational analysis or post-translational modifications of LD-associated proteins such as PLIN2 and PLIN5 represent promising directions for linking molecular changes to disease phenotypes. Moreover, the platforms could serve as a basis for studying drug interactions, lipid trafficking inhibitors, or nanocarrier systems targeting LD-related pathways in cancer and metabolic disorders.

7. References

1. J. A. Olzmann, P. Carvalho. Dynamics and functions of lipid droplets. Nat Rev Mol Cell Biol. 2019, 20(3):137-155.
2. M. Schuldiner, M. Bohnert. A Different Kind of Love - Lipid Droplet Contact Sites, Biochimica et Biophysica Acta (BBA) - Molecular and Cell Biology of Lipids, Volume 1862, Issue 10, Part B, 2017. Pages 1188-1196.
3. S. Fasciano, S. Wang. Recent advances of droplet-based microfluidics for engineering artificial cells. SLAS Technology. 2024, 29, 2, 100090.
4. B. Alberts, R. Heald, A. Johnson, D. Morgan, M. Raff, K. Roberts, P. Walter and J.Wilson. Molecular Biology of the Cell, 7th edition. 4022.
5. G. M. Cooper, R. E. Hausman. The Cell: A Molecular Approach. 6th Edition. 2013. Sinauer Associates: Sunderland, MA.
6. M. A. Weltea, A. P. Gouldb. Lipid Droplet Functions Beyond Energy Storage. Biochimica et Biophysica Acta (BBA) - Molecular and Cell Biology of Lipids, Volume 1862. 2017. Pages 1260-12.
7. A. R. Thiam, R.V. Farese Jr., T. C. Walther. The Biophysics and Cell Biology of Lipid Droplets, Nat Rev Mol Cell Biol. 2013; 14(12): 775-786.
8. M. F. Renne, H. Hariri, Lipid Droplet-Organelle Contact Sites as Hubs for Fatty Acid Metabolism, Trafficking, and Metabolic Channeling, Frontiers in Cell and Developmental Biology, Volume 9, 2021.
9. H. Yang, A. Galea, V. Sytnyk, M. Crossley. Controlling the size of lipid droplets : lipid and protein factors. Curr Opin Cell Biol. 2012, 24:509-16.
10. C. Zhang, M. Zheng, R. Bai, J. Chen, H. Yang, and G. Luo. Molecular mechanisms of lipid droplets-mitochondria coupling in obesity and metabolic syndrome: insights and pharmacological implications. Frontiers in Physiology. 2024, vol. 15.
11. T. Horii, J. Kozawa, Y. Fujita, S. Kawata, H. Ozawa, C. Ishibashi, S. Yoneda, T. Nammo, J. I. Miyagawa, H. Eguchi, I. Shimomura. Lipid droplet accumulation in β cells in patients with type 2 diabetes is associated with insulin resistance, hyperglycemia and β cell dysfunction involving decreased insulin granules. Front Endocrinol (Lausanne). 2022.
12. C. Y. Park, D. Kim, M. K. Seo, J. Kim, H. Choe, J. H. Kim, J. P. Hong, Y. J. Lee, Y. Heo, H. J. Kim, H. S. Park, Y. J. Jang. Dysregulation of Lipid Droplet Protein Expression in Adipose Tissues and Association with Metabolic Risk Factors in Adult Females with Obesity and Type 2 Diabetes. J Nutr. 2023, 153(3):691-702.
13. A. Zadoorian, X. Du, H. Yang. Lipid droplet biogenesis and functions in health and disease. Nat Rev Endocrinol. 2023, 19, 443-459.

14. A. C. Sheka, O. Adeyi, J. Thompson, B. Hameed, P. A. Crawford, S. Ikramuddin. Non-alcoholic steatohepatitis: a review. JAMA. 2020, 323, 1175-1183.
15. R. Ramkissoon, & T. B. Gardner. Pancreatic steatosis: an emerging clinical entity. Am. J. Gastroenterol. 2019, 114, 1726-1734.
16. M. S. Petrov, & R. Taylor. Intra-pancreatic fat deposition: bringing hidden fat to the fore. Nat. Rev. Gastroenterol. Hepatol. 2022, 19, 153-168.
17. M. Nakamura. Lipotoxicity as a therapeutic target in obesity and diabetic cardiomyopathy. Journal of Pharmacy & Pharmaceutical Sciences. 2024, vol. 27.
18. T. Xin, & S. Roland. Lipid Droplets Protect Human β-Cells from Lipotoxicity-Induced Stress and Cell Identity Changes. Diabetes. 2021, 70, 11, 2595-2607.
19. I. J. Goldberg, I. J. et al. Deciphering the role of lipid droplets in cardiovascular disease: a report from the 2017 National Heart, Lung, and Blood Institute Workshop. Circulation, 2018, 138, 305-315.
20. C. L. Yen, S. J. Stone, S. Koliwad, C. Harris, R. V. Farese Jr. Thematic review series: glycerolipids. DGAT enzymes and triacylglycerol biosynthesis. J Lipid Res. 2008, 49:2283-2301.
21. L. Sandager, M. H. Gustavsson, U. Stahl, A. Dahlqvist, E. Wiberg, A. Banas, M. Lenman, H. Ronne, S. Stymne. Storage lipid synthesis is non-essential in yeast. J Biol Chem. 2002, 277:6478-6482.
22. S. J. Stone, H. M. Myers, S. M. Watkins, B. E. Brown, K. R. Feingold, P. M. Elias, R. V. Farese Jr. Lipopenia and skin barrier abnormalities in DGAT2-deficient mice. J Biol Chem. 2004, 279:11767-11776.
23. G. Onal, O. Kutlu, D. Gozuacik, S. Dokmeci Emre. Lipid Droplets in Health and Disease. Onal et al. Lipids in Health and Disease, 2017, 16:128.
24. M. A. Welte. Expanding roles for lipid droplets. Curr Biol. 2015, 25:R470-81.
25. A. P. Long, A. K. Manneschmidt, B. VerBrugge, M. R. Dortch, S. C. Minkin, K. E. Prater, et al. Lipid droplet de novo formation and fission are linked to the cell cycle in fission yeast. Traffic. 2012, 13:705-14.
26. H. Khandelia, L. Duelund, K.I. Pakkanen, J.H. Ipsen. Triglyceride blisters in lipid bilayers: implications for lipid droplet biogenesis and the mobile lipid signal in cancer cell membranes. PLoS One. 2010, 5:e12811.
27. A. Kassan, A. Herms, A. Fernandez-Vidal, M. Bosch, N. L. Schieber, B. J. Reddy, A. Fajardo, M. Gelabert-Baldrich, F. Tebar, C. Enrich, et al. Acyl-CoA synthetase 3 promotes lipid droplet biogenesis in ER microdomains. J Cell Biol. 2013, 203:985-1001.
28. J. M. Shockey, S. K. Gidda, D. C. Chapital, J. C. Kuan, P. K. Dhanoa, J. M. Bland, S. J. Rothstein, R. T. Mullen, J. M. Dyer. Tung tree DGAT1 and DGAT2 have nonredundant

functions in triacylglycerol biosynthesis and are localized to different subdomains of the endoplasmic reticulum. Plant Cell. 2006, 18:2294-2313.

29. J. R. Skinner, T. M. Shew, D. M. Schwartz, A. Tzekov, C. M. Lepus, N. A. Abumrad, N. E. Wolins. Diacylglycerol enrichment of endoplasmic reticulum or lipid droplets recruits perilipin 3/TIP47 during lipid storage and mobilization. J Biol Chem. 2009, 284:30941-30948.
30. F. Wilfling, J. T. Haas, T. C. Walther, R. V. Farese Jr.. Lipid Droplet Biogenesis. Curr Opin Cell Biol. 2014, 29: 39-45.
31. K. G. Soni, G. A. Mardones, R. Sougrat, E. Smirnova, C. L. Jackson, J. S. Bonifacino. Coatomer-dependent protein delivery to lipid droplets. J Cell Sci. 2009, 122:1834-1841.
32. K. Tauchi-Sato, S. Ozeki, T. Houjou, R. Taguchi, T. Fujimoto. The surface of lipid droplets is a phospholipid monolayer with a unique Fatty Acid composition. J Biol Chem. 2002, 277:44507-12.
33. T. Fujimoto, Y. Ohsaki, J. Cheng, M. Suzuki, Y. Shinohara. Lipid droplets: a classic organelle with new outfits. Histochem Cell Biol. 2008, 130:263-79.
34. Wilfling F, Haas JT, Walther TC, Farese RV Jr. Lipid droplet biogenesis. Curr Opin Cell Biol. 2014, 29:39-45.
35. Bartz R, Li W-H, Venables B, Zehmer JK, Roth MR, Welti R, et al. Lipidomics reveals that adiposomes store ether lipids and mediate phospholipid traffic. J Lipid Res. 2007, 48:837-47.
36. W.S. Blaner, S.M. O'Byrne, N. Wongsiriroj, J. Kluwe, D. M. D'Ambrosio, H. Jiang, et al. Hepatic stellate cell lipid droplets: a specialized lipid droplet for retinoid storage. Biochim Biophys Acta Mol Cell Biol Lipids. 2009, 1791:467-73.
37. T. Fujimoto, R. G. Parton. Not just fat: the structure and function of the lipid droplet. Cold Spring Harb Perspect Biol. 2011, 3.
38. H. C. Wan, R. C. Melo, Z. Jin, A. M. Dvorak, P. F. Weller. Roles and origins of leukocyte lipid bodies: proteomic and ultrastructural studies. FASEB J. 2007, 21:167-78.
39. C. Chitraju, M. Trotzmuller, J. Hartler, H. Wolinski, G. G. Thallinger, A. Lass, et al. Lipidomic analysis of lipid droplets from murine hepatocytes reveals distinct signatures for nutritional stress. J Lipid Res. 2012, 53:2141-52.
40. A. Penno, G. Hackenbroich, C. Thiele. Phospholipids and lipid droplets. Biochim Biophys Acta. 1831, 2013:589-94.
41. A. L. McIntosh, S. M. Storey, B. P. Atshaves. Intracellular lipid droplets contain dynamic pools of sphingomyelin: ADRP binds phospholipids with high affinity. Lipids. 2010, 45:465-77.

42. W. Fei, G. Shui, Y. Zhang, N. Krahmer, C. Ferguson, T. S. Kapterian, et al. A role for phosphatidic acid in the formation of “supersized” lipid droplets. PLoS Genet. 2011, 7:e1002201.
43. J. Zanghellini, F. Wodlei, H. von Grünberg. Phospholipid demixing and the birth of a lipid droplet. J Theor Biol. 2010, 264:952-61.
44. C. M. Blouin, S. Le Lay, A. Eberl, H. C. Köfeler, I. C. Guerrera, C. Klein, et al. Lipid droplet analysis in caveolin-deficient adipocytes: alterations in surface phospholipid composition and maturation defects. J Lipid Res. 2010, 51:945-56.
45. D. L. Brasaemle, N. E. Wolins. Packaging of fat: an evolving model of lipid droplet assembly and expansion. J Biol Chem. 2012, 287:2273-9.
46. K. Liu, M. J. Czaja. Regulation of lipid stores and metabolism by lipophagy. Cell Death Differ. 2013, 20:3-11.
47. R. Singh, A. M. Cuervo. Lipophagy: connecting autophagy and lipid metabolism. Int J Cell Biol. 2012, 2012:282041.
48. V. Choudhary, G. Golani, A. S. Joshi, S. Cottier, R. Schneiter, W. A. Prinz, M. M. Kozlov. Architecture of Lipid Droplets in Endoplasmic Reticulum Is Determined by Phospholipid Intrinsic Curvature. Current Biology. 2018, 28, 6, 915-926, e9.
49. L. Yang, Y. Ding, Y. Chen, S. Zhang, C. Huo, Y. Wang, et al. The proteomics of lipid droplets: structure, dynamics, and functions of the organelle conserved from bacteria to humans. J Lipid Res. 2012, 53:1245-53.
50. N. Krahmer, Y. Guo, F. Wilfling, M. Hilger, S. Lingrell, K. Heger, H. W. Newman, M. Schmidt-Supprian, D. E. Vance, M. Mann, R. V. Jr. Farese, T. C. Walther. Phosphatidylcholine synthesis for lipid droplet expansion is mediated by localized activation of CTP: phosphocholine cytidylyltransferase. Cell Metab. 2011, 14, 4, 504-15.
51. X. Xiang, J. Chen, L. Che. Emerging roles and therapeutic implications of lipid droplet protein perilipin 2 in liver disease. Genes & Diseases. 2025, 101712, 2352-3042.
52. P. E. Bickel, J. T. Tansey, M. A. Welte. PAT proteins, an ancient family of lipid droplet proteins that regulate cellular lipid stores. Biochim Biophys Acta Mol Cell Biol Lipids. 2009, 1791:419-40.
53. E. Griseti, A. A. Bello, E. Bieth, B. Sabbagh, J. S. Iacovoni, J. Bigay, H. Laurell, A. Čopič. Molecular mechanisms of perilipin protein function in lipid droplet metabolism. FEBS Lett. 2024, 598(10):1170-1198.
54. D. L. Brasaemle, B. Rubin, I. A. Harten, J. Gruia-Gray, A. R. Kimmel, C. Londos, Perilipin A increases triacylglycerol storage by decreasing the rate of triacylglycerol hydrolysis, J Biol Chem. 2000; 275:38486-93.

55. J. Tansey, C. Sztalryd, J. Gruia-Gray, D. Roush, J. Zee, O. Gavrilova, et al. Perilipin ablation results in a lean mouse with aberrant adipocyte lipolysis, enhanced leptin production, and resistance to diet-induced obesity. Proc Natl Acad Sci. 2001, 98:6494-9.
56. C. Sztalryd, D. L. Brasaemle. The perilipin family of lipid droplet proteins: Gatekeepers of intracellular lipolysis. Biochim Biophys Acta Mol Cell Biol Lipids. 2017, 1862(10 Pt B):1221-1232.
57. Y. Zhao, E. Albrecht, Z. Li, J. Schregel, Q. L. Sciascia, C. C. Metges, S. Maak. Distinct Roles of Perilipins in the Intramuscular Deposition of Lipids in Glutamine-Supplemented, Low-, and Normal-Birth-Weight Piglets. Frontiers in Veterinary Science. 2021, 8, 633898.
58. S. Kim, J. M.J. Swanson. The Surface and Hydration Properties of Lipid Droplets. Biophysical Journal. 2020, 119, 10, 1958-1969.
59. S.J. Peters, I.A. Samjoo, M.C. Devries, I. Stevic, H.A. Robertshaw, M.A. Tarnopolsky. Perilipin family (PLIN) proteins in human skeletal muscle: the effect of sex, obesity, and endurance training. Appl. Physiol. Nutr. Metab. 37. 2012, 724-735.
60. G. E. Miner, C. M. So, W. Edwards, J. V. Ragusa, J. T. Wine, D. Wong Gutierrez, M. V. Airola, L. E. Herring, R. A. Coleman, E. L. Klett, S. Cohen. PLIN5 interacts with FATP4 at membrane contact sites to promote lipid droplet-to-mitochondria fatty acid transport. Dev Cell. 2023, 58(14):1250-1265.e6.
61. A. Bezawork-Geleta, C. J. Devereux, S. N. Keenan, J. Lou, E. Cho, S. Nie, D. P. De Souza, V. K. Narayana, N. A. Siddall, C. H. M. Rodrigues, S. Portelli, T. Zheng, H. T. Nim, M. Ramialison, G. R. Hime, G. T. Dodd, E. Hinde, D. B. Ascher, D. A. Stroud, M. J. Watt. Proximity proteomics reveals a mechanism of fatty acid transfer at lipid droplet-mitochondria- endoplasmic reticulum contact sites. Nat Commun. 2025, 16, 2135.
62. B. D. Hodges, C. C. Wu. Proteomic insights into an expanded cellular role for cytoplasmic lipid droplets. J Lipid Res. 2010, 51:262-73.
63. M. A. Welte. Proteins under new management: lipid droplets deliver. Trends Cell Biol. 2007, 17:363-9.
64. W. Yu, J. Cassara, P.F. Weller. Phosphatidylinositide 3-kinase localizes to cytoplasmic lipid bodies in human polymorphonuclear leukocytes and other myeloid-derived cells. Blood. 2000, 95:1078-85.
65. W. Yu, P. T. Bozza, D. M. Tzizik, J. P. Gray, J. Cassara, A. M. Dvorak, et al. Co-compartmentalization of MAP kinases and cytosolic phospholipase A2 at cytoplasmic arachidonate-rich lipid bodies. Am J Pathol. 1998, 152:759.
66. T. V. Kurzchalia, R. G. Partan. Membrane microdomains and caveolae. Curr Opin Cell Biol. 1999, 11:424-31.
67. T. Fujimoto, H. Kogo, K. Ishiguro, K. Tauchi, R. Nomura. Caveolin-2 is targeted to lipid droplets, a new “membrane domain” in the cell. J Cell Biol. 2001, 152:1079-86.

68. G. van Meer. Caveolin, cholesterol, and lipid droplets? J Cell Biol. 2001, 152:F29-34.
69. J. K. Zehmer, Y. Huang, G. Peng, J. Pu, R. G. Anderson, P. Liu. A role for lipid droplets in inter-membrane lipid traffic. Proteomics. 2009, 9:914-21.
70. V. T. Salo. Seipin, still a mysterious protein? Front. Cell Dev. Biol., 03. 2023.
71. Y. Jin., Y. Tan, J. Wu, Z. Ren. Lipid droplets: a cellular organelle vital in cancer cells. Cell Death Discoverv. 9, 254. 2023.
72. K.M. Szymanski, D. Binns, R. Bartz, N. V. Grishin, W. P. Li, A. K. Agarwal, A. Garg, R. G. Anderson, J. M. Goodman. The lipodystrophy protein seipin is found at endoplasmic reticulum lipid droplet junctions and is important for droplet morphology. Proc Natl Acad Sci U S A. 2007, 104:20890-20895.
73. S. K. Tiwari, S. Bhat, & K. K. Mahato. Design and Fabrication of Low-cost Microfluidic Channel for Biomedical Application. Sci Rep, 2020. 10, 9215.
74. W. Fei, H. Wang, X. Fu, C. Bielby, H. Yang. Conditions of endoplasmic reticulum stress stimulate lipid droplet formation in Saccharomyces cerevisiae. Biochem J. 2009, 424:61-67.
75. N. Krahmer, M. Hilger, N. Kory, F. Wilfling, G. Stoehr, M. Mann, R. V. Farese Jr., T. C. Walther. Protein correlation profiles identify lipid droplet proteins with high confidence. Mol Cell Proteomics. 2013, 12:1115-1126.
76. E. Herker, M. Ott. Unique ties between hepatitis C virus replication and intracellular lipids. Trends Endocrinol Metab. 2011, 22:241-248.
77. A. D. Barbosa, H. Sembongi, W. M. Su, S. Abreu, F. Reggiori, G. M. Carman, S. Siniossoglou, Lipid partitioning at the nuclear envelope controls membrane biogenesis, Mol. Biol. Cell 26. 2015, 3641-3657.
78. H. Senoo, N. Kojima, M. Sato. Vitamin A-storing cells (stellate cells), Vitam. Horm. 75. 2007, 131-159.
79. E. Chang, Y. Kim. Vitamin D decreases adipocyte lipid storage and increases NAD-SIRT1 pathway in 3T3-L1 adipocytes. Nutrition. Volume 32, Issue 6. 2016, 702-708.
80. R. T. Brookheart, C. I. Michel, J. E. Schaffer. As a matter of fat. Cell Metab. 2009, 10, 1, 9-12.
81. C. P. Najt, M. Devarajan, D. G. Mashek. Perilipins at a glance. J Cell Sci. 2022, 135, 5, jcs259501.
82. W. M. Henne, M. L. Reese, J. M. Goodman. The assembly of lipid droplets and their roles in challenged cells. The EMBO Journal. 2018, 37, 12, e98947.
83. L. Scorrano, M. A. De Matteis, S. Emr, F. Giordano, G. Hajnóczky, B. Kornmann, L. L. Lackner, T. P. Levine, L. Pellegrini, K. Reinisch, R. Rizzuto, T. Simmen, H. Stenmark, C. Ungermann, M. Schuldiner. Coming together to define membrane contact sites. Nat Commun 10, 1287, 2019.

84. J. Magre, M. Delepine, E. Khallouf, T. Gedde-Dahl Jr., L. Van Maldergem, E. Sobel, J. Papp, M. Meier, A. Megarbane, A. Bachy, A. Verloes, F.H. d'Abronzo, E. Seemanova, R. Assan, N. Baudic, C. Bourut, P. Czernichow, F. Huet, F. Grigorescu, M. de Kerdanet, D. Lacombe, P. Labrune, M. Lanza, H. Loret, F. Matsuda, J. Navarro, A. Nivelon-Chevalier, M. Polak, J.J. Robert, P. Tric, N. Tubiana-Rufi, C. Vigouroux, J. Weissenbach, S. Savasta, J.A. Maassen, O. Trygstad, P. Bogalho, P. Freitas, J.L. Medina, F. Bonnicci, B.I. Joffe, G. Loyson, V.R. Panz, F.J. Raal, S. O'Rahilly, T. Stephenson, C.R. Kahn, M. Lathrop, J. Capeau, B.W. Group, Identification of the gene altered in Berardinelli-Seip congenital lipodystrophy on chromosome 11q13, Nat. Genet. 28. 2001, 365-370.
85. C. Wang, Y. Zhao, X. Gao, L. Li, Y. Yuan, F. Liu, L. Zhang, J. Wu, P. Hu, X. Zhang, Y. Gu, Y. Xu, Z. Wang, Z. Li, H. Zhang, J. Ye, Perilipin 5 improves hepatic lipotoxicity by inhibiting lipolysis, Hepatology 61. 2015, 870-882.
86. N.E. Wolins, B.K. Quaynor, J.R. Skinner, A. Tzekov, M.A. Croce, M.C. Gropler, V. Varma, A. Yao-Borengasser, N. Rasouli, P.A. Kern, B.N. Finck, P.E. Bickel. OXPAT/PAT-1 is a PPAR-induced lipid droplet protein that promotes fatty acid utilization, Diabetes 55. 2006, 3418-3428.
87. H. Hariri, S. Rogers, R. Ugrankar, Y. L. Liu, J. R. Feathers, W. M. Henne. Insights into ER-lipid droplet tethering. Journal of Cell Biology. 2019, 218, 4, 1089-1100.
88. M. Bohnert. Tether Me, Tether Me Not: Dynamic Organelle Contact Sites in Metabolic Rewiring. Developmental Cell 54, 2020. 212-225.
89. V. Choudhary and R. Schneiter. A unique junctional interface at contact sites between the endoplasmic reticulum and lipid droplets. Frontiers in cell and developmental biology. 2021, vol. 9, p. 650186.
90. E. Quon and C. T. Beh. Membrane contact sites: complex zones for membrane association and lipid exchange. Lipid Insights.2015, vol. 8, pp. LPI-S37190.
91. H. Wang, M. Becuwe, B.E. Housden, C. Chitraju, A.J. Porras, M.M. Graham, X.N. Liu, A.R. Thiam, D.B. Savage, A.K. Agarwal, A. Garg, M.J. Olarte, Q. Lin, F. Frohlich, H.K. Hannibal-Bach, S. Upadhyayula, N. Perrimon, T. Kirchhausen, C.S. Ejsing, T.C. Walther, R.V. Farese, Seipin is required for converting nascent to mature lipid droplets, elife 5 (2016).
92. F. Wilfling, H. Wang, J.T. Haas, N. Krahmer, T.J. Gould, A. Uchida, J.X. Cheng, M. Graham, R. Christiano, F. Frohlich, X. Liu, K.K. Buhman, R.A. Coleman, J. Bewersdorf, R.V. Farese Jr., T.C. Walther, Triacylglycerol synthesis enzymes mediate lipid droplet growth by relocalizing from the ER to lipid droplets. Dev. Cell 24, 2013, 384-399.
93. Y. Ohsaki, J. Cheng, M. Suzuki, A. Fujita, T. Fujimoto. Lipid droplets are arrested in the ER membrane by tight binding of lipidated apolipoprotein B-100, J. Cell Sci. 121, 2008, 2415-2422.

94. D. Binns, T. Januszewski, Y. Chen, J. Hill, V.S. Markin, Y. Zhao, C. Gilpin, K.D. Chapman, R.G. Anderson, J.M. Goodman. An intimate collaboration between peroxisomes and lipid bodies, J. Cell Biol. 173, 2006, 719-731.
95. D. Lumaquin, E. Johns, E. Montal, J. M. Weiss, D. Ola, A. Abuhashem, R. M. White. An in vivo reporter for tracking lipid droplet dynamics in transparent zebrafish. Elife. 2021, 10, e64744.
96. S. A. Gandhi, S. Parveen, M. Alduhailan, R. Tripathi, N. Junedi, M. Saqallah, M. A. Sanders, P. M. Hoffmann, K. Truex, J. G. Granneman, C. V. Kelly. Methods for making and observing model lipid droplets. Cell Rep Methods. 2024, 20, 4, 5, 100774.
97. E. Fernandes, V. F. Cardoso, S. Lanceros-Méndez, M. Lúcio. Lipid Microfluidic Biomimetic Models for Drug Screening: A Comprehensive Review. Advanced Functional Materials. 2024, 34, 315166.
98. B. G. Segars, M. Makhoul-Mansour, J. Beyrouthy, E. C. Freeman. Measuring the Transmembrane Registration of Lipid Domains in Droplet Interface Bilayers through Tensiometry. American Chemical Society. 2024, 40, 21, 11228-11238.
99. P. Zhao, Z. Zhao, Z. Yu, L. Chen, Y. Jin, J. Wu, Z. Ren. Application of synthetic lipid droplets in metabolic diseases. Clin Transl Med. 2023, 13(11):e1441.
100. J. A. Julien, A. L. Pellett, S. S. Shah, N. J. Wittenberg, K. J. Glover. Preparation and characterization of neutrally-buoyant oleosin-rich synthetic lipid droplets. Biochimica et Biophysica acta. Biomembranes. 2021, 1863(8):183624.
101. E. Ntone, B. Rosenbaum, S. Sridharan, S. B. J. Willems, O. A. Moultos, T. J. H. Vlugt, M. B. J. Meinders, L. M. C. Sagis, J. H. Bitter, C. V. Nikiforidis. The dilatable membrane of oleosomes (lipid droplets) allows their in vitro resizing and triggered release of lipids. Soft Matter. 2023, 23;19(33):6355-6367.
102. S. Tamilvanan. Oil-in-water lipid emulsions: implications for parenteral and ocular delivering systems. Progress in Lipid Research. 2004, 43, 6, 489-533.
103. A. Chorlay, A. Santinho, A. R. Thiam. Making Droplet-Embedded Vesicles to Model Cellular Lipid Droplets, STAR Protocols. Volume 1, Issue 3, 2020, 100116.
104. A. Chorlay, A. R. Thiam. An Asymmetry in Monolayer Tension Regulates Lipid Droplet Budding Direction. Biophysical Journal. 2018, 114, 3, 631-640.
105. D. Onan, M. Özder, M. I. Sipahi, N. Poyraz, C. Apaydın, G. Erel-Akbaba, H. Akbaba. Microfluidics Based Particle and Droplet Generation for Gene and Drug Delivery Approaches. J Biomed Mater Res B Appl Biomater. 2025, 113, 2, e35530.
106. S. K. Tiwari, S. Bhat, & K. K. Mahato. Design and Fabrication of Low-cost Microfluidic Channel for Biomedical Application. Sci Rep, 2020. 10, 9215.

107. H. N. Joensson. Microfluidics: Revolutionizing Science through Miniaturization. Pharm. Bioprocess. 2023. 11(6).
108. T. Trantidou, M. S. Friddin, A. Salehi-Reyhani, O. Ces, and Y. Elani. Droplet microfluidics for the construction of compartmentalised model membranes. Lab Chip. 2018, 18, 17, 2488-2509.
109. P. Mruetusatorn, J. B. Boreyko, G. A. Venkatesan, S. A. Sarles, D. G. Hayes, C. P. Collier. Dynamic morphologies of microscale droplet interface bilayers. Soft Matter. 2014, 10, 2530-2538.
110. S. Damiati, U. B. Kompella, S. A. Damiati, R. Kodzius. Microfluidic Devices for Drug Delivery Systems and Drug Screening. Genes (Basel). 2018, 16, 9, 2, 103.
111. Z. Hayat and A. E. Abed. Microfluidic Based Fast and Dynamic Droplet Interface Bilayer System (DIBS). Biomedical, Journal of Scientific & Technical Research. 2019, 21,1, 15611-15619.
112. S. Bachler, D. Haidas, M. Ort, T. M. Duncombe, P. S. Dittrich. Microfluidic platform enables tailored translocation and reaction cascades in nanoliter droplet networks. Commun Biol 3. 2020, 769.
113. J. N. Israelachvili, Intermolecular and surface forces. Academic press, 2011.
114. H. Martinez-Seara, T. Róg, M. Pasenkiewicz-Gierula, I. Vattulainen, M. Karttunen, R. Reigada. Interplay of unsaturated phospholipids and cholesterol in membranes: effect of the double-bond position. Biophys J. 2008, 95, 7, 3295-305.
115. S. Ballweg, E. Sezgin, M. Doktorova, R. Covino, J. Reinhard, D. Wunnicke, I. Hänelt, I. Levental, G. Hummer, R. Ernst. Regulation of lipid saturation without sensing membrane fluidity. Nat Commun. 2020, 11, 756.
116. S. Kim, G. A. Voth. Physical Characterization of Triolein and Implications for Its Role in Lipid Droplet Biogenesis. J Phys Chem B. 2021, 125, 25, 6874 - 6888.
117. Avanti Polar Lipids, Inc. Available online: https://avantilipids.com/.
118. B. Qiu, M. C. Simon. BODIPY 493/503 Staining of Neutral Lipid Droplets for Microscopy and Quantification by Flow Cytometry. Bio Protoc. 2016, 6, 17, e1912.
119. S. Asfia, R. Seemann, J.B. Fleury. Phospholipids diffusion on the surface of model lipid droplets. BBA - Biomembranes 1865, 2023, 184074.
120. J. L. Robeson, R. D. Tilton. Effect of concentration quenching on fluorescence recovery after photobleaching measurements. Biophys J. 1995, 68, 5, 2145-55.
121. L. Caillon, V. Nieto, P. Gehan, M. Omrane, N. Rodriguez, L. Monticelli, A.R. Thiam. Triacylglycerols sequester monotopic membrane proteins to lipid droplets, Nature Commun. 2020, 11, 1, 3944.

122. H. Bayley, B. Cronin, A. Heron, M.A. Holden, W.L. Hwang, R. Syeda, J. Thompson, M. Wallace. Droplet interface bilayers, Mol. BioSyst. 2008, 4, 12, 1191-1208.
123. S. Puza, S. Caesar, C. Poojari, M. Jung, R. Seemann, J.S. Hub, B. Schrul, J.-B. Fleury. Lipid Droplets Embedded in a Model Cell Membrane Create a Phospholipid Diffusion Barrier, Small. 2022, 18, 12, , e2106524.
124. K. Ben M'barek, D. Ajjaji, A. Chorlay, S. Vanni, L. Forêt, A.R. Thiam. ER Membrane Phospholipids and Surface Tension Control Cellular Lipid Droplet Formation, Dev. Cell. 2017, 41, 6, 591-604, e7.
125. J. M. Andreas, E. A. Hauser, W. B. Tucker, W. B. Boundary Tension by Pendant Drops. Journal of Physical Chemistry. 1938, 42, 8, 1001-1019.
126. J. D. Berry, M. J. Neeson, R. R. Dagastine, D. Y. Chan, R. F. Tabor. Measurement of surface and interfacial tension using pendant drop tensiometry. Journal of Colloid and Interface Science. 2015, 454, 226-237.
127. Y. Rotenberg, L. Boruvka, A. W. Neumann. Determination of surface tension and contact angle from the shapes of axisymmetric fluid interfaces. Journal of Colloid and Interface Science. 1983, 93, 1, 169-183.
128. J. D. Berry, M. J. Neeson, R. R. Dagastine, D. Y. C. Chan, R. F. Tabor. Measurement of surface and interfacial tension using pendant drop tensiometry. Journal of Colloid and Interface Science. 2015, 454, 226-237.
129. A. W. Adamson, A. P. Gast. Physical Chemistry of Surfaces (6th ed.). Wiley-Interscience. 1997.
130. J. Drelich, C. Fang, C. L. White. Measurement of interfacial tension in fluid-fluid systems. Encyclopedia of Surface and Colloid Science. 2002, 3, 3157-3163.
131. M. Kang, C. A. Day, A. K. Kenworthy, & E. DiBenedetto, E. Simplified equation to extract diffusion coefficients from confocal FRAP data. Traffic. 2012, 13, 12, 1589-1600.
132. Y. Li, P. Khanal, F. Norheim, M. Hjorth, T. Bjellaas, C.A. Drevon, J. Vaage, A.R. Kimmel, K.T. Dalen. Plin2 deletion increases cholesteryl ester lipid droplet content and disturbs cholesterol balance in adrenal cortex, J. Lipid Res.2021, 62, 100048.
133. K. Hsieh, Y.K. Lee, C. Londos, B.M. Raaka, K.T. Dalen, A.R. Kimmel. Perilipin family members preferentially sequester to either triacylglycerol-specific or cholesteryl-ester-specific intracellular lipid storage droplets, J. Cell Sci. 2012, 125, 17, 4067-4076.
134. S. Xu, X. Zhang, P. Liu, Lipid droplet proteins and metabolic diseases, Biochim. Biophys. Acta (BBA) - Mol. Basis Dis. 2018, 1864, 5, Part B, 1968-1983.
135. A. Chorlay, L. Monticelli, J.V. Ferreira, K.B. M'barek, D. Ajjaji, S. Wang, E. Johnson, R. Beck, M. Omrane, M. Beller, P. Carvalho, A.R. Thiam. Membrane Asymmetry Imposes Directionality on Lipid Droplet Emergence from the ER, Dev. Cell. 2019, 50, 1, 25-42.e7.

136. R. B. Gennis. Biomembranes: Molecular Structure and Function. Springer Advanced texts in Chemistry. 2013, Chapter 1.
137. R. Macháň and M. Hof. Lipid diffusion in planar membranes investigated by fluorescence correlation spectroscopy. Biochimica et Biophysica Acta (BBA) - Biomembranes. 2010, 1808, 7, 1377-1391.
138. V. Zoni, V. Nieto, L. J. Endter, H. J. Risselada, L. Monticelli, S. Vanni. To Bud or Not to Bud: A Perspective on Molecular Simulations of Lipid Droplet Budding. Front. Mol. Biosci. 2019, 6, 124.
139. V. Zoni, R. Khaddaj, P. Campomanes, A. R. Thiam, R. Schneiter, S. Vanni. Pre-existing bilayer stresses modulate triglyceride accumulation in the ER versus lipid droplets. eLife 2021, 10, e62886.
140. C. M. Fader Kaiser, P. S. Romano, M. C. Vanrell, C. A. Pocognoni, J. Jacob, B. Caruso, L. R. Delgui. Biogenesis and Breakdown of Lipid Droplets in Pathological Conditions. Front. Cell Dev. Biol. 2022, 9, 3870.

8. List of Publications

(I) **Shima Asfia**, Ralf Seemann, Jean-Baptiste Fleury. Phospholipids diffusion on the surface of model lipid droplets. BBA - Biomembranes 1865, 2023, 184074.

(II) Sevde Puza, **Shima Asfia**, Ralf Seemann and Jean-Baptiste Fleury. Bilayer-Embedded Lipid Droplets Coated with Perilipin-2 Display a Pancake Shape. Int. J. Mol. Sci. 2023, 24, 2072.

(III) Mahsa Mohammadian‡, **Shima Asfia**‡, Ralf Seemann. Influence of PLIN5 and Lipid Composition on Lipid Droplet Contact Sites with other Organelles (‡ Authors contributed equally).

(IV) Vahideh Sardari, Mahsa Mohammadian, **Shima Asfia**, Felix Maurer, Diana Or̈um, Ralf Seemann, Thomas John, Lars Kaestner, Christian Wagner, Maniya Malekia, Alexis Darras. Deposit of Red Blood Cells at low concentrations in evaporating droplets is dominated by a central edge growth. Journal of Colloid and Interface Science. 2024, 679, Part A, 939-946.

Appendices

Appendix (I) Phospholipids diffusion on the surface of model lipid droplets

Authors: Shima Asfia, Ralf Seemann, Jean-Baptiste Fleury

Experimental Physics, Saarland University, 66123 Saarbrücken, Germany

https://doi.org/10.1016/j.bbamem.2022.184074

Author contributions:

Fabrication of microfluidic device, running the experiments, and interpreting the analysis wereconducted by S. Asfia. The paper was written by S. Asfia, R. Seemann, and J.B. Fleury. The research was directed by R. Seemann.

Abstract:

Lipid droplets (LD) are organelles localized in the membrane of the Endoplasmic Reticulum (ER) that play an important role in metabolic functions. They consist of a core of neutral lipids surrounded by a monolayer of phospholipids and proteins resembling an oil-in-water emulsion droplet. Many studies have focused on the biophysical properties of these LDs. However, despite numerous efforts, we are lacking information on the mobility of phospholipids on the LDs surface, although they may play a key role in the protein distribution. In this article, we developed a microfluidic setup that allows the formation of a triolein-buffer interface decorated with a phospholipid monolayer. Using this setup, we measured the motility of phospholipid molecules by performing Fluorescent Recovery After Photobleaching (FRAP) experiments for different lipidic compositions. The results of the FRAP measurements reveal that the motility of phospholipids is controlled by the monolayer packing decorating the interface.

BBA - Biomembranes 1865 (2023) 184074

Contents lists available at ScienceDirect

BBA - Biomembranes

journal homepage: www.elsevier.com/locate/bbamem

Phospholipids diffusion on the surface of model lipid droplets

Shima Asfia, Ralf Seemann, Jean-Baptiste Fleury *

Universität des Saarlandes, Experimental Physics and Center for Biophysics, 66123 Saarbrücken, Germany

ARTICLE INFO

Keywords:
Phospholipid
Lipid droplet
Diffusion
FRAP

ABSTRACT

Lipid droplets (LD) are organelles localized in the membrane of the Endoplasmic Reticulum (ER) that play an important role in metabolic functions. They consist of a core of neutral lipids surrounded by a monolayer of phosphoplipids and proteins resembling an oil-in-water emulsion droplet. Many studies have focused on the biophysical properties of these LDs. However, despite numerous efforts, we are lacking information on the mobility of phospholipids on the LDs surface, although they may play a key role in the protein distribution. In this article, we developed a microfluidic setup that allows the formation of a triolein–buffer interface decorated with a phospholipid monolayer. Using this setup, we measured the motility of phospholipid molecules by performing Fluorescent Recovery After Photobleaching (FRAP) experiments for different lipidic compositions. The results of the FRAP measurements reveal that the motility of phospholipids is controlled by the monolayer packing decorating the interface.

1. Introduction

Lipid droplets are organelles present in the Endoplasmic Reticulum (ER) membrane [1,2]. They attract many interest due to their role in several diseases like cancer and metabolic problems [3–5]. One of their functions is to store lipids and to regulate their consumption based on mechanisms that are not yet understood [6]. Lipid droplets (LDs) are composed of a core of neutral lipids and are surrounded by a phospholipid monolayer [7,8]. Their biogenesis is assumed to occur in three consecutive steps [2,9]. First, neutral lipids are synthesized in the ER membrane. Then, they accumulate and segregate into the ER bilayer core and form a lenticular droplet [2,10,11]. And finally, they grow through the accumulation of lipids until budding and sometimes pinch-off from the ER membrane [2,12–15]. Many of the biophysical properties of LDs have been investigated over the last decade using model systems [6]. As example, droplet interface bilayers (DiB), advanced free-standing bilayer (AFB), and giant unilamellar vesicles (GUVs) have been extensively used to reconstitute artificial and natural LDs in such lipid membranes [16–21]. After successful reconstitution of LDs in a bilayer, the morphology of LDs was studied as function of the phospholipidic composition of the DiBs, GUVs or AFB systems [18–20]. It has been shown that the shape of LDs in a bilayer is determined by the balance of surface forces at the contact line between the embedded-LDs and the bilayer [18–20]. Thus, the associated contact angle of LDs can be predicted using wetting theory [11,22]. Accordingly, numerical simulations based on continuum models were able to confirm many experimental results obtained on microscopic LDs [15,18,23–27].

In addition to the equilibrium shape determined by a force balance, non-equilibrium phenomena related to LDs have also attracted attention in recent years. A key example is protein partitioning, which is used to understand the dynamic distribution of specific proteins between the monolayer covering the LD and the bilayer in which the LDs are embedded [6,16]. Indeed, protein partitioning seems highly dependent of the physical properties of the lipid monolayer (packing, fluidity) that surrounds the LD surface [17,18]. However, to the best of our knowledge, there are no experimental measurements on phospholipid properties such as motility at the LD surface. One reason for this lack of knowledge could be the small size of the reconstituted LDs in the artificial systems (DiB, AFB, GUVs), which make FRAP experiments and extraction of precise diffusion coefficients challenging [17,28]. As a consequence, there are only a few experimental studies in the literature that address diffusion [24]. Interestingly, this fact is not limited to experimental studies but also occurs in theoretical studies with numerical simulations [18,25,29].

In this article, we experimentally investigate the motility of phospholipids covering the interface between an aqueous and an oily phase. For this purpose, we have developed a microfluidic setup that enables the formation of a triolein–buffer interface decorated with phospholipids and have performed FRAP experiments directly at this interface (Fig. 1). Here, the planar phospholipid monolayer at the triolein–buffer interface mimicks the surface of a LD. We used triolein as neutral lipid because it is an important component of the biological LD [5] and varied the molecular composition of the monolayer to

* Corresponding author.
E-mail address: jean-baptiste.fleury@physik.uni-saarland.de (J.-B. Fleury).

https://doi.org/10.1016/j.bbamem.2022.184074
Received 1 July 2022; Received in revised form 13 October 2022; Accepted 15 October 2022
Available online 23 October 2022

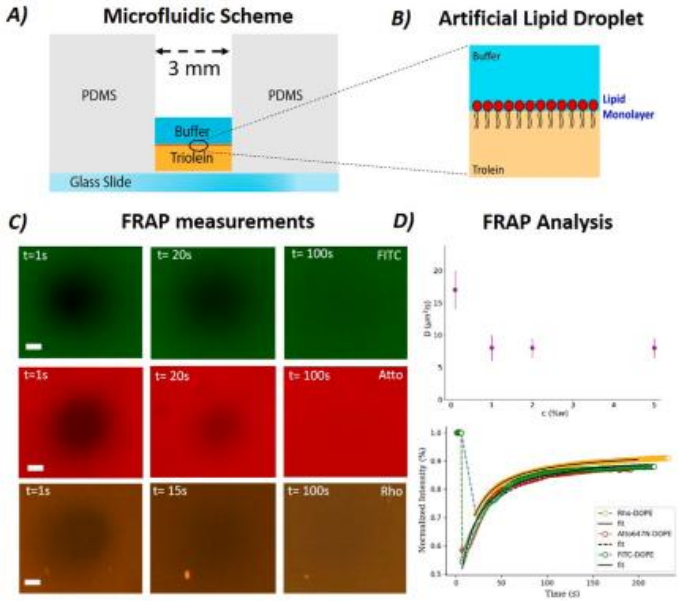

Fig. 1. (A) Sketch of the microfluidic device. (B) Schematic of the phospholipid decorated triolein–buffer interface. (C) Examples of FRAP measurements on a pure DOPE bilayer with FITC-DOPE (top), Atto647N-DOPE (middle) and Rho-DOPE (bottom). The time $t = 0$ corresponds to the moment when the bleaching was stopped. The length bar denotes 50 μm and corresponds to the radius of the bleached area. (D) Upper panel: Measured diffusion constant for a pure DOPE monolayer with 2% Atto647N-DOPE (in molar ratio) for different phospholipid concentration (expressed in weight ratio). Bottom panel: Experimental intensity data, as obtained from a FRAP measurement plotted together with the Soumpasis equation fitted to these data (dashed line); orange dots represent Rho-DOPE, red dots represent Atto647N-DOPE and orange dots represent FITC-DOPE [32]. Fits correspond to continuous and dashed dark lines (and all fits yield $D \approx 17\ \mu m^2\ m^{-1}$).

Table 1
Table summarizing the measured surface tensions γ and diffusion constants D for triolein–buffer interfaces decorated with monolayers made of a single lipidic component. More results including lipid mixtures are available in the plots shown in Figs. 2–4.

Lipids	DOPC	DOPE	POPC	DPPC	DSPA	SM
γ (m N/m)	1.5 ± 0.3	2.3 ± 0.3	1.3 ± 0.3	1.1 ± 0.3	2.6 ± 0.3	1.2 ± 0.3
D ($\mu m^2/s$)	8.2 ± 1	17.1 ± 1.6	7 ± 1	6 ± 0.6	20.1 ± 1.8	8.1 ± 0.9

assess the influence of the most common molecules that make up the LD surface in living cells. These molecules are mainly phospholipids and cholesterol. Because native biological LDs may contain cholesterol ester [30,31], we also investigated the influence of LD-core composition on phospholipid motility by adding some cholesterol ester (chol-ester) to the neutral lipid (triolein). Our measurements show that the motility of amphiphilic lipids is directly influenced by the packing of these molecules coating the interface.

2. Results and discussion

Liquid droplets (LDs) originate in the ER membrane, and the phospholipid monolayer that decorates LDs is therefore composed mainly of phospholipids, sterols and proteins [33–37], with phospholipids making up the vast majority and proteins and sterols being present in only a small percentage. The decorating phospholipids can be distinguished in two families, saturated and unsaturated. Accordingly, we start our discussion with the most common lipids and presented the results sorted by lipid families: unsaturated phospholipids, saturated phospholipids, and sterols.

Unsaturated phospholipids: DOPC, DOPE, N-DOPE, POPC, LPC. A relevant biophysical composition for a phospholipid monolayer covering LDs localized in the ER membrane can be approximated by a DOPC/DOPE mixture with a molar ratio between 1:1 and 3:1 [7,8,17,18]. For completeness, we vary the composition from pure DOPC to a pure DOPE monolayer. The extracted diffusion constants are presented in Fig. 2 and Table 1. The diffusion constant of a pure DOPC monolayer is $D \approx 8\ \mu m^2\ s^{-1}$, i.e. close to, or slightly lower than, the DOPC fluidity observed in giant vesicles [37] and in free-standing bilayer [28]. For increasing DOPE content, the fluidity monotonically increases reaching $D \approx 17\ \mu m^2\ s^{-1}$ for a pure DOPE monolayer.

To also compare the observed motility of a DOPE monolayer with that of a bilayer, bilayer motility was determined using a free-standing DOPE bilayer as described in [28]. The formed free-standing DOPE/DOPC bilayers (with a 1:1 molar ratio) were formed using a 3D microfluidic chip as described in detail in Ref. [28]. Interestingly, the diffusion constant determined by FRAP measurements on a free-standing DOPE/DOPC (1:1) bilayer with 2% DOPE-Atto647 (in molar ratio) reveals ≈11 $\mu m^2/s$, which is very close to the diffusion constant in giant vesicle (≈10 $\mu m^2/s$) but lower than that of a DOPE monolayer [38]. So in contrast to monolayer, no clear dependence on the bilayer motility was observed for different lipids.

The observed dependence of monolayer motility on the type of lipid can be easily understood considering the lipid packing that results from the geometry of these two molecules. DOPC can be approximated as a cylinder, while the shape of DOPE is closer to a truncated cone [39]. Assuming a cylindrical shape, the volume of a single phospholipid molecule can be approximated by the cross sectional area of its head a_0 and its tail length l, as $V_{DOPC} \approx l \cdot a_0$ for DOPC and $l \cdot \frac{1}{2} a_0 < V_{DOPE} < l \cdot a_0$ for DOPE. Thus, the corresponding critical packing parameter $\rho = V/a_0 \cdot l$ is $\rho_{DOPC} \approx 1$ for a monolayer consisting only of DOPC molecules and $0.5 < \rho_{DOPE} < 1$ for a monolayer consisting only of

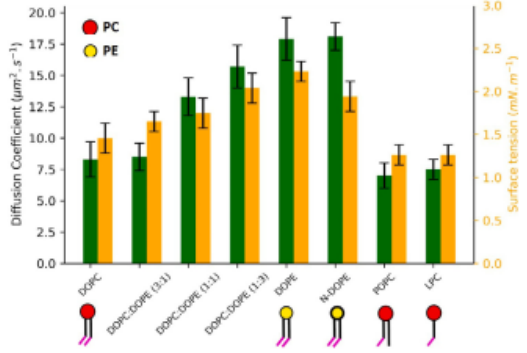

Fig. 2. FRAP experiments yielded diffusion constants D (green bars) and surface tension values (yellow bars) for several saturated phospholipids (DOPC, DOPE, N-DOPE, POPC, LPC) and mixtures of DOPC and DOPE at a triolein–buffer interface. Schematic representations of the various lipids are provide for PE (red head), PC (yellow head) where pink tails indicate one unsaturation.

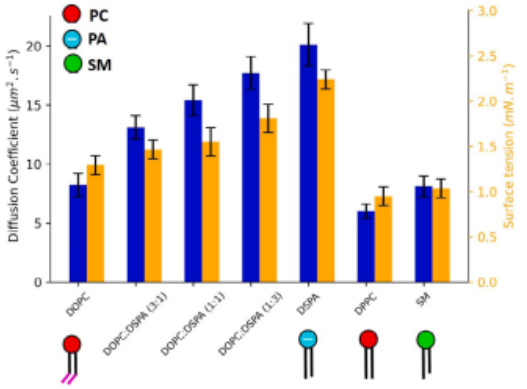

Fig. 3. From FRAP experiments, diffusion constants D (green bars) and surface tension values (yellow bars) for unsaturated phospholipids (DSPA, DPPC, and SM) and mixtures of DOPC and DSPA were extracted and compared to DOPC values. A schematic representation is provided for PC lipids (red head), SM (green head) and the charged PA (light blue head).

DOPE molecules [39]. For a flat interface, a DOPC monolayer obviously has a higher lipid packing than a DOPE monolayer. In consequence, at equivalent surface coverage, the average motility of a single DOPE molecule is larger than that of a single DOPC molecule. Accordingly, packing density and mobility of DOPC and DOPE mixtures interpolate between the limits of a pure DOPC and DOPE monolayer, respectively.

As the increased lipids density at the triolein–buffer interface lowers the surface tension, differences in surface coverage can also be confirmed by differences in surface tension measured by the pending drop method as $\gamma_{DOPC} \approx 1.5$ m N/m and $\gamma_{DOPE} \approx 2.3$ m N/m, for DOPC and DOPE, respectively. These surface tension values are consistent with expectations based on geometry dependent lipid packing and the experimentally observed lipid motility.

To confirm the influence of the lipid packing on lipid motility in a monolayer, we repeated the experiments described above with monolayers consisting of N-DOPE, POPC and LPC molecules. Compared to DOPE, has N-DOPE an additional methyl group in the PE head, thus this molecule is slightly less conical than DOPE but also less cylindrical than DOPC (Fig. 2). The measured diffusion constant for a pure N-DOPE monolayer is $D \approx 17.5\ \mu m^2\ s^{-1}$ and the corresponding surface tension is ≈ 2 m N/m. As expected from the N-DOPE geometry, are both diffusion constant and surface tension rather comparable to pure DOPE monolayer.

POPC has the same hydrophilic head as DOPC and the same length of the hydrophobic tail, but only one unsaturation in its tail [34,35]. Thus, due to this little difference, a POPC monolayer is expected to present a similar packing than a DOPC monolayer [27,33,40,41]. And consistently with the geometry of the molecules and the expected monolayer packing, we measured the diffusion constant and the surface tension of POPC as $D = 7\ \mu m^2\ s^{-1}$ and $\gamma \approx 1.3$ mN/m, that are very similar to those of a pure DOPC monolayer, see Fig. 2.

LPC is a single tail lipid with one unsaturation in its tail and an inverted conical geometry. The measured diffusion constant for a pure LPC monolayer is $D \approx 7\ \mu m^2\ s^{-1}$ and its surface tension is $\gamma \approx 1.3$ m N/m, see Fig. 2. Thus, this LPC appears to have a motility close to POPC and DOPC. This result is a little surprising, as *a priori*, we may have expected to measure a stronger difference between a monolayer composed of lipids with a single tail or a double tail. However, the correlation between low surface tension resembling high lipid packing and low lipid motility still holds true.

Saturated phospholipids (DPPC, DSPA) and sphingolipids (SM). The motility of unsaturated lipids that make up the majority of the lipids covering LDs [42] was explored in the previous section. In this section, we continue our study by exploring the motility of saturated phospholipids on the surface of model lipid droplets. Due to the absence of unsaturations, the packing of unsaturated (neutral) phospholipids may be expected to be denser than that of unsaturated phospholipids. Following our findings for unsaturated lipids, the corresponding motility of saturated lipids, like DPPC, is generally expected to be lower than that of DOPC. However, the degree of saturation is not the only interaction that controls the monolayer packing. As example, electrostatic interactions can also strongly influence the packing of lipid monolayers. For this reason, we also explored mixtures between saturated DSPA molecules having an negatively charged hydrophilic head group and uncharged and unsaturated DOPC molecules. In addition to saturated lipids, we also consider the case of sphingolipids (SM).

DPPC is a saturated lipid with a cylindrical shape that self-assembles in an highly packed monolayer [43]. The measured diffusion constant for a pure DPPC monolayer is $D \approx 5.5\ \mu m^2\ s^{-1}$, which is a little slower to that of unsaturated DOPC and POPC phospholipids, that are also expected to be densely packed (see, Fig. 3). The high DPPC packing at the triolein–buffer interface also coincides with a low surface tension, $\gamma \approx 1.1$ m N/m, which is also very similar to surface tension values for DOPC and POPC.

DSPA is a saturated double-tailed lipid with a head that is negatively charged with a conical shape. Due to electrostatic repulsion, the lipid packing of a pure PA monolayer is smaller than that of other lipids [44]. In addition to a large motility of $D \approx 20\ \mu m^2\ s^{-1}$ of a pure DSPA monolayer, the comparatively low packing density also leads to a comparatively large surface tension at the triolein–buffer interface, which was measured to be $\gamma \approx 2.6$ m N/m, see Table 1. Mixtures of DOPC and DSPA molecules show motilities intermediate between those of a pure DOPC and a pure DSPA monolayer. Presumably due to the repulsion of the charged DSPA molecules, the measured diffusion constants are already quite large at a DSPA content of 25% and increase even further with increasing DSPA content, see Fig. 3.

Sphingolipids are a family of lipids that are synthesized in the (ER) membrane, where they can be found in low amounts, as well as at the trans Golgi [45–47]. Due to the possible role of sphingolipids in the LD biogenesis, they have attracted a growing attention in recent years [45–47]. Sphingomyelin (SM) has a PC head with a fatty acid

group and a tail that has a single saturation in contact with the head. Thus, we study this lipids with other saturated lipids. SM molecule has a slightly conical geometry close to a cylindrical molecule. The relatively low diffusion constant of a pure SM monolayer of $D \approx 8\ \mu m^2\ s^{-1}$, and the corresponding low surface tension $\gamma \approx 1.2$ m N/m, Fig. 3, indicate that despite of the slightly conical shape of the SM, the associated lipid packing is dense, similar to an assembly of cylindrical molecules, in agreement with literature [39,48].

Sterol and sterol ester. Sterols like cholesterol (chol) and cholesteryl ester (chol ester) are also important components of LDs [7,8]. However, these molecules differ from previous lipids, as they are unable to form a lipid bilayer on their own. As example, chol ester is not a surface active molecule, it is a component of the LD core and not of the LD surface. Nevertheless, these sterols are important lipids and it is interesting to investigate their influence on the properties of phospholipid monolayers.

Cholesterol (Chol) is present in the ER membrane only in small amounts, namely below 6% percent. Nevertheless, Chol may play a role in metabolic diseases that are involving LDs [4,49]. Chol drastically alters the biophysical properties of the plasma membrane and thus, it is interesting to investigate the case of a lipid monolayer enriched with Chol. It is known that Chol increases both the bilayer tension and the bilayer fluidity, at least at low temperatures [50–52]. The measured surface tension for a DOPC monolayer with 10% Chol is ≈ 1.7 m N/m, while the surface tension of a DOPE monolayer with 10% Chol is ≈ 2.5 m N/m, i.e. the surface tension for both phospholipids are increased by about 10% compared to pure DOPC or DOPE monolayer, respectively, see Table 1. The observed increase in surface tension indicates a reduced packing density of lipids, which is expected to increase lipid diffusion. In fact, the measured diffusion constant for a DOPC monolayer with 10% Chol gives a value of $\approx 10\ \mu m^2\ s^{-1}$, while that of a DOPE monolayer with 10% Chol gives $\approx 20\ \mu m^2\ s^{-1}$, see Fig. 4, i.e. the diffusion constant also increased by about 10% compared to pure DOPC or DOPE monolayer. This suggests that the increase in surface tension and lipid diffusion is indeed due to decreased lipid packing.

Cholesteryl ester, a dietary lipid, is an ester of cholesterol found in LDs [53]. This molecule differs from the previous molecules in that it is not localized at the surface of LDs but it is only present in the LD core. This is interesting because cholesterol ester appears to affect the recruitment of some LD proteins when they enrich the LD composition [30,31]. The surface tension of a DOPC monolayer at the interface between triolein–buffer with 15% cholesteryl ester in triolein was measured to be $\gamma \approx 1.5$ m N/m, i.e. the same value as for triolein not containing cholesteryl ester. Similarly, we also measured the surface tension for a DOPE monolayer to be ≈2.3 m N/m no matter if the triolein contains 15% cholesteryl ester or not. The corresponding measured diffusion constant yields a value of $D \approx 8\ \mu m^2\ s^{-1}$ for a DOPC monolayer with 15% cholesteryl ester in triolein, and a diffusion constant $D \approx 17\ \mu m^2\ s^{-1}$ for DOPE monolayer with 15% cholesteryl ester in triolein, see Fig. 4. From this, we can conclude that cholesteryl ester molecules remain in the triolein phase and hardly change the surface properties of the lipid decorated triolein–buffer interface. Similarly, we observed no measurable change in the surface tension of the phospholipid-decorated triolein–buffer interface or in the corresponding diffusion constant compared to a pure DOPC or a pure DOPE monolayer, respectively (cf. Fig. 4).

3. Conclusion

We investigated the diffusion properties of lipids on the surface of model lipid droplets. For that, we produced a model lipid droplet interface made of a triolein–buffer interface in a microfluidic chamber that is decorated with a lipid monolayer of variable composition. FRAP experiments were conducted directly at this interface and the corresponding diffusion constants for the lipids were obtained as function of the molecular composition of the lipid monolayer. Based on geometrical (cylindrical, conical) and chemical (electrostatic charge, saturation) properties of the respective lipids, we argue that the lipid packing is the key parameter to understand the measured results. In this context, monolayers with high lipid packing have low lipid motility. And monolayers with low lipid packing have high lipid motility. This reasoning is supported by surface tension measurements as high lipid packing means low interfacial tension and low lipid packing means high interfacial tension. By extrapolation, this study provides an estimate of defect density on the LD surface for the lipids composition tested. This point is important because defects seem to play a key role in protein partitioning on LD surface [17].

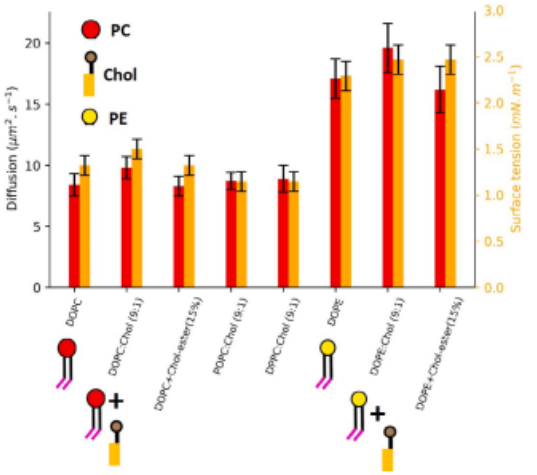

Fig. 4. Diffusion coefficients D (red bars) are derived from FRAP experiments and surface tension values (yellow bars) for cholesterol-containing DOPC, DOPE, POPC, and DPPC monolayers at the triolein–buffer interface, as well as DOPC and DOPE monolayers at the cholesterol-ester interface. Schematic representation is provide for cholesterol and DOPC.

4. Methods

Molecules. For the preparation of molecular monolayer that cover the model lipid droplets, i.e. the triolein–buffer interface, the following molecules were purchased from Avanti Polar Lipids: 1,2-dioleoyl-sn-glycero-3-phosphocholine (DOPC), 1,2-dioleoyl-sn-glycero-3-phosphoethanolamine (DOPE), 1,2-distearoyl-sn-glycero-3-phosphate (sodium salt) (DSPA), 1-palmitoyl-2-oleoyl-sn-glycero-3-phosphocholine (POPC), 1-(10Z-heptadecenoyl)-2-hydroxy-sn-glycero-3-phosphocholine (LPC), 1,2-dipalmitoyl-sn-glycero-3-phosphocholine (DPPC), 1,2-dioleoyl-sn-glycero-3-phosphoethanolamine-N-methyl (N-DOPE), cholesterol (Chol), N-stearoyl-D-erythro-sphingosylphosphorylcholine (SM), 1,2-dipalmitoyl-sn-glycero-3-phosphocholine (DPPC), Cholesteryl ester (Chol ester). Glyceryl trioleate (triolein) and squalene were purchased from Sigma-Aldrich. Recombinant human denatured perilipin 2 protein (PL2) was purchased from Abcam (ab181932). To allow for FRAP experiments, the following fluorescent labeled lipids were used: (FITC-DOPE) 1,2-dioleoyl-sn-glycerol-phosphoethanolamine Fluorescein purchased from ChemCruz (Santa Cruz Biotechnology), 1,2-dioleoyl-sn-glycero-3-phosphoethanolamine-N-(lissamine rhodamine B sulfonyl) (ammonium salt) (Rho-DOPE) purchased from Avanti Polar lipids, and 1,2-Dioleoyl-sn-glycero-3-phosphoethanolamine labeled with Atto 647N (Atto647N-DOPE) purchased from Sigma-Aldrich.

Interfacial tension measurements. The interfacial tension of phospholipid decorated triolein–buffer interfaces was determined by the pendant drop method using a contact angle measurement device OCA 20 (DataPhysics, Germany). For this method, a transparent cuvette is filled with the lower density fluid, here the triolein–phospholipid mixture (ρ_{oil} = 0.91 g/cm^3) and a pendant drop containing a defined volume of the denser fluid, here the buffer solution (ρ_{buffer} = 0.998 g/cm^3), is produced from a hollow needle immersed in this liquid. While gravity drags the droplet down, buoyancy and surface forces keep the droplet in place. Based on a contour fit to the pendant droplet, the software SCA 20 extracts both size and shape of the droplet and automatically computes the corresponding interfacial tension. This procedure is most reliable when the droplet size is close to detachment from the needle, and we thus set the droplet volume to (2.0 ± 0.5) µl.

µ*Chip fabrication and monolayer formation.* Using computer software (Autocad), we created a drawing in the form of a cylinder with 3 mm diameter, which was produced using a 3D printer. This cylinder was positioned in the center of a glass Petri dish. After setting up the mold, mixed and degassed PDMS (Sylgard 184 – Dow Corning) was poured onto the mold with a resulting layer thickness of about 3 mm so that the cylinder is not fully immersed in the PDMS. After curing the PDMS at 60 °C for 6–7 h, the cylinder was removed and square pieces with the cylindrical hole in the center were cut from the PDMS and removed from the Petri dish. The final device was fabricated by attaching the square PDMS piece to a PDMS coated glass cover slip (Sylgard 184 spin coated for 5 min at 3000 rpm) using plasma bonding (Diener electronics). The thus fabricated device was placed on a hot plate at 60 °C for 1 h to achieve higher bonding strength.

To produce the triolein–lipid mixture, a specific amount of lipid was dissolved in Ethanol. This solution was then dried under vacuum. Triolein was added to the dried components and mixed in an ultrasonic bath. The resulting phospholipid concentration in triolein is always equal to 2% w/w, which is above the critical concentration needed to form stable droplet interface bilayers in triacylglycerol oil [17,54]. A 2% molar ratio of FITC-DOPE as a fluorescent probe. Such concentrations are typically employed for the production of stable artificial lipid droplets in literature [18,55].

To form a monolayer, 6 µl of the as-prepared triolein–lipid mixture was first placed in the cylindrical opening of the PDMS micro chip, and then 20 µl of 150 M KCl buffer was added on top. Within seconds, a phospholipid monolayer forms at the triolein–buffer interface, with a composition similar to the lipid composition of the originally prepared triolein solution.

FRAP experiments. Confocal images were acquired with an inverted microscope (Nikon Ti-Eclipse) with an Intensilight Epi-fluorescence light source and a laser unit (LU-NV, Nikon). The confocal microscope was equipped with a Yokogawa spinning disk head (CSU-W1; Andor Technology) and a fluorescence recovery after photo-bleaching module (FRAPPA; Andor Technology). Confocal imaging was conducted using excitation wavelengths of 481 nm (for FITC-DOPE 495/515) and 561 nm (for Rho-DOPE 560/583, Atto647-DOPE 643/665). The used emission filters have the wavelengths/bandwidths of 525/30 nm, 607/36 nm and 685/40 nm, respectively. For the FRAP experiments, a pinhole size of 50 µm was used with 40× oil objective having a working distance of 220 µm. Prior to bleaching, a circular stimulation area with diameter ranging between 5 and 50 micrometer was selected inside the bilayer (to increase measurements quality). Prior to a FRAP measurement, fluorescence imaging was performed for 20 s for each individual experiment. Then, bleaching was performed by increasing the laser power on the stimulation area to the maximum laser power for 20 s (70 mW for 481 and 561 nm, 125 mW for 647 nm) including 10 loops that were repeated for three times. During the recovery, image acquisition was continued for at least 5 min to be able to observe all the changes after recovery. Then, the obtained fluorescence recovery (FRAP) data are directly fitted with the Soupmasis equation using Python. All the experiments were performed at room temperature of 23 °C.

Interestingly, similar FRAP curves (and identical bleached area) and fits were obtained for three types of dyes on a pure DOPE monolayer: FITC-DOPE, Rho-DOPE and Atto647-DOPE (see Fig. 1). A notable difference between these dyes is that Rho-DOPE appeared more difficult to bleach than Atto647N-DOPE or FITC-DOPE.

CRediT authorship contribution statement

Shima Asfia: Performed the experiments, Analyzed the data, Writing – original draft. **Ralf Seemann:** Writing – original draft. **Jean-Baptiste Fleury:** Designed the experimental setup and the research, Writing – original draft.

Declaration of competing interest

The authors declare that they have no known competing financial interests or personal relationships that could have appeared to influence the work reported in this paper.

Data availability

The datasets generated during and/or analyzed during the current study are available from the corresponding author on reasonable request.

Acknowledgments

Financial support is acknowledged by the Deutsche Forschungsgemeinschaft (DFG), Germany, SFB1027 (project B4).

Appendix A. Supplementary data

Supplementary material related to this article can be found online at https://doi.org/10.1016/j.bbamem.2022.184074.

References

[1] Y. Guo, K.R. Cordes, R.V. Farese, T.C. Walther, Lipid droplets at a glance, J. Cell Sci. 122 (6) (2009) 749–752, http://dx.doi.org/10.1242/jcs.037630, Publisher: The Company of Biologists Ltd Section: Cell Science at a Glance. URL https://jcs.biologists.org/content/122/6/749.

[2] T.C. Walther, J. Chung, R.V. Farese, Lipid Droplet Biogenesis, Annu. Rev. Cell Dev. Biol. 33 (1) (2017) 491–510, http://dx.doi.org/10.1146/annurev-cellbio-100616-060608, _eprint:https://doi.org/10.1146/annurev-cellbio-100616-060608.

[3] P.T. Bozza, J.P.B. Viola, Lipid droplets in inflammation and cancer, Prostaglandins Leukot. Essent. Fatty Acids (PLEFA) 82 (4) (2010) 243–250, http://dx.doi.org/10.1016/j.plefa.2010.02.005, URL https://www.sciencedirect.com/science/article/pii/S0952327810000499.

[4] G. Onal, O. Kutlu, D. Gozuacik, S. Dokmeci Emre, Lipid Droplets in Health and Disease, Lipids Health Dis. 16 (1) (2017) 128, http://dx.doi.org/10.1186/s12944-017-0521-7.

[5] S. Xu, X. Zhang, P. Liu, Lipid droplet proteins and metabolic diseases, Biochim. Biophys. Acta (BBA) - Mol. Basis Dis. 1864 (5, Part B) (2018) 1968–1983, http://dx.doi.org/10.1016/j.bbadis.2017.07.019, URL https://www.sciencedirect.com/science/article/pii/S0925443917302454.

[6] R. Dhiman, S. Caesar, A.R. Thiam, B. Schrul, Mechanisms of protein targeting to lipid droplets: A unified cell biological and biophysical perspective, Semin. Cell Dev. Biol. (2020) http://dx.doi.org/10.1016/j.semcdb.2020.03.004.

[7] Y. Guo, T.C. Walther, M. Rao, N. Stuurman, G. Goshima, K. Terayama, J.S. Wong, R.D. Vale, P. Walter, R.V. Farese, Functional genomic screen reveals genes involved in lipid-droplet formation and utilization, Nature 453 (7195) (2008) 657–661, http://dx.doi.org/10.1038/nature06928, URL https://www.ncbi.nlm.nih.gov/pmc/articles/PMC2734507/.

[8] M.A. Welte, A.P. Gould, Lipid droplet functions beyond energy storage, Biochim. Biophys. Acta (BBA) - Mol. Cell Biol. Lipids 1862 (10, Part B) (2017) 1260–1272, http://dx.doi.org/10.1016/j.bbalip.2017.07.006, URL http://www.sciencedirect.com/science/article/pii/S1388198117301373.

[9] J.A. Olzmann, P. Carvalho, Dynamics and functions of lipid droplets, Nat. Rev. Mol. Cell Biol. 20 (3) (2019) 137–155, http://dx.doi.org/10.1038/s41580-018-0085-z, URL http://www.nature.com/articles/s41580-018-0085-z.

[10] H. Khandelia, L. Duelund, K.I. Pakkanen, J.H. Ipsen, Triglyceride Blisters in Lipid Bilayers: Implications for Lipid Droplet Biogenesis and the Mobile Lipid Signal in Cancer Cell Membranes, PLOS ONE 5 (9) (2010) e12811, http://dx.doi.org/10.1371/journal.pone.0012811, Publisher: Public Library of Science. URL https://journals.plos.org/plosone/article?id=10.1371/journal.pone.0012811.

[11] M.J. Greenall, C.M. Marques, Hydrophobic droplets in amphiphilic bilayers: a coarse-grained mean-field theory study, Soft Matter 8 (12) (2012) 3308, http://dx.doi.org/10.1039/c2sm07193b, URL http://xlink.rsc.org/?DOI=c2sm07193b.

[12] K.D. Chapman, J.M. Dyer, R.T. Mullen, Biogenesis and functions of lipid droplets in plants, J. Lipid Res. 53 (2) (2012) 215–226, http://dx.doi.org/10.1194/jlr.R021436, URL https://www.ncbi.nlm.nih.gov/pmc/articles/PMC3269164/.

[13] V. Choudhary, N. Ojha, A. Golden, W.A. Prinz, A conserved family of proteins facilitates nascent lipid droplet budding from the ER, J. Cell Biol. 211 (2) (2015) 261–271, http://dx.doi.org/10.1083/jcb.201505067, Publisher: The Rockefeller University Press. URL https://rupress.org/jcb/article/211/2/261/38599/A-conserved-family-of-proteins-facilitates-nascent.

[14] A. Masedunskas, Y. Chen, R. Stussman, R. Weigert, I.H. Mather, Kinetics of milk lipid droplet transport, growth, and secretion revealed by intravital imaging: lipid droplet release is intermittently stimulated by oxytocin, MBoC 28 (7) (2017) 935–946, http://dx.doi.org/10.1091/mbc.e16-11-0776, Publisher: American Society for Cell Biology (mboc). URL https://www.molbiolcell.org/doi/10.1091/mbc.e16-11-0776.

[15] V. Zoni, V. Nieto, L.J. Endter, H.J. Risselada, L. Monticelli, S. Vanni, To Bud or Not to Bud: A Perspective on Molecular Simulations of Lipid Droplet Budding, Front. Mol. Biosci. 6 (2019) http://dx.doi.org/10.3389/fmolb.2019.00124, Publisher: Frontiers. URL https://www.frontiersin.org/articles/10.3389/fmolb.2019.00124/full.

[16] A.R. Thiam, I. Dugail, Lipid droplet–membrane contact sites – from protein binding to function, J. Cell Sci. 132 (12) (2019) http://dx.doi.org/10.1242/jcs.230169, Publisher: The Company of Biologists Ltd Section: Review. URL https://jcs.biologists.org/content/132/12/jcs230169.

[17] L. Caillon, V. Nieto, P. Gehan, M. Omrane, N. Rodriguez, L. Monticelli, A.R. Thiam, Triacylglycerols sequester monotopic membrane proteins to lipid droplets, Nature Commun. 11 (1) (2020) 3944, http://dx.doi.org/10.1038/s41467-020-17585-8, Number: 1 Publisher: Nature Publishing Group. URL https://www.nature.com/articles/s41467-020-17585-8.

[18] S. Puza, S. Caesar, C. Poojari, M. Jung, R. Seemann, J.S. Hub, B. Schrul, J.-B. Fleury, Lipid Droplets Embedded in a Model Cell Membrane Create a Phospholipid Diffusion Barrier, Small n/a (n/a) 2106524, http://dx.doi.org/10.1002/smll.202106524, _eprint: https://onlinelibrary.wiley.com/doi/pdf/10.1002/smll.202106524. URL https://onlinelibrary.wiley.com/doi/abs/10.1002/smll.202106524.

[19] A. Chorlay, A.R. Thiam, An Asymmetry in Monolayer Tension Regulates Lipid Droplet Budding Direction, Biophys. J. 114 (3) (2018) 631–640, http://dx.doi.org/10.1016/j.bpj.2017.12.014, Publisher: Elsevier. URL https://www.cell.com/biophysj/abstract/S0006-3495(17)35094-4.

[20] A. Chorlay, L. Monticelli, J.V. Ferreira, K.B. M'barek, D. Ajjaji, S. Wang, E. Johnson, R. Beck, M. Omrane, M. Beller, P. Carvalho, A.R. Thiam, Membrane Asymmetry Imposes Directionality on Lipid Droplet Emergence from the ER, Dev. Cell 50 (1) (2019) 25–42.e7, http://dx.doi.org/10.1016/j.devcel.2019.05.003, Publisher: Elsevier. URL https://www.cell.com/developmental-cell/abstract/S1534-5807(19)30374-0.

[21] A. Chorlay, A. Santinho, A.R. Thiam, Making Droplet-Embedded Vesicles to Model Cellular Lipid Droplets, STAR Protocols 1 (3) (2020) 100116, http://dx.doi.org/10.1016/j.xpro.2020.100116, URL https://www.sciencedirect.com/science/article/pii/S2666166720301039.

[22] P.G. de Gennes, Wetting: statics and dynamics, Rev. Modern Phys. 57 (3) (1985) 827–863, http://dx.doi.org/10.1103/RevModPhys.57.827, Publisher: American Physical Society. URL https://link.aps.org/doi/10.1103/RevModPhys.57.827.

[23] V. Zoni, R. Khaddaj, P. Campomanes, A.R. Thiam, R. Schneiter, S. Vanni, Pre-existing bilayer stresses modulate triglyceride accumulation in the ER versus lipid droplets, eLife 10 (2021) e62886, http://dx.doi.org/10.7554/eLife.62886, Publisher: eLife Sciences Publications, Ltd. URL https://doi.org/10.7554/eLife.62886.

[24] A. Bacle, R. Gautier, C.L. Jackson, P.F.J. Fuchs, S. Vanni, Interdigitation between Triglycerides and Lipids Modulates Surface Properties of Lipid Droplets, Biophys. J. 112 (7) (2017) 1417–1430, http://dx.doi.org/10.1016/j.bpj.2017.02.032, URL https://www.sciencedirect.com/science/article/pii/S0006349517302461.

[25] G. Bussi, D. Donadio, M. Parrinello, Canonical sampling through velocity rescaling, J. Chem. Phys. 126 (1) (2007) 014101, http://dx.doi.org/10.1063/1.2408420.

[26] M.J. Abraham, T. Murtola, R. Schulz, S. Páll, J.C. Smith, B. Hess, E. Lindahl, GROMACS: High performance molecular simulations through multi-level parallelism from laptops to supercomputers, SoftwareX 1–2 (2015) 19–25, http://dx.doi.org/10.1016/j.softx.2015.06.001, URL https://www.sciencedirect.com/science/article/pii/S2352711015000059.

[27] L. Vamparys, R. Gautier, S. Vanni, W.F.D. Bennett, D.P. Tieleman, B. Antonny, C. Etchebest, P.F.J. Fuchs, Conical Lipids in Flat Bilayers Induce Packing Defects Similar to that Induced by Positive Curvature, Biophys. J. 104 (3) (2013) 585–593, http://dx.doi.org/10.1016/j.bpj.2012.11.3836, URL https://www.sciencedirect.com/science/article/pii/S0006349512051429.

[28] P. Heo, S. Ramakrishnan, J. Coleman, J.E. Rothman, J.-B. Fleury, F. Pincet, Highly Reproducible Physiological Asymmetric Membrane with Freely Diffusing Embedded Proteins in a 3D-Printed Microfluidic Setup, Small 15 (21) (2019) 1900725, http://dx.doi.org/10.1002/smll.201900725, _eprint: https://onlinelibrary.wiley.com/doi/pdf/10.1002/smll.201900725. URL https://www.onlinelibrary.wiley.com/doi/abs/10.1002/smll.201900725.

[29] C. Tempra, O.H.S. Ollila, M. Javanainen, Accurate Simulations of Lipid Monolayers Require a Water Model With Correct Surface Tension, 2021, http://dx.doi.org/10.26434/chemrxiv-2021-ws71h, URL https://chemrxiv.org/engage/chemrxiv/article-details/6152338087a02d9ab04af36a.

[30] Y. Li, P. Khanal, F. Norheim, M. Hjorth, T. Bjellaas, C.A. Drevon, J. Vaage, A.R. Kimmel, K.T. Dalen, Plin2 deletion increases cholesteryl ester lipid droplet content and disturbs cholesterol balance in adrenal cortex, J. Lipid Res. 62 (2021) 100048, http://dx.doi.org/10.1016/j.jlr.2021.100048, URL https://www.sciencedirect.com/science/article/pii/S0022227521000286.

[31] K. Hsieh, Y.K. Lee, C. Londos, B.M. Raaka, K.T. Dalen, A.R. Kimmel, Perilipin family members preferentially sequester to either triacylglycerol-specific or cholesteryl-ester-specific intracellular lipid storage droplets, J. Cell Sci. 125 (17) (2012) 4067–4076, http://dx.doi.org/10.1242/jcs.104943, URL https://www.ncbi.nlm.nih.gov/pmc/articles/PMC3482316/.

[32] D.M. Soumpasis, Theoretical analysis of fluorescence photobleaching recovery experiments, Biophys. J. 41 (1) (1983) 95–97, URL https://www.ncbi.nlm.nih.gov/pmc/articles/PMC1329018/.

[33] P.J. Quinn, F. Joo, L. Vigh, The role of unsaturated lipids in membrane structure and stability, Prog. Biophys. Mol. Biol. 53 (2) (1989) 71–103, http://dx.doi.org/10.1016/0079-6107(89)90015-1.

[34] N. Kučerka, F.A. Heberle, J. Pan, J. Katsaras, Structural Significance of Lipid Diversity as Studied by Small Angle Neutron and X-ray Scattering, Membranes 5 (3) (2015) 454–472, http://dx.doi.org/10.3390/membranes5030454, Number: 3 Publisher: Multidisciplinary Digital Publishing Institute. URL https://www.mdpi.com/2077-0375/5/3/454.

[35] W. Ding, M. Palaiokostas, G. Shahane, W. Wang, M. Orsi, Effects of High Pressure on Phospholipid Bilayers, J. Phys. Chem. B 121 (41) (2017) 9597–9606, http://dx.doi.org/10.1021/acs.jpcb.7b07119, Publisher: American Chemical Society. URL https://doi.org/10.1021/acs.jpcb.7b07119.

[36] G. Onal, O. Kutlu, D. Gozuacik, S. Dokmeci Emre, Lipid Droplets in Health and Disease, Lipids Health Dis. 16 (1) (2017) 128, http://dx.doi.org/10.1186/s12944-017-0521-7, URL http://lipidworld.biomedcentral.com/articles/10.1186/s12944-017-0521-7.

[37] R. Dimova, C. Marques, C. Marques, The Giant Vesicle Book, CRC Press, 2019, http://dx.doi.org/10.1201/9781315152516, URL https://www.taylorfrancis.com/books/e/9781315152516.

[38] N. Kahya, D. Scherfeld, K. Bacia, P. Schwille, Lipid domain formation and dynamics in giant unilamellar vesicles explored by fluorescence correlation spectroscopy, J. Struct. Biol. 147 (1) (2004) 77–89, http://dx.doi.org/10.1016/j.jsb.2003.09.021, URL http://www.sciencedirect.com/science/article/pii/S1047847703001667.

[39] J.N. Israelachvili, Intermolecular and Surface Forces, 3e éd., Academic Press Inc, Burlington (Mass.), 2011.

[40] M. Raja, Do Small Headgroups of Phosphatidylethanolamine and Phosphatidic Acid Lead to a Similar Folding Pattern of the K+ Channel? J. Membr. Biol. 242 (3) (2011) 137–143, http://dx.doi.org/10.1007/s00232-011-9384-4, URL https://www.ncbi.nlm.nih.gov/pmc/articles/PMC3146712/.

[41] G. Cevc, Phospholipids Handbook, CRC Press, 1993, Google-Books-ID: 2ZxaucDNWHcC.

[42] The ins and outs of endoplasmic reticulum-controlled lipid biosynthesis, EMBO Rep. 18 (11) (2017) 1905–1921, http://dx.doi.org/10.15252/embr.201643426, Publisher: John Wiley & Sons, Ltd. URL https://www.embopress.org/doi/full/10.15252/embr.201643426.

[43] L. Qiao, A. Ge, Y. Liang, S. Ye, Oxidative Degradation of the Monolayer of 1-Palmitoyl-2-Oleoyl-sn-Glycero-3-Phosphocholine (POPC) in Low-Level Ozone, J. Phys. Chem. B 119 (44) (2015) 14188–14199, http://dx.doi.org/10.1021/acs.jpcb.5b08985, Publisher: American Chemical Society. URL https://doi.org/10.1021/acs.jpcb.5b08985.

[44] W. Kulig, H. Korolainen, M. Zatorska, U. Kwolek, P. Wydro, M. Kepczynski, T. Róg, Complex Behavior of Phosphatidylcholine–Phosphatidic Acid Bilayers and Monolayers: Effect of Acyl Chain Unsaturation, Langmuir 35 (17) (2019) 5944–5956, http://dx.doi.org/10.1021/acs.langmuir.9b00381, Publisher: American Chemical Society. URL https://doi.org/10.1021/acs.langmuir.9b00381.

[45] A.L. McIntosh, S.M. Storey, B.P. Atshaves, Intracellular Lipid Droplets Contain Dynamic Pools of Sphingomyelin: ADRP Binds Phospholipids with High Affinity, Lipids 45 (6) (2010) 465–477, http://dx.doi.org/10.1007/s11745-010-3424-1, URL https://www.ncbi.nlm.nih.gov/pmc/articles/PMC3065392/.

[46] D.K. Breslow, Sphingolipid Homeostasis in the Endoplasmic Reticulum and Beyond, Cold Spring Harb. Perspect. Biol. 5 (4) (2013) a013326, http://dx.doi.org/10.1101/cshperspect.a013326, URL https://www.ncbi.nlm.nih.gov/pmc/articles/PMC3683901/.

[47] G.M. Deevska, M.N. Nikolova-Karakashian, The expanding role of sphingolipids in lipid droplet biogenesis, Biochim. Biophys. Acta Mol. Cell Biol. Lipids 1862 (10 Pt B) (2017) 1155–1165, http://dx.doi.org/10.1016/j.bbalip.2017.07.008.

[48] F.M. Goñi, A. Alonso, Biophysics of sphingolipids I. Membrane properties of sphingosine, ceramides and other simple sphingolipids, Biochim. Biophys. Acta (BBA) - Biomembr. 1758 (12) (2006) 1902–1921, http://dx.doi.org/10.1016/j.bbamem.2006.09.011, URL https://www.sciencedirect.com/science/article/pii/S0005273606003579.

[49] D. Casares, P.V. Escribá, C.A. Rosselló, Membrane Lipid Composition: Effect on Membrane and Organelle Structure, Function and Compartmentalization and Therapeutic Avenues, Int. J. Mol. Sci. 20 (9) (2019) 2167, http://dx.doi.org/10.3390/ijms20092167, URL https://www.ncbi.nlm.nih.gov/pmc/articles/PMC6540057/.

[50] Y. Guo, M. Werner, R. Seemann, V.A. Baulin, J.-B. Fleury, Tension-Induced Translocation of an Ultrashort Carbon Nanotube through a Phospholipid Bilayer, ACS Nano 12 (12) (2018) 12042–12049, http://dx.doi.org/10.1021/acsnano.8b04657, Publisher: American Chemical Society. URL https://doi.org/10.1021/acsnano.8b04657.

[51] F. Lolicato, R. Saleppico, A. Griffo, B. Pokrandt, H.-M. Müller, H. Ewers, H. Hähl, J.-B. Fleury, R. Seemann, B. Brügger, K. Jacobs, I. Vattulainen, W. Nickel, Cholesterol Promotes Both Head Group Visibility and Clustering of PI(4,5)P2 Driving Unconventional Secretion of Fibroblast Growth Factor 2, Tech. rep., bioRxiv, 2021, http://dx.doi.org/10.1101/2021.04.16.440132, Section: New Results Type: article. URL https://www.biorxiv.org/content/10.1101/2021.04.16.440132v1.

[52] The Effect of Cholesterol on the Lateral Diffusion of Phospholipids in Oriented Bilayers | Elsevier Enhanced Reader. http://dx.doi.org/10.1016/S0006-3495(03)70033-2. URL https://reader.elsevier.com/reader/sd/pii/S0006349503700332?token=D174135284A6750C4C8C01396F72C8C4681860FF9AAC469D6C4BDD009DC31A8B41E9CBBE56A222D90717BE658D13911D.

[53] G.R. Phillips, S.E. Hancock, S.H.J. Brown, A.M. Jenner, F. Kreilaus, K.A. Newell, T.W. Mitchell, Cholesteryl ester levels are elevated in the caudate and putamen of Huntington's disease patients, Sci. Rep. 10 (2020) 20314, http://dx.doi.org/10.1038/s41598-020-76973-8, URL https://www.ncbi.nlm.nih.gov/pmc/articles/PMC7680097/.

[54] H. Bayley, B. Cronin, A. Heron, M.A. Holden, W.L. Hwang, R. Syeda, J. Thompson, M. Wallace, Droplet interface bilayers, Mol. BioSyst. 4 (12) (2008) 1191–1208, http://dx.doi.org/10.1039/B808893D, Publisher: The Royal Society of Chemistry. URL https://pubs.rsc.org/en/content/articlelanding/2008/mb/b808893d.

[55] K. Ben M'barek, D. Ajjaji, A. Chorlay, S. Vanni, L. Forêt, A.R. Thiam, ER Membrane Phospholipids and Surface Tension Control Cellular Lipid Droplet Formation, Dev. Cell 41 (6) (2017) 591–604.e7, http://dx.doi.org/10.1016/j.devcel.2017.05.012, URL http://www.sciencedirect.com/science/article/pii/S1534580717303945.

Appendix (II) Bilayer-Embedded Lipid Droplets Coated with Perilipin-2 Display a Pancake Shape

Authors: Sevde Puza, Shima Asfia, Ralf Seemann and Jean-Baptiste Fleury

Experimental Physics, Saarland University, 66123 Saarbrücken, Germany

https://doi.org/10.3390/ijms24032072

Author contributions:

S. Puza and J.B. Fleury performed the experiments and analyzed the data with the suspended lipid bilayer. S. Asfia and J.B. Fleury performed the experiments and analyzed the data for the monolayer. J.B. Fleury designed the research. All the authors analyzed and discussed the results. All the authors wrote the manuscript. All authors have read and agreed to the published version of the manuscript.

Abstract:

Lipid droplets (LD) are organelles localized in the membrane of the endoplasmic reticulum (ER) that play an important role in many biological functions. Free LDs that have been released from the ER membrane and are present in the cytosol resemble an oil-in-water emulsion. The surface of an LD is coated with a phospholipid monolayer, and the core of an LD is composed of neutral lipids. Adipose differentiation-related protein (ADRP), also known as perilipin-2, is a protein that surrounds the LD, together with the phospholipid monolayer. ADRP molecules are involved in assisting in the storage of neutral lipids within LDs. In this article, we focus our interest on the influence of ADRP molecules on the 3D shape of bilayer-embedded LDs and the diffusion of phospholipids in the monolayer covering LDs. For this study, we employed two different microfluidic setups: one to produce and explore bilayer-embedded LDs and a second one to mimic the surface of a single LD. Using the first setup, we demonstrate that ADRP molecules stay preferentially localized on the surfaces of bilayer-embedded LDs, and we study their 3D-shape in the presence of ADRP. Using the second setup, we performed FRAP experiments to measure the phospholipid diffusion on a model LD surface as a function of the ADRP concentration. Although the presence of proteins on the LD surface minimally affects the phospholipid and protein motility, ADRP appears to have a significant effect on the 3D structure of LDs embedded in the bilayer.

International Journal of
Molecular Sciences

MDPI

Article

Bilayer-Embedded Lipid Droplets Coated with Perilipin-2 Display a Pancake Shape

Sevde Puza, Shima Asfia, Ralf Seemann and Jean-Baptiste Fleury *

Experimental Physics and Center for Biophysics, Saarland University, 66123 Saarbrücken, Germany
* Correspondence: jean-baptiste.fleury@physik.uni-saarland.de

Abstract: Lipid droplets (LD) are organelles localized in the membrane of the endoplasmic reticulum (ER) that play an important role in many biological functions. Free LDs that have been released from the ER membrane and are present in the cytosol resemble an oil-in-water emulsion. The surface of an LD is coated with a phospholipid monolayer, and the core of an LD is composed of neutral lipids. Adipose differentiation-related protein (ADRP), also known as perilipin-2, is a protein that surrounds the LD, together with the phospholipid monolayer. ADRP molecules are involved in assisting in the storage of neutral lipids within LDs. In this article, we focus our interest on the influence of ADRP molecules on the 3D shape of bilayer-embedded LDs and the diffusion of phospholipids in the monolayer covering LDs. For this study, we employed two different microfluidic setups: one to produce and explore bilayer-embedded LDs and a second one to mimic the surface of a single LD. Using the first setup, we demonstrate that ADRP molecules stay preferentially localized on the surfaces of bilayer-embedded LDs, and we study their 3D-shape in the presence of ADRP. Using the second setup, we performed FRAP experiments to measure the phospholipid diffusion on a model LD surface as a function of the ADRP concentration. Although the presence of proteins on the LD surface minimally affects the phospholipid and protein motility, ADRP appears to have a significant effect on the 3D structure of LDs embedded in the bilayer.

Keywords: lipid droplet; diffusion; FRAP; phospholipid; ADRP

Citation: Puza, S.; Asfia, S.; Seemann, R.; Fleury, J.-B. Bilayer-Embedded Lipid Droplets Coated with Perilipin-2 Display a Pancake Shape. *Int. J. Mol. Sci.* **2023**, *24*, 2072. https://doi.org/10.3390/ijms24032072

Academic Editor: Konstantin K. Turoverov

Received: 5 December 2022
Revised: 13 January 2023
Accepted: 18 January 2023
Published: 20 January 2023

1. Introduction

In recent years, lipid droplets (LDs) have attracted attention due to their roles in several diseases, metabolic disorders, and atherosclerosis [1–3]. LDs are organelles that are produced by the endoplasmic reticulum (ER) membrane [4,5] and are composed of a core made of neutral lipids, such as triglycerides and sterol esters, surrounded by a phospholipid monolayer [4,5]. The origin of their biogenesis is still under debate [6]. However, it is generally accepted that their biogenesis occurs in three steps [6,7]. First, neutral lipids are synthesized in the ER membrane [8]. In a second step, these neutral lipids diffuse in the membrane and agglomerate to produce nanometer-size oil inclusions. These nanometric hydrophobic inclusions are LDs that are supposed to have an initial diameter of approximately 50 nm [9,10]. The growth and enlargement of these LDs are caused by the ongoing production of neutral lipids inside the ER membrane. The LDs can spontaneously bud in the ER membrane as they grow, and are released into the cytosol when they pinch off from the membrane in the final step [11]. After release, the LDs can be observed via fluorescent microscopy, or by transmission electron microscopy. It appears that LDs are relatively spherical, having diameters ranging from 0.1 to 5 to 100 µm, depending on the cell type [12]. Aside from phospholipids, the surfaces of these LDs are decorated with either peripheral proteins or integral membrane proteins that adopt a monotopic topology and that are involved in metabolic and other biological functions [13]. Proteins of the perilipin family are known to be associated with the surfaces of LDs [14]. Adipose differentiation-related protein (ADRP or perilipin-2), is a lipid droplet protein from the

perilipin family that is found in most cells and tissues [15]. Perilipin controls important intracellular lipases, although to a very different degree [16]. Perilipin-2 has been proposed to play a role in LD budding [17]. Studies on the subcellular localization of LDs suggest that the budding of LDs from the ER may take place in perilipin2-enriched domains in the ER membrane [17,18]. This is a crucial step, as the budding step precedes the release of the LDs into the cytosol, where they can transport material to other organelles in the cell [19,20].

The full-length perilipin-2 protein is made of 437 amino acids and is self-assembled in several α-helices. Its secondary structure available from the AlphaFold openIA database [21]. It is supposed that ADRP plays a key role in the management of neutral lipid stores [15,22]. How perilipin-2 proteins target and bind to lipid droplets (LDs) is poorly understood, even if alpha helices seem to play a key role in the targeting mechanism [23,24]. In living cells or in artificial LDs, ADRP has been found to barely affect the phospholipid diffusion properties [25].

In this manuscript, we investigate the effects of ADRP on phospholipid diffusion and the 3D shape of lipid droplets embedded in a bilayer. For that, we used two different microfluidic setups: One for the fabrication of bilayer-embedded LDs and a second to mimic the surface of a single LD [26,27]. Using the first setup, we found that ADRP remains preferentially localized on the surfaces of bilayer-embedded LDs and investigated the impact of ADRP on the 3D geometry of bilayer-embedded LDs. In addition, we measured the effect of ADRP concentration on the exchange rate of phospholipid molecules between the monolayer and bilayer [26] by performing fluorescent recovery after photobleaching (FRAP) experiments. With the second setup, we determined the phospholipid diffusion on an artificial LD's surface as a function of ADRP concentration [27] by FRAP measurements.

2. Results and Discussion

2.1. LD Insertion and ADRPs' Localization in a Free-Standing Bilayer

We employed a 3D microchip [26] that enables the formation of a free-standing horizontal lipid bilayer at a desired position (see Figure 1, as detailed in the Section 3). The bilayer consisted of DOPC:DOPE with a molar ratio 3:1, which can be considered as a model endoplasmic reticulum membrane [28]. After lipid bilayer formation, we dispensed protein containing LDs through the bottom channel of the chip. From now on, LDs always refer to lipid droplets enriched with some high concentration of ADRP protein, if not mentioned otherwise (see Section 3). Due to their preparation, the LDs were normally about 15 µm in size. Fluorescent visualization of the LDs in buffer revealed that the protein was present throughout the entire LD, and not only on the surface. The same observation was made for several type of LDs coated with perilipins [23–25]. The estimated diffusion coefficient of a freely dispersed LD of about 15 µm is ≈0.03–0.04 $\mu m^2 \cdot s^{-1}$ [29]. This diffusion coefficient is sufficient for the LDs to diffuse freely and to finally reach the lipid bilayer. A LD in contact with a bilayer can insert into the bilayer core, creating an inclusion with a distinctive shape [26,30], and stops moving [26]. This insertion into the bilayer was verified by 3D confocal scans; see Figure 2. The absence of any detectable fluorescent signal from ADRP in the bilayer demonstrates that the proteins stay localized in and on the bilayer-embedded LD. However, it might still be possible that some negligible amounts of protein move in the bilayer. To test this, we bleached the proteins present in the core and on the surface of a single bilayer-embedded LD and waited 1 h for any fluorescent protein signal to recover. However, no fluorescence recovery was observed during that time, indicating that there is in fact neither ADRP in the bilayer nor any measurable protein transport between different bilayer-embedded LDs. This point is interesting, as it was also observed in living cells [25].

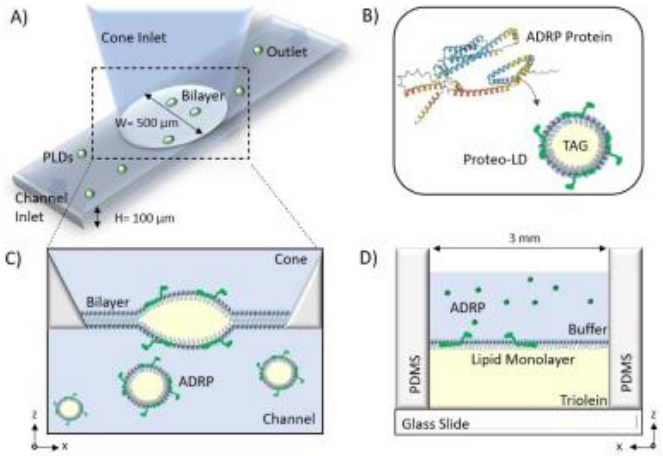

Figure 1. (**A**) Schematic of the microfluidic system to form a free-standing bilayer containing Proteo-LDs. (**B**) The secondary structure of ADRP was provided by the AlphaFold AI database. ADRP is reconstituted in the PC:PE monolayer covering the LD. (**C**) A bilayer is formed at the aperture between the channel and the cone, and LDs containing ADRP protein are introduced from the bottom channel and insert into the bilayer. (**D**) Schematic of the microfluidic device to form the free-standing monolayer. A phospholipid monolayer is formed at the buffer–triolein interface.

2.2. *Influence of ADRP on the Shape of Bilayer-Embedded LD*

Having inserted LDs into a free-standing lipid bilayer, we explored their 3D shape in view of the acting surface forces. The LDs were consequently divided into two groups: tiny drops and pancakes. Tiny droplets are too small to have their geometry analyzed in detail. In consequence, we ignored these tiny droplets in the following analysis. Pancake droplets have a diameter of about 20 µm and a height of about 5 µm, which was sufficiently large to resolve that their shapes escaped slightly from the expected ideal lens shape with spherical interfaces (Video S1). LDs without proteins, however, revealed a larger contact angle, and the shape of the two lens surfaces was spherical; see Figure 2B and Table 1 [10,30,31]. Indeed, surface-tension measurements revealed that ADRP is highly surface active. For example, a triolein–buffer interface with 1 µM of ADRP, directly dispersed into the buffer, revealed a surface tension of ≈10 mN/m, which is only one third of the surface tension of a triolein–buffer surface (≈30 mN/m) not containing and surface active molecules (as determined by pendant-droplet method). Thus, the reduced contact angle and the slightly flattened LD shape with ADRP molecules being present of the LD surface might have resulted from an inhomogeneous distribution of the surface active ADRP molecules (see Section 3 and Table 1), which might have an increased presence close to the circumference of the LD, lowering the local surface tension.

To check the shape of the LDs' and their influence on the wetting properties in some more detail, we measured the shapes of the LDs with bilayers having different cholesterol concentrations. The usage of cholesterol is not biorelevant, as ER membranes do not contain cholesterol. However, it allowed us to tune the surface forces applied to the LDs [26]. Interestingly, cholesterol appears to increase the LD surface tension as measured by the pendant-droplet method and also increased the contact angle of the LDs (see Table 1). However, the pancake-like shape in the presence of ADRP molecules remained and seemed even more pronounced; the larger the cholesterol concentration, the larger the contact angle α. This may suggest that the inhomogeneous distribution of ADRP on the LD's surface is even enhanced in the presence of cholesterol.

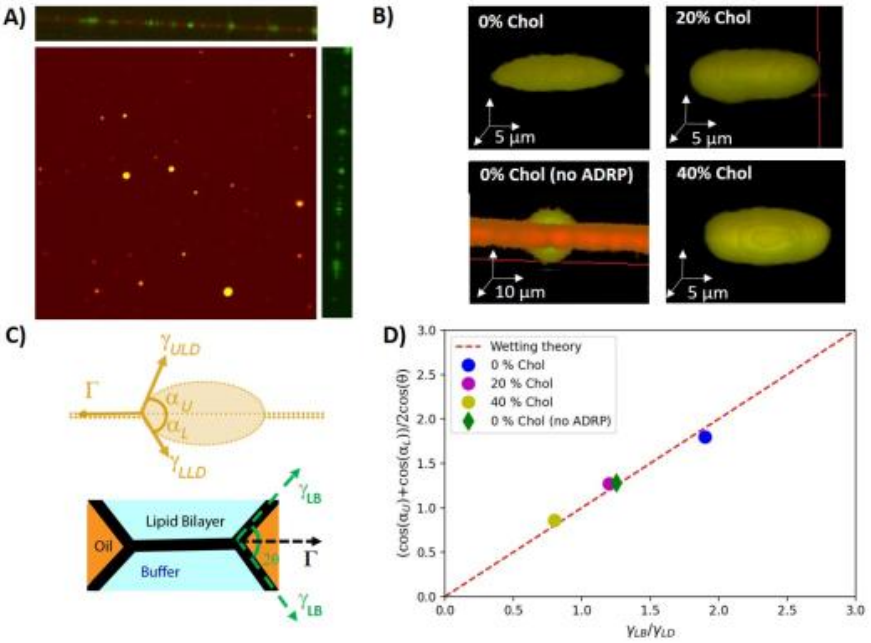

Figure 2. (**A**) Top view of a free-standing bilayer containing LDs. A side view of a 3D scan is provided in the top panel. The right panel provides the corresponding side view with only the protein channel. All the proteins are labeled in green (Alexa 488) and 2% (molar ratio) DOPE is labeled in red (Cy5). (**B**) 3D reconstructions of individual bilayer-embedded LDs for 0%, 20%, and 40% cholesterol, respectively (with 1 µM ADRP). For comparison, the 3D reconstructions of a bilayer-embedded LD with 0% cholesterol are given, and no ADRP was added. In the latter case, the neutral lipids were stained with BODIPY. (**C**) Scheme of the surface forces acting on a bilayer-embedded LD with an ideal lens shape (upper panel). Scheme of the surface forces acting on the bilayer (lower paner). (**D**) Comparison between wetting theory and the balance of surface forces as extracted from the symmetric 3D LD geometry.

The shape of embedded LDs is defined by the balance between the bilayer tension Γ and the tensions applied by the horizontal components of the surface tensions of the upper LD leaflet $\Gamma_{ULD} = \gamma_{ULD} \cdot \cos(\alpha_U)$ and the lower leaflet $\Gamma_{LLD} = \gamma_{LLD} \cdot \cos(\alpha_L)$ close to the three-phase contact line, such as:

$$\Gamma = \gamma_{ULD} \cdot \cos(\alpha_U) + \gamma_{LLD} \cdot \cos(\alpha_L). \quad (1)$$

where α_U, α_L are the angles measured from the 3D images, as defined in Figure 2C. In equilibrium, the bilayer tension can be determined by the Young–Dupré law, $\Gamma = 2\gamma_{LB} \cdot \cos(\theta)$ [31], where γ_{LB} is the surface tension of a monolayer-decorated oil–water interface and 2θ is the contact angle of the plateau border; see Figure 2C (measured by scanning directly the contact angle via confocal microscopy). As ADRP is partially soluble in the core of the LD, after a short equilibration time, it can be assumed that the amount of proteins at the interface of the LDs and thus the surface tension of both droplet interfaces are equal on average. As a reasonable simplification, we can thus assume $\gamma_{ULD} = \gamma_{LLD} = \gamma_{LD}$ and reformulate Equation (1) to

$$\frac{\gamma_{LB}}{\gamma_{LD}} = \frac{\cos(\alpha_U) + \cos(\alpha_L)}{2\cos(\theta)}, \quad (2)$$

From the independently measured angles α and θ and the measured surface tensions values γ_{LB} and γ_{LD} (see Table 1), we could verify that these values satisfy Equation (2), as plotted in Figure 2D. It results that the measured pancake shapes correspond to an equilibrium wetting morphology, and the reduction of the insertion angle with increasing cholesterol concentration appears to be a consequence of increased bilayer tension as a function of increasing cholesterol concentration, which is consistent with some literature [32,33]. It also indicates that ADRP proteins qualitatively change the surface properties of bilayer-embedded LDs, as they do not exhibit a lens-like shape but a pancake shape (see Figure 2). In view of the quantitative agreement of the measured LD shape with bulk surface-tension measurements, it can be even assumed that the LD surface remote from the three-phase contact line is depleted of ADRP molecules.

Table 1. Physical characterization of a symmetric bilayer and LDs inserted in it. The phospholipids diffused between the monolayer covering the LD and the bilayer, so the LD monolayer's phospholipidic composition was the same as that of the bilayer after a long time. LD surface tension γ_{LD} was obtained from pendant drop measurements, bilayer tension Γ was obtained from optically determined contact angles θ and γ_{LD} using Equation (2), and LD contact angles were obtained from 3D confocal micrographs. Each value was obtained by averaging 30 different measurements.

Protein (μM)	Chol (%)	Bilayer Tension Γ	LB Contact Angle θ	LD Tension γ_{LD}	LD Contact Angle α_U	LD Contact Angle α_L
1	0%	2 mN/m	(64 ± 3)°	1.06 mN/m	(42 ± 3)°	(35 ± 3)°
1	20%	2.4 mN/m	(67 ± 3)°	2.01 mN/m	(65 ± 3)°	(55 ± 3)°
1	40%	3.1 mN/m	(69 ± 2)°	3.9 mN/m	(75 ± 3)°	(65 ± 3)°
0	0%	2 mN/m	(63 ± 2)°	1.6 mN/m	(49 ± 3)°	(51 ± 3)°

2.3. Effect of ADRP on the Phospholipid Diffusion Properties of an LD Embedded in a Bilayer

In this section, we study the phospholipid diffusion properties in the presence of ADRPs. In this context, there are two aspects of particular interest to us: the influence of ADRP on the phospholipid exchange rate between the LD monolayer and the bilayer (in the case of a bilayer-embedded LD) and the influence of phospholipid diffusion on the LD monolayers themselves.

We begin our discussion by studying the phospholipid diffusion on an artificial LD surface. For this purpose, we realized a model LD surface using the microfluidic setup described in Figure 1D. The model LD surface was covered with a phospholipid monolayer at the buffer–triolein interface composed of DOPC:DOPE with a molar ratio of 3:1. As DOPE contains 2 w% of the fluorescent phospholipid DOPE-Cy5, we can perform FRAP experiments on this monolayer (see Figure 3) [27]. The diffusion coefficient extracted from the FRAP data is ≈8 $\mu m^2 \cdot s^{-1}$ when the total phospholipid concentration in triolein used to form the monolayer is equal or above 1 w%; see Figure 3 [34]. Smaller phospholipid concentrations lead to an increased diffusion constant, which is expected for a monolayer with incomplete surface coverage. When these experiments were repeated with 1 μM ADRP, we observed that the ADRP molecules were slightly inhomogeneously distributed and seemed to cluster, showing granularity on the length scale of about 1 μm and 5 μm in fluorescent images. This indicates that the ADRP proteins do not remarkably affect the motility of a phospholipid monolayer. This feature seems to be consistent with results reported in the literature [23]. We also performed FRAP measurements on fluorescently labeled (ADRP-Alexa488) proteins (c ≈ 1 μM) present on the lipid monolayer. The thus extracted ADRP diffusion coefficient is ≈0.3 $\mu m^2 \cdot s^{-1}$ when the total phospholipid concentrations used to form the monolayer were equal or above 1%w. This diffusion coefficient was more than 20 times smaller than that of the phospholipids, indicating slow motility of the proteins on the LD surface; however, this motility is still not negligible. Interestingly, to the best of our knowledge, this manuscript offers the first measurements of ADRP diffusion in a lipid monolayer.

The diffusion coefficient of PE in a bilayer is about 10 $\mu m^2 \cdot s^{-1}$ [26]—i.e., very close to the diffusion coefficient of about 8 $\mu m^2 \cdot s^{-1}$ measured for a densely packed DOPC/DOPE monolayer with or without ADRP present in the monolayer. However, despite the similar motilities in the bilayer and monolayer, it was found in previous experiments that a diffusion barrier between monolayer and bilayer exists in this system [26], which reduces the molecular transport rate between the bilayer and the monolayer. This was shown in [26] by the cone-shaped DOPE lipids, which are able to stabilize the negative membrane curvature along the LD edge and provide a structural source for the diffusion barrier, in line with other recent studies [35–37].

To test the possible existence of such a diffusion barrier also in the presence of ADRP molecules, we performed FRAP experiments on bilayer-embedded LDs; see Figure 3B. For that, we fabricated a free-standing bilayer composed of DOPC:DOPE with a molar ratio of 3:1 and inserted ADRP-enriched LDs into the bilayer, as was described previously. We bleached the fluorescent phospholipids (DOPE-Cy5) on the entire surface of the LD and measured the fluorescence recovery due to the transport of fluorescent phospholipids coming from the bilayer. Surprisingly, in the presence of ADRP, we measured that the DOPE-Cy5 fluorescence recovery curve is very similar to the one measured in a phospholipid mono- or bilayer. This result indicates that the presence of ADRP disassembles the hypothetic metastable PE ring and facilitates the molecular transport between the bilayer and the monolayer. This finding agrees perfectly with a preferential presence of ADRP molecules near the three-phase contact line, as already suspected based on the pancake-like shape of the LDs in the presence of ADRP molecules.

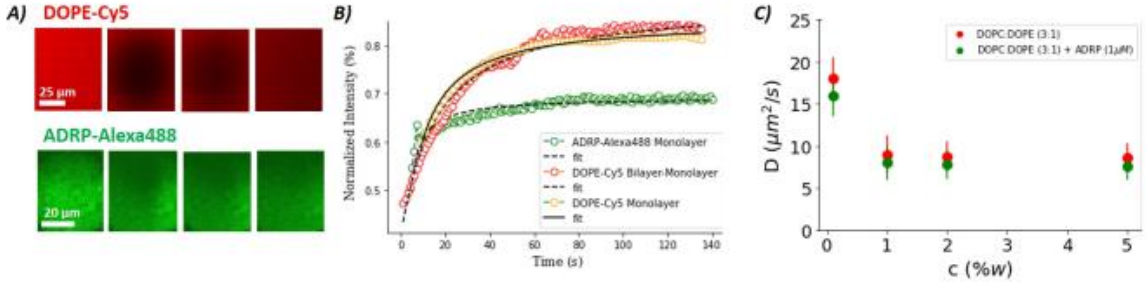

Figure 3. (**A**) Series of fluorescence images showing a lipid monolayer (DOPC:DOPE, 3:1) between buffer and triolein before bleaching and during recovery. (Upper panel) DOPE-Cy5, 2% molar ratio; (Lower panel) ADRP-Alexa488, 1 µM. (**B**) FRAP curves extracted from fluorescence images, such as the one shown in (**A**) with the corresponding Soumpasis fits for DOPE-Cy5 (red dots) and ADRP-Alexa488 (green dots). Yellow dots correspond to the recovery of the DOPE-Cy5 fluorescence obtained by bleaching the entire bilayer-embedded LD surface, with same bilayer composition as in (**A**). (**C**) Diffusion coefficients of DOPE in the lipid monolayer, as a function of total lipid concentration and in the presence and absence of ADRP. The error bars are presented by the continuous lines. In (**A–C**), each value was obtained by averaging ≈ 30 different measurements.

3. Materials and Methods

3.1. Molecules

1,2-Dioleoyl-sn-glycero-3-phosphocholine (DOPC), 1,2-dioleoyl-sn-glycero-3-phosphoethanolamine (DOPE), and cholesterol were purchased from Avanti Polar Lipids. Glyceryl trioleate (triolein, T7140) and squalene (S3626) were purchased from Sigma-Aldrich. BODIPY (493/503, D3922) was purchased from Thermo-Fisher. Recombinant human denaturated full length perilipin-2 protein (ADRP) was purchased from Abcam (ab181932). We purchased (DOPE-Cy5.5)1,2-dioleoyl-sn-glycero-3-phosphoethanolamine-N-(cyanine 5.5) from Avanti Polar Lipid. Adipose differentiation-related protein (ADRP) is turned fluorescent by

the Alexa Fluor 488 conjugation kit (Abcam-ab236553), following the procedure described in the next section. In this manuscript, buffer solution refers to 150 mM potassium chloride.

3.2. ADRP Protein Conjugation

Prior to conjugation, a stock solution with a concentration of 0.5 mg/mL was prepared by mixing the recombinant human ADRP protein with ultra-pure water (Thermo Fisher, Waltham, MA, USA). To label the proteins with the Alexa Fluor 488 conjugation kit (Abcam-ab236553), 5 µg of the proteins was used. For that, first, 1 µL of the modifier agent was added to 10 µL of the ADRP stock solution (buffer) and mixed gently. The mixed sample was pipetted into the reagent. This solution was kept standing in a dark room for 15 min, before mixing with 1 µL of the quenching agent. The conjugated proteins were ready to use after 5 min.

3.3. Free-Standing Bilayer Formation

A sketch of the 3D microfluidic device is shown in Figure 1A). The device consists of a horizontal channel at the bottom with an attached truncated cone and was fabricated in PDMS (Sylgard 184, Dow Corning) from a 3D mold following soft-lithographic protocols. Details of the design and the fabrication of the microfluidic 3D device can be found in [26].

We employed a bilayer with a constant DOPC:DOPE composition of 3:1 (unless mentioned otherwise), which can be considered as a model endoplasmic reticulum membrane [26,37]. All the phospholipids were prepared with a concentration of 5 mg/mL in squalene oil. The lipid–oil solution was mixed at 50 °C for 3–4 h to allow the lipids to dissolve completely in the oil. The bilayer formation in the 3D microfluidic device was done following three steps. First, the bottom channel was filled completely with the buffer solution. The height of the buffer was set so that its meniscus was located at the aperture formed by the intersection of the bottom channel and the upper cone. Then, gently, a 4 µL drop of lipid–oil mixture was pipetted into the upper cone, whereby the entire meniscus was covered with the lipid–oil mixture to form a first water–oil interface. Subsequently, a 5 µL drop of buffer was pipetted into the cone to cover the lipid–oil mixture and to form a second water–oil interface. The phospholipids cover the water–oil interfaces and form two separated phospholipid monolayers. At the same time, squalene is adsorbed by the PDMS, eventually bringing the two separate phospholipid monolayers into contact and forming a bilayer. Depending on the amount of the lipid–oil mixture trapped between the two buffer phases, the time required for the formation of a bilayer varies from 10 min to 2 h. When the formation of the bilayer begins, a small circle appears in the center of the aperture. This circle enlarges and eventually fills the entire aperture, which is the sign of complete zipping of the two monolayers and the formation of the bilayer [38]. All experiments were performed at a room temperature of 23 °C.

3.4. LD Preparation

Phospholipids (DOPC and DOPE) and triolein were used from their stock solution (10 mg/mL). In total, 30 µL of triolein with DOPC:DOPE (1:1 in molar ratio, and 2% of phospholipid in total weight ratio) was dried in a glass falcon under vacuum for 1 h. The composition of the phospholipid monolayer on the LD surface was chosen to allow easy LD insertion inside the free-standing bilayer (see [26]). For one experiment detailed in Figure 2B, showing a LD without ADRP, BODIPY was added to triolein to stain neutral lipids. Then, 1 µM of the conjugated protein solution was diluted in 10 µL PBS. This triolein–lipid mixture and 200 µL PBS were added to a falcon tube and stored at 4 °C overnight. Afterwards, the mixture was sonicated for 5 min to obtain LDs. The sizes of the obtained LDs were measured to be round 15 µm by optical microscopy. We injected 1 µM of ADRP into the LD dispersion and let them find and bind to the LD by diffusion. In summary, the formed LDs were coated with a PC:PE monolayer (molar ratio 1:1) containing ADRP proteins. Then, the LDs were dispersed around the bilayer by flowing them into the

bottom channel of device 1; cf. Figure 1A. After (10–15) min, the spontaneous insertion of several of these LDs into the bilayer was observed using confocal microscopy [26].

Finally, to demonstrate the presence of ADRP on the LD surface, we repeated the formation of LDs without the use of phospholipids. Thus, we produced an emulsion of triolein in water with only ADRP as an emulsifier. The resulting triolein droplets were stable for at least of a few hours and presented a size in the range of 50–100 µm. This finding would be impossible to achieve if the ADRP were not surface active (as demonstrated by the surface-tension measurements).

3.5. Free-Standing Monolayer Formation

The device used to study phospholipid monolayer was a simplified version of the previously described one and consisted essentially of a cylindrical hole in a PDMS (Sylgard 184) matrix that was bonded to a glass substrate; cf. Figure 1D. Details of the fabrication and chip geometry, can be found in ref. [27].

To produce the triolein–lipid mixture, a specific lipid composition (2% of phospholipids in total weight ratio) was dissolved in chloroform. This solution was then dried under vacuum. Triolein was added to the dried components and mixed in an ultrasonic bath. The resulting phospholipid mixture also contained 2% (in molar ratio) of DOPE-Cy5 as a fluorescent probe. To form a monolayer, 6 µL of the as-prepared triolein–lipid mixture was first placed in the cylindrical opening of the PDMS microchip, and then 20 µL of 150 M KCl buffer was added on top. This buffer also contained 1 µM of fluorescent ADRP. Within seconds, a phospholipid monolayer formed at the triolein–buffer interface, with a composition similar to the lipid composition of the originally prepared triolein solution. All experiments were performed at a room temperature of 23 °C.

3.6. Confocal Imaging and FRAP Experiments

Confocal images were acquired with an inverted microscope (Nikon Ti-Eclipse) with an Intensilight Epi-fluorescence light source and a laser unit (LU-NV, Nikon). The confocal microscope was equipped with a Yokogawa spinning disk head (CSU-W1; Andor Technology) and a module for fluorescence recovery after photo-bleaching (FRAPPA; Andor Technology). Confocal imaging was conducted using excitation wavelengths of 481 nm (for Alexa488) and 647 nm (for DOPE-Cy5). The used emission filters had the wavelengths/bandwidths of 525/30 nm and 685/40 nm, respectively. For the FRAP experiments, a pinhole size of 50 µM was used in combination with a 40× oil objective having a working distance of 220 µm. Prior to bleaching, a circular stimulation area with diameter ranging between 5 and 50 µm was selected inside the bilayer (to increase measurement quality). At the beginning of a FRAP measurement, fluorescence imaging was performed for 20 s for each individual experiment. Then, bleaching was performed by increasing the laser power in the stimulation area (defined by the pinhole size) to the maximum laser power for 20 s (70 mW for 481 and 561 nm, 125 mW for 647 nm). During the following fluorescence recovery, image acquisition was continued for at least 5 min to be able to observe the full recovery. The thus obtained fluorescence recovery (FRAP) data were directly fitted with the Soumpasis equation using Python [26,27,34]. All experiments were performed at a room temperature of 23 °C.

3.7. Surface Tension Measurement

Surface tensions were determined by the pending-drop method using a contact angle measurement device, an OCA 20 (DataPhysics, Filderstadt, Germany). For this method, a droplet with a defined volume of the denser fluid, here the buffer solution (ρ_{buffer} = 0.998 g/cm^3), is created at the tip of a needle, which is immersed in a transparent cuvette filled with the fluid of lesser density—here, the squalene–phospholipid mixture (ρ_{oil} = 0.858 g/cm^3). While gravity drags the droplet down, buoyancy and surface forces keep the droplet in place. The surface tension can then be determined based on a Young–Laplace fit to an shadow image of the droplet, which is automatically accomplished by

the software SCA 20. For best quality of the fitted data, the droplet volume should be chosen to be as large as possible, yet on the other hand, the detachment droplet volume at a fully lipid-decorated oil–water interface defines an upper limit of the droplet's size. As an optimum for the considered system, we set the droplet volume to 2.0 ± 0.5 µL.

From the surface tension values obtained from those pendant drop measurements (listed in Table 1), and the bilayer contact angle 2θ obtained from optical micrographs (listed in Table 1), cf. Figure 2C, the bilayer tension can be calculated using Young's equation:

$$\Gamma = 2\gamma \, cos(\theta). \quad (3)$$

All those measured surface tension and contact angle values and those calculated from them are listed in Table 1.

4. Conclusions

In this manuscript, we have extended previous works by successfully reconstituting a full-length LD protein (ADRP) in a bilayer-embedded LD. We focused our interests on the influence of ADRPs on the phospholipid diffusion and the 3D shape of bilayer-embedded LDs. We observed that the surface-active ADRP molecules strongly affect the shape of the bilayer-embedded LDs. The traditional expected lens shape is believed to have vanished in favor of a pancake shape as a result of the non-homogeneous protein decoration on the LD's surface, i.e., a relative enrichment of ADRP molecules close to the three-phase contact line and a depletion at the center of the droplet. This spontaneous asymmetry may facilitate spontaneous droplet bulging and have consequences for LD biogenesis [39]. This specific pancake-like droplet shape was maintained (or even enhanced) for varying surface tension tuned by increasing cholesterol concentration. However, despite the unexpected pancake shape, the contact angles measured locally on the three-phase contact line are in agreement with expectations from wetting theory, assuming contact angles averaged for several droplets and surface tensions obtained from bulk measurements. We think that the unexpected shape of these LDs may affect how they work, how they grow, or how they bulge.

Additionally, we also studied the diffusion properties of phospholipids and ADRP within our system. In particular, we measured that the ADRP molecules can diffuse freely throughout the LD's surface. Consistently, the phospholipid diffusion properties on a LD surface were very similar to those of a bilayer and were barely affected by the presence of ADRP. This point seems to be in agreement with the literature. However, ADRPs facilitate the transport of phospholipids between a bilayer and a bilayer-embedded LD, presumably by destroying the hypothesized PE-ring around an LD forming the structural origin of the diffusion barrier [26]. These results show that all molecules may diffuse freely, proving that the pancake shape is not the result of a diffusion-related artifact, but rather the consequence of the accumulation of ADRP molecules close to the three-phase contact line.

Supplementary Materials: The following supporting information can be downloaded at: https://www.mdpi.com/article/10.3390/ijms24032072/s1.

Author Contributions: S.P. and J.-B.F. performed the experiments and analyzed the data with the suspended lipid bilayer. S.A. and J.-B.F. performed the experiments and analyzed the data for the monolayer. J.-B.F. designed the research. All the authors analyzed and discussed the results. All the authors wrote the manuscript. All authors have read and agreed to the published version of the manuscript.

Funding: This research was funded by Deutsche Forschungsgemeinschaft grant number sfb1027, project B4.

Data Availability Statement: The datasets generated during and/or analyzed during the current study are available from the corresponding author on reasonable request.

Acknowledgments: The authors acknowledge that financial support was from the Deutsche Forschungsgemeinschaft (DFG), SFB1027 (project B4).

Conflicts of Interest: The authors declare no conflict of interest.

References

1. Greenberg, A.S.; Coleman, R.A.; Kraemer, F.B.; McManaman, J.L.; Obin, M.S.; Puri, V.; Yan, Q.W.; Miyoshi, H.; Mashek, D.G. The role of lipid droplets in metabolic disease in rodents and humans. *J. Clin. Investig.* **2011**, *121*, 2102–2110. [CrossRef] [PubMed]
2. Bozza, P.T.; Viola, J.P.B. Lipid droplets in inflammation and cancer. *Prostaglandins Leukot. Essent. Fat. Acids (PLEFA)* **2010**, *82*, 243–250. [CrossRef] [PubMed]
3. Melo, R.C.N.; Dvorak, A.M. Lipid Body–Phagosome Interaction in Macrophages during Infectious Diseases: Host Defense or Pathogen Survival Strategy? *PLoS Pathog.* **2012**, *8*, e1002729. [CrossRef] [PubMed]
4. Welte, M.A.; Gould, A.P. Lipid droplet functions beyond energy storage. *Biochim. Biophys. Acta (BBA)-Mol. Cell Biol. Lipids* **2017**, *1862*, 1260–1272. [CrossRef] [PubMed]
5. Guo, Y.; Walther, T.C.; Rao, M.; Stuurman, N.; Goshima, G.; Terayama, K.; Wong, J.S.; Vale, R.D.; Walter, P.; Farese, R.V. Functional genomic screen reveals genes involved in lipid-droplet formation and utilization. *Nature* **2008**, *453*, 657–661. [CrossRef] [PubMed]
6. Walther, T.C.; Chung, J.; Farese, R.V. Lipid Droplet Biogenesis. *Annu. Rev. Cell Dev. Biol.* **2017**, *33*, 491–510. [CrossRef]
7. Olzmann, J.A.; Carvalho, P. Dynamics and functions of lipid droplets. *Nat. Rev. Mol. Cell Biol.* **2019**, *20*, 137–155. [CrossRef]
8. Chitraju, C.; Mejhert, N.; Haas, J.T.; Diaz-Ramirez, L.G.; Grueter, C.A.; Imbriglio, J.E.; Pinto, S.; Koliwad, S.K.; Walther, T.C.; Farese, R.V. Triglyceride Synthesis by DGAT1 Protects Adipocytes from Lipid-Induced ER Stress during Lipolysis. *Cell Metab.* **2017**, *26*, 407–418.e3. [CrossRef]
9. Khandelia, H.; Duelund, L.; Pakkanen, K.I.; Ipsen, J.H. Triglyceride Blisters in Lipid Bilayers: Implications for Lipid Droplet Biogenesis and the Mobile Lipid Signal in Cancer Cell Membranes. *PLoS ONE* **2010**, *5*, e12811. [CrossRef]
10. Greenall, M.J.; Marques, C.M. Hydrophobic droplets in amphiphilic bilayers: A coarse-grained mean-field theory study. *Soft Matter* **2012**, *8*, 3308. [CrossRef]
11. Wilfling, F.; Haas, J.T.; Walther, T.C.; Farese, R.V. Lipid Droplet Biogenesis. *Curr. Opin. Cell Biol.* **2014**, *29*, 39–45. [CrossRef]
12. Fujimoto, T.; Parton, R.G. Not Just Fat: The Structure and Function of the Lipid Droplet. *Cold Spring Harb Perspect Biol.* **2011**, *3*, a004838. [CrossRef] [PubMed]
13. Dhiman, R.; Caesar, S.; Thiam, A.R.; Schrul, B. Mechanisms of protein targeting to lipid droplets: A unified cell biological and biophysical perspective. *Semin. Cell Dev. Biol.* **2020**, *108*, 4–13. [CrossRef] [PubMed]
14. Itabe, H.; Yamaguchi, T.; Nimura, S.; Sasabe, N. Perilipins: A diversity of intracellular lipid droplet proteins. *Lipids Health Dis.* **2017**, *16*, 83. [CrossRef] [PubMed]
15. Brasaemle, D.L.; Barber, T.; Wolins, N.E.; Serrero, G.; Blanchette-Mackie, E.J.; Londos, C. Adipose differentiation-related protein is an ubiquitously expressed lipid storage droplet-associated protein. *J. Lipid Res.* **1997**, *38*, 2249–2263. [CrossRef]
16. Ajjaji, D.; Ben M'barek, K.; Mimmack, M.L.; England, C.; Herscovitz, H.; Dong, L.; Kay, R.G.; Patel, S.; Saudek, V.; Small, D.M.; et al. Dual binding motifs underpin the hierarchical association of perilipins1–3 with lipid droplets. *MBoC* **2019**, *30*, 703–716. [CrossRef]
17. Robenek, H.; Hofnagel, O.; Buers, I.; Robenek, M.J.; Troyer, D.; Severs, N.J. Adipophilin-enriched domains in the ER membrane are sites of lipid droplet biogenesis. *J. Cell Sci.* **2006**, *119*, 4215–4224. [CrossRef]
18. Xu, S.; Zou, F.; Diao, Z.; Zhang, S.; Deng, Y.; Zhu, X.; Cui, L.; Yu, J.; Zhang, Z.; Bamigbade, A.T.; et al. Perilipin 2 and lipid droplets provide reciprocal stabilization. *Biophys. Rep.* **2019**, *5*, 145–160. [CrossRef]
19. Chapman, K.D.; Dyer, J.M.; Mullen, R.T. Biogenesis and functions of lipid droplets in plants. *J. Lipid Res.* **2012**, *53*, 215–226. [CrossRef]
20. Schuldiner, M.; Bohnert, M. A different kind of love—Lipid droplet contact sites. *Biochim. Biophys. Acta (BBA)-Mol. Cell Biol. Lipids* **2017**, *1862*, 1188–1196. [CrossRef]
21. Callaway, E. DeepMind's AI predicts structures for a vast trove of proteins. *Nature* **2021**, *595*, 635. [CrossRef]
22. Ducharme, N.A.; Bickel, P.E. Minireview: Lipid Droplets in Lipogenesis and Lipolysis. *Endocrinology* **2008**, *149*, 942–949. [CrossRef] [PubMed]
23. Giménez-Andrés, M.; Emeršič, T.; Antoine-Bally, S.; D'Ambrosio, J.M.; Antonny, B.; Derganc, J.; Čopič, A. Exceptional stability of a perilipin on lipid droplets depends on its polar residues, suggesting multimeric assembly. *eLife* **2021**, *10*, e61401. [CrossRef] [PubMed]
24. Čopič, A.; Antoine-Bally, S.; Giménez-Andrés, M.; La Torre Garay, C.; Antonny, B.; Manni, M.M.; Pagnotta, S.; Guihot, J.; Jackson, C.L. A giant amphipathic helix from a perilipin that is adapted for coating lipid droplets. *Nat. Commun.* **2018**, *9*, 1332. [CrossRef] [PubMed]
25. Targett-Adams, P.; Chambers, D.; Gledhill, S.; Hope, R.G.; Coy, J.F.; Girod, A.; McLauchlan, J. Live cell analysis and targeting of the lipid droplet-binding adipocyte differentiation-related protein. *J. Biol. Chem.* **2003**, *278*, 15998–16007. [CrossRef]
26. Puza, S.; Caesar, S.; Poojari, C.; Jung, M.; Seemann, R.; Hub, J.S.; Schrul, B.; Fleury, J.B. Lipid Droplets Embedded in a Model Cell Membrane Create a Phospholipid Diffusion Barrier. *Small* **2022**, *18*, 2106524. [CrossRef]
27. Asfia, S.; Seemann, R.; Fleury, J.B. Phospholipids diffusion on the surface of model lipid droplets. *Biochim. Biophys. Acta (BBA)-Biomembr.* **2022**, *1865*, 184074. [CrossRef]
28. Fouillen, L.; Maneta-Peyret, L.; Moreau, P. ER Membrane Lipid Composition and Metabolism: Lipidomic Analysis. *Methods Mol. Biol.* **2018**, *1691*, 125–137. [CrossRef]

29. Ferrari, P.A.; Goldstein, S.; Lebowitz, J.L. Diffusion, Mobility and the Einstein Relation. In *Statistical Physics and Dynamical Systems: Rigorous Results*; Fritz, J.; Jaffe, A.; Szász, D., Eds.; Progress in Physics; Birkhäuser: Boston, MA, USA, 1985; pp. 405–441. [CrossRef]
30. Choudhary, V.; Golani, G.; Joshi, A.S.; Cottier, S.; Schneiter, R.; Prinz, W.A.; Kozlov, M.M. Architecture of lipid droplets in endoplasmic reticulum is determined by phospholipid intrinsic curvature. *Curr. Biol.* **2018**, *28*, 915–926.e9. [CrossRef]
31. de Gennes, P.G. Wetting: Statics and dynamics. *Rev. Mod. Phys.* **1985**, *57*, 827–863. [CrossRef]
32. Takei, T.; Yaguchi, T.; Fujii, T.; Nomoto, T.; Toyota, T.; Fujinami, M. Measurement of membrane tension of free standing lipid bilayers via laser-induced surface deformation spectroscopy. *Soft Matter* **2015**, *11*, 8641–8647. [CrossRef] [PubMed]
33. Lolicato, F.; Saleppico, R.; Griffo, A.; Pokrandt, B.; Müller, H.M.; Ewers, H.; Hähl, H.; Fleury, J.B.; Seemann, R.; Brügger, B.; et al. Cholesterol Promotes Both Head Group Visibility and Clustering of PI(4,5)P2 Driving Unconventional Secretion of Fibroblast Growth Factor 2. *bioRxiv* **2021**. [CrossRef]
34. Soumpasis, D.M. Theoretical analysis of fluorescence photobleaching recovery experiments. *Biophys J.* **1983**, *41*, 95–97. [CrossRef] [PubMed]
35. Zoni, V.; Nieto, V.; Endter, L.J.; Risselada, H.J.; Monticelli, L.; Vanni, S. To Bud or Not to Bud: A Perspective on Molecular Simulations of Lipid Droplet Budding. *Front. Mol. Biosci.* **2019**, *6*, 124. [CrossRef]
36. Zoni, V.; Khaddaj, R.; Campomanes, P.; Thiam, A.R.; Schneiter, R.; Vanni, S. Pre-existing bilayer stresses modulate triglyceride accumulation in the ER versus lipid droplets. *eLife* **2021**, *10*, e62886. [CrossRef]
37. Caillon, L.; Nieto, V.; Gehan, P.; Omrane, M.; Rodriguez, N.; Monticelli, L.; Thiam, A.R. Triacylglycerols sequester monotopic membrane proteins to lipid droplets. *Nat. Commun.* **2020**, *11*, 3944. [CrossRef]
38. Heo, P.; Ramakrishnan, S.; Coleman, J.; Rothman, J.E.; Fleury, J.B.; Pincet, F. Highly Reproducible Physiological Asymmetric Membrane with Freely Diffusing Embedded Proteins in a 3D-Printed Microfluidic Setup. *Small* **2019**, *15*, 1900725. [CrossRef]
39. Fader Kaiser, C.M.; Romano, P.S.; Vanrell, M.C.; Pocognoni, C.A.; Jacob, J.; Caruso, B.; Delgui, L.R. Biogenesis and Breakdown of Lipid Droplets in Pathological Conditions. *Front. Cell Dev. Biol.* **2022**, *9*, 3870. [CrossRef]

Appendix (III) Influence of PLIN5 and Lipid Composition on Lipid Droplet Contact Sites with other Organelles

Authors: Mahsa Mohammadian‡, Shima Asfia‡ and Ralf Seemann

‡ Authors contributed equally

Experimental Physics, Saarland University, 66123 Saarbrücken, Germany

Author contributions:

Shima Asfia & Mahsa Mohammadian: Investigation, Formal analysis, Software, Writing - original draft. Ralf Seemann: Conceptualization, Funding acquisition, Supervision, Writing - review and editing.

Abstract:

Lipid droplets (LDs) play an important role in cellular energy storage and supplying components for the structure of organelle membranes. As the biology of lipid droplets relies on close coordination and communication with other cellular organelles, studying their interactions is crucial. The role of the protein perilipin 5 (PLIN5), known to mediate the regulation of LD dynamics and metabolism in cells, is of particular interest. To investigate the impact of PLIN5 on the formation of contact sites between LDs and a bilayer, LDs composed of triolein and surrounded by a DOPE or DOPC monolayer with or without PLIN5 are brought in contact with large unilamellar vesicles (LUVs) composed of a DOPC and DOPE mixture close to the ER membrane composition. To detect different contact interactions of the LUVs with the monolayer coating the LDs, the LUVs were double fluorescence labeled, on the one hand, with a rhodamine-labeled phospholipid in the bilayer and, on the other hand, with water-soluble Cy5-labeled dextran in the core. When spots with both fluorescence dyes are observed on the surface of the LDs, the LUVs stay in contact with the LDs and protein tethers can be assumed to have formed between LUVs and LDs. When instead a uniform colored 'rhodamine signal' appears on the surface of the LDs, the fluorescent phospholipid of the LUVs merged with LDs monolayer. Our study investigates the influence of lipid composition and protein interactions on the formation of lipid bridges and protein tethers between LDs and the membranes of other organelles.

Influence of PLIN5 and Lipid Composition on Lipid Droplet Contact Sites with other Organelles

Mahsa Mohammadian[1,‡], Shima Asfia[1,‡] and Ralf Seemann[1,*]

June 20, 2025

Department of Experimental Physics and Center for Biophysics, Saarland University, Saarbrücken, Germany
‡ Authors contributed equally
* Correspondance to: r.seemann@physik.uni-saarland.de

Abstract

Lipid droplets (LDs) play an important role in cellular energy storage and supplying components for the structure of organelle membranes. As the biology of lipid droplets relies on close coordination and communication with other cellular organelles, studying their interactions is crucial. The role of the protein perilipin 5 (PLIN5), known to mediate the regulation of LD dynamics and metabolism in cells, is of particular interest. To investigate the impact of PLIN5 on the formation of contact sites between LDs and a bilayer, LDs composed of triolein and surrounded by a DOPE or DOPC monolayer with or without PLIN5 are brought in contact with large unilamellar vesicles (LUVs) composed of a DOPC and DOPE mixture close to the ER membrane composition. To detect different contact interactions of the LUVs with the monolayer coating the LDs, the LUVs were double fluorescence labeled, on the one hand, with a rhodamine-labeled phospholipid in the bilayer and, on the other hand, with water-soluble Cy5-labeled dextran in the core. When spots with both fluorescence dyes are observed on the surface of the LDs, the LUVs stay in contact with the LDs and protein tethers can be assumed to have formed between LUVs and LDs. When instead a uniform colored 'rhodamine signal' appears on the surface of the LDs, the fluorescent phospholipid of the LUVs merged with LDs monolayer. Our study investigates the influence of lipid composition and protein interactions on the formation of lipid bridges and protein tethers between LDs and the membranes of other organelles.

Keywords: Lipid droplet, Large unilamellar vesicle, Contact site, Lipidic bridge, Protein tether, Perilipin 5, PLIN5

1 Introduction

Lipid droplets (LDs) are known to serve as reservoirs for neutral lipids and play an important role in the control of energy and lipid metabolic processes, membrane biogenesis and the synthesis of signaling molecules. LDs consist of the neutral lipids in their core, primarily triacylglycerol (TAG) and sterol esters (SE), which are surrounded by a phospholipid monolayer with different proteins decorating the surface [1, 2], see Fig. 1. To fulfill their crucial function, lipid droplets are known to interact extensively with various cellular organelles [3, 4]. One of the most significant interaction sites is the endoplasmic reticulum (ER), which serves as a key platform for LD formation, expansion, and budding. Another important organelle in this network is the mitochondrion, where LDs supply fatty acids derived from stored neutral lipids for oxidation and energy production[5]. Additionally, peroxisomes establish specialized contact sites with LDs, known as pexopodia [6]. These structures enable peroxisomal protrusions, lined by the inner bilayer leaflet of the peroxisome, to extend into the lipid droplet core. Notably, pexopodia are enriched with components involved in β oxidation, highlighting their potential role in lipid metabolism [7].

When two organelles are in close proximity (typically 10-70 nm apart) and physically linked, they form contact sites that enable the efficient and rapid exchange of different molecules through active or passive transport [1, 5], Fig. 2. The formed contact sites are typically protein-based structures that

are known as "molecular tethers" [8]. These protein tethers play an important role in keeping the interacting organelles at a specific distance, thereby establishing the framework for the architecture of the contact site (Fig. 2) [1]. These contact sites contain various proteins, categorized as either "effectors," which carry out specific functions like material transfer, or "regulators," which modulate the contact site based on the cell's functional state [1, 8].

Although protein tethers are the main topic in the field of contact site investigation, also lipidic structures forming connections between LDs and the endoplasmic reticulum (ER), and in some cases with other organelles, have been frequently observed [9, 10]. These findings have drawn attention to the possible involvement of lipidic bridges in facilitating the formation of LD contact sites [3]. Lipidic bridges can serve as channels connecting the phospholipid membrane of LDs to the outer leaflet of the phospholipid bilayer of the ER (Fig. 2). These architectural features have been documented across various cell types and have been reported to establish connections between nearly all intracellular LDs and the ER in yeast [11]. Since these lipidic bridges may not be rigid enough for inter-organelle contacts, they probably coexist with, rather than replacing, protein-based tethers, which are essential for maintaining structural integrity of these contact sites [1]. Studies have shown that similar lipidic bridges have been seen mostly in the LD-Peroxisome connections and LD-ER bridges, which can form de novo, reconnecting LDs that were previously detached from the ER. This suggests that these bridges have a more active role than just being leftovers from the LD biogenesis process [7, 12, 13].

In mammalian cells, the predominant component of the phospholipid monolayer covering an LD is phosphatidylcholine (DOPC), which can make up up to 60 % of the total membrane composition. After DOPC, the next most common phospholipid is phosphatidylethanolamine (DOPE) and, with smaller amounts, phosphatidylinositol (DOPI), phosphatidylserine (DOPS), and sphingomyelin (SM) [14]. The phospholipid monolayer of a LD is enriched with specific proteins [1, 2] that facilitate various cellular processes. So far, it has been shown that there are different types and classes of proteins decorating LDs and two of these classes have been broadly studied. Class I proteins, which possess hydrophobic hairpin motifs are thought to localize into LDs from the ER during their formation. Class II proteins access the LD's surface directly from the cytosol through amphipathic helices or via multiple amphipathic and hydrophobic helices [15, 16].

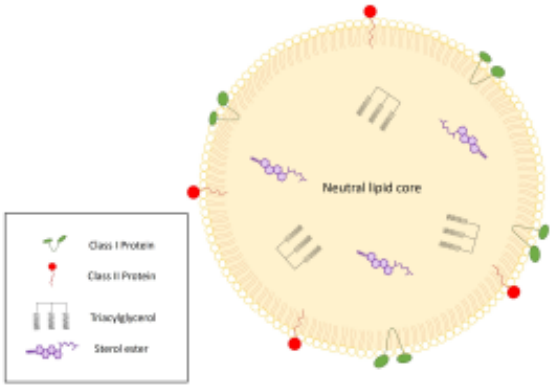

Figure 1: Schematic of a LD including various protein classes embedded in the phospholipid monolayer decorating the LD.

There are several proteins contained in the LD coating that are associated with the connection of LDs with different organelles. Among these, Seipin and Perilipin 5 (PLIN5) (one of the known proteins from PLIN family protein) are both well-conserved transmembrane proteins, which show their importance in the cellular energy homeostasis [3, 17]. Seipin, classified as a class I LD-associated proteins has been studied as a contact protein between LD and ER contact sites. PLIN5 , a class II protein is known for the LD-mitochondria connection and recognized as a LD targeting protein [18].

PLIN5, on one hand, helps to stabilize lipid droplets, preventing their coalescence and fusion and is involved in the storage of lipids within the LDs [19, 20]. On the other hand, PLIN5 helps to keep triglycerides and other neutral lipids safely stored inside the lipid droplet, protecting them from

degradation [21]. Besides, PLIN5 plays a role in regulating lipolysis, the process by which stored triglycerides are broken down into fatty acids and released into the cell for energy production. It can either promote or inhibit lipolysis depending on the cellular context and signaling pathways [22]. Moreover, PLIN5 in addition to having a potential role in LD budding, can interact with other proteins involved in lipid metabolism and intracellular signaling pathways [23, 24]. These proteins can interact with other proteins of the PLIN family, such as PLIN1 and PLIN2 to regulate LD function collectively [23, 25].

Studies have shown that mutation and dysfunction of LD proteins such as perilipin family members and seipin can be associated with several human diseases, including obesity, diabetes, steatohepatitis and lipodystrophy [26, 27, 28]. An in-depth understanding of the functionality of the LD contact site network holds significant promise in shedding light on the underlying mechanisms of lipid-associated pathological conditions [29, 30].

In this study, LDs were brought into contact with LUVs containing a phospholipid dye (rhodamine) in their outer membrane and a water-soluble dye (Cy5 labeled dextran) in their core (Fig. 2). After incubation, the mixture was observed in a microfluidic channel with a fluorescence microscope. Our findings reveal that LDs coated with DOPE or DOPC form lipidic bridges with LUVs, leading to membrane fusion, while the probability for fusion is substantially increased for DOPE coated LDs. When adding PLIN5 to the phospholipid LD coating, LUVs are kept in close contact to the LDs, indicating protein tethers and the fusion events are reduced. Furthermore, we studied different phospholipids in LD monolayers to investigate their role in fusion tendencies.

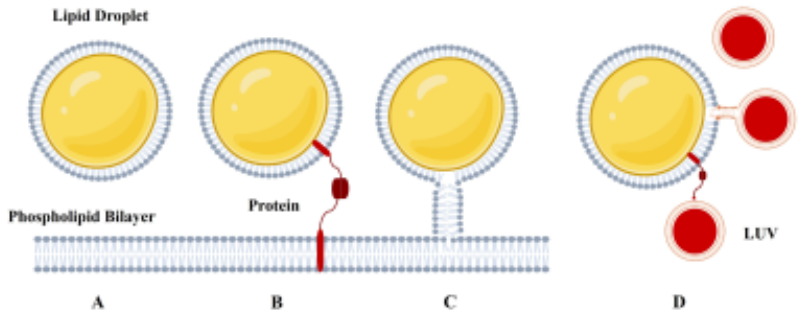

Figure 2: Schematic of possible ways of LD contact sides with and without protein connection. (A) LDs and Phospholipid bilayer in close proximity (B) Protein tethers connecting LDs with phospholipid bilayer (C) Lipidic bridge connecting LDs with phospholipid bilayer (D) in vitro method to model LDs contact sites with LUVs.

2 Results and Discussion

2.1 Lipidic bridge in LD's contact sites with LUVs

Figure 3 shows results of the first set of experiments where DOPE or DOPC covered LDs were brought in contact with LUVs composed of DOPC and DOPE with a molar ratio of 60:40. After the incubation time of 60 min, a certain fraction of the initially invisible LDs turned orange showing a rhodamine fluorescent signal. A parallel Cy5 fluorescent signal from the core of the LUVs could not be observed. This indicates that lipidic bridges between LDs and LUVs were formed and rhodamine-PE was transferred into the LD's monolayer. In our experiments, it remains unclear whether the LUVs fully fused with the LDs, completely donating their phospholipid bilayer to the LD monolayer, or if they only made short contact, exchanged some phospholipids, and then detached. However, the lack of Cy5 signal on the surface of the LDs clearly indicates that the LUVs do not remain attached, suggesting that the formed lipidic bridges are transient.

To evaluate how lipid composition affects the formation of lipidic bridges, defined here as the transfer of rhodamine-PE from LUVs to the LD monolayer, we compared LDs coated with DOPC and DOPE monolayers. After 60 minutes of incubation, only about 35–40% of the DOPC-coated LDs displayed rhodamine fluorescence, indicating phospholipid uptake from the LUVs. In contrast, approximately 95% of DOPE-coated LDs showed strong rhodamine signals, suggesting a significantly higher fusion efficiency, see Fig. 4. This difference in fusion probability of the LDs aligns with the larger surface tension of a DOPE covered triolein-water interface with respect to a DOPC covered triolein-water interface of $\approx 2.3\,mN/m$ and $1.5\,mN/m$, respectively, and the higher diffusion rate of DOPE phospholipids in comparison with DOPC phospholipids of $\approx 8\,\mu m^2/s$ and $18\,\mu m^2/s$, respectively [31, 32].

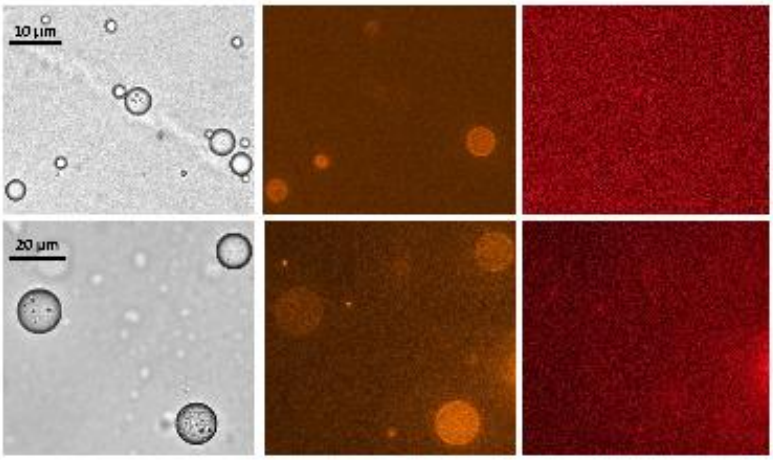

Figure 3: Fusion behavior of LD's monolayer with LUVs after the incubation time. LD's monolayer consists of DOPC (top row) and DOPE (bottom row). The different columns show the same spot of one sample with different microscopy contrast methods, respectively fluorescent wavelengths. (left) Bright field micrographs, (middle) rhodamine dye channel and (right) Cy5 dye channel.

2.2 Role of PLIN5 in LD contact sites

To additionally investigate the role of PLIN5 proteins in forming contact sites between LDs and LUVs, a similar set of experiments was conducted but with PLIN5 contained in the phospholipid monolayer covering the LDs. Similarly to the previous experiments, we also find LDs that show a fairly homogeneous rhodamine signal after the incubation time, Fig. 5. But the probability of finding LDs with a homogeneous rhodamine signal dropped to 5 %, and 70 %, respectively. In the presence of PLIN5, the total probability of phospholipid uptake from LUVs decreased by factors of 1.3 for DOPE-coated LDs and 8 for DOPC-coated LDs, respectively.

In this set of experiments with PLIN5, in comparison to the previous condition without PLIN5, we additionally find LDs with distinct individual fluorescence spots with both rhodamine and Cy5 signal, which are not visible in the bright field micrographs. These bright spots can thus be identified as LUVs that remain attached to the LDs by so-called protein tethers without undergoing fusion. While in previous observations lipidic bridges formed only transiently, protein tethers remained stable over a longer period of time.

The qualitative observation of these LUVs that are attached to the LDs, together with the quantitative observation of a smaller percentage of LDs that fused with LUVs suggests that PLIN5 stabilizes LUV-LD contacts without promoting fusion, or even prevents fusion of LUVs with LDs. This observation strongly supports the interpretation of PLIN5-mediated interactions at LD-LUV contact sites, known as protein tethers (see Fig. 5) that keep the LUVs at a certain distance and thus rather prohibit unspecific fusion.

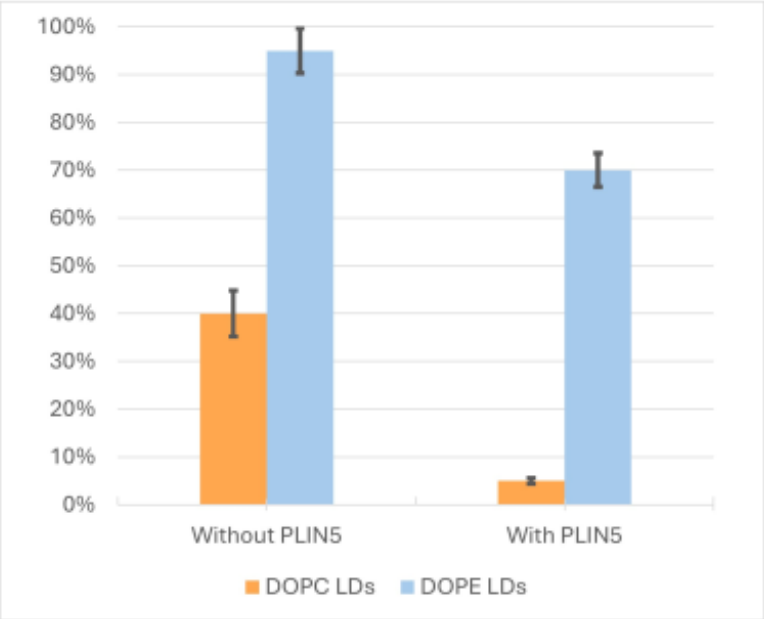

Figure 4: Probability of LD and LUV fusion as function of the LD's monolayer. *Left* LDs coated with DOPC (orange) and DOPE (blue), *right* LDs coated with DOPC (orange) and DOPE (blue) and with PLIN5. These statistics were obtained by counting the observed LDs in all experiments.

3 Conclusion and Outlook

In this study, we introduced a model system to investigate the contact sites of LDs and LUVs, representing the interaction of LDs with the bilayer membrane of cell organelles. To test the effect of the LD's membrane, respectively phospholipid composition, we conducted experiments with two different phospholipid compositions (DOPC and DOPE) with and without additional PLIN5. While DOPE enhances the formation of transient lipidic bridges and thus the fusion probability of LUVs with LDs, PLIN5 leads to the formation of protein tethers that keeps the LUVs at a fixed distance and strongly reduces the fusion probability of the LUVs with LDs. Our observations also demonstrate that lipidic bridges form more often or faster with LDs composed of DOPE compared to DOPC, which can be attributed to the characteristics of DOPC and DOPE phospholipids. The increased fusion probability for DOPE covered LDs can be attributed to the higher lipid mobility and reduced packing density compared to DOPC [33]. These differences in mobility or packing density, respectively, can be understood by the truncated conical geometry of DOPE and the cylindrical geometry of DOPC [31, 33]. Their impact on the fusion probability emphasizes the significance of the biophysical properties of lipid monolayers in mediating inter-organellar communication and structural interactions.According to our results, the presence of PLIN5 in the LDs' monolayer clearly enables protein-mediated tethering, which keeps vesicles in close contact with the LD's surface but prevents their fusion.

Our findings thus support the idea that PLIN5 plays a regulatory role in forming functional connections between LDs and other organelles, such as mitochondria, potentially influencing lipid metabolism and energy homeostasis. These insights advance our understanding of the molecular mechanisms regulating LD interactions and provide a foundation for future research into the dynamic regulation of organelle communication. Finally, understanding how these molecular interactions contribute to broader cellular processes, such as lipid metabolism, energy homeostasis, and signal transduction, could pave the way for therapeutic interventions targeting metabolic disorders and related diseases.

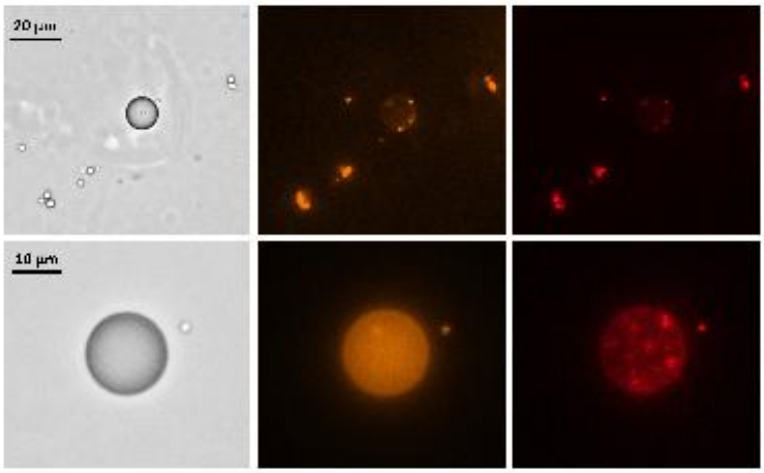

Figure 5: Fusion behavior of PLIN5-decorated LDs with LUVs after the incubation time. LD's monolayer consists of DOPC (top row) and DOPE (bottom row), plus PLIN5. Different columns show bright field images (left), rhodamine dye channel (middle) and Cy5 channel (right). The different columns show the same spot of one sample with different microscopy contrast methods, respectively fluorescent wavelengths.

4 Materials & Methods

4.1 Molecules

1,2-Dioleoyl-sn-glycero-3-phosphocholine (DOPC), 1,2-dioleoyl-sn-glycero-3-phospho-ethanolamine (DOPE) and 1,2-dioleoyl-snglycero-3-phosphoethanolamine-N-(lissamine rhodamine B sulfonyl) (rhodamine-PE) were acquired from Avanti Polar Lipids and Cy5 labeled dextran was purchased from Creative Biolabs. Glyceryl trioleate (triolein, T7140) and squalene (S3626) were purchased from Sigma-Aldrich. Recombinant Bovine Perilipin-5 (PLIN5) were ordered from Cusabio Technology LLC. For microfluidic device preparation, Sylgard 184 Silicone Elastomer Kit (PDMS) was obtained from Dow Corning. In this manuscript, buffer solution refers to 150 mM potassium chloride (KCl) purchased from Sigma-Aldrich. All the phospholipid stocks were dissolved in chloroform and stored at $-20\,^{\circ}C$.

4.2 3D-Chip Fabrication

The layout of the microfluidic structure was designed using AutoCAD software. The design consisted of one straight channel with dimensions $15\,mm \times 1\ mm \times 100\,\mu m$ (length × width × height). The positive mold of this structure was fabricated by standard contact photolithography using the negative photoresist SU-8 on 2 inch Si-wafer. Sylgard 184 was prepared following the instructions of the manufacturer including a thorough mixing and degassing period of 15 minutes. Subsequently, the degassed PDMS mixture was poured directly onto the SU-8 photoresist master and cured at a temperature of $100\,^{\circ}C$ for a duration of 2 hours. Upon completion of the curing process, the cured PDMS material was separated from the SU-8 mold and inlet and outlet holes were punched into the PDMS at the two ends of the bottom channels. The thus prepared PDMS microchip was sealed with a glass cover slip using plasma bonding (Diener Electronics). The assembled microfluidic device was heated at $95\,^{\circ}C$ for 1 hour to increase the bonding strength between PDMS and glass.

4.3 Large unilamellar vesicle (LUV) preparation

Large unilamellar vesicles (LUVs) were prepared using DOPC and DOPE in a 60:40 molar ratio, incorporating two fluorescent dyes (Rhod-PE and Dextran-Cy5) at 2% of the total phospholipid concentration, to facilitate monitoring the vesicles and distinguishing different interaction pathways with

LDs. rhodamine-PE is a fluorescent-labeled phospholipid and Dextran-Cy5 is a fluorescent-labeled sugar, which enable them to locate on the surface and in the core of LUVs, respectively. Lipids and fluorescence dyes were mixed with the previously mentioned molar ratios and with a total concentration of 1 mg/mL in chloroform and vacuum dried for about one hour to ensure complete evaporation of the solvent. The dried lipid powders were re-suspended in 150 mM KCl buffer by pipetting and vortexing. Using an Avanti mini extruder, the suspension was subsequently passed 10 times through a 1 μm polycarbonate filter (Avanti) at 50 °C, according to the company's instructions. To optimize the number of vesicles for each experiment, serial dilutions of LUVs were prepared and tested prior to the experiments. A 1:100 dilution of the original solution showed better visibility of the LUVs with minimal background noise and resulted in a final concentration of 8.67×10^8 vesicles per mL of KCl buffer.

4.4 Lipid droplet (LD) preparation

For the preparation of the lipid droplets, a chloroform droplet containing 2 w% of phospholipid (DOPC or DOPE phospholipid based on the experiment) was dried in a glass falcon under vacuum for 60 minutes to fully evaporate the existing chloroform in the sample. To the dried phospholipids, 250 μL triolein oil and for some cases, where PLIN5 was tested in the experiments, 4 μL of 0.1 mg/mL protein solution (prepared as recommended by the company instructions) were added. In the next step, the mixture was diluted with (8-10) mL KCl buffer, then a solution of lipid–oil droplets in buffer was formed by mixing the suspension with a magnetic stirrer for about 5 minutes at 250 rpm. The size of lipid droplets was controlled by the intensity and the speed of the stirrer; longer and faster stirring resulted in smaller sizes of LDs. To be able study the LDs individually and more conveniently under our fluorescence microscope, the mentioned time and speed were chosen that resulted in LDs with a size range of 5μm - 20 μm. To observe the lipid droplets in contact with LUVs under the fluorescence microscope, 10 μL of the LUV solution was added to 60 μL of LDs dispersion in a vial (6:1 volume ratio) and incubated for 60 minutes. Afterwards, the LD-LUV solution was injected by pipetting into the microchip channel and observed by optical fluorescence microscopy.

4.5 Inverted fluorescence microscopy

Fluorescence microscopy images were acquired with an inverted AXIO Observer 7 microscope (Carl Zeiss Microscopy GmbH) equipped with a fluorescence LED (Colibri7) and a CMOS camera (Axiocam 712). The fluorescence imaging was conducted using the filter excitation wavelengths of 538-562 nm (for Rhodamine) and 614-647 nm (for Cy5) and the filter emission wavelengths of 570-640 nm and 659-759 nm, respectively. The images were obtained with a 40× objective (NA: 0.95) and 150 ms exposure time. It is worth mentioning that all experiments were performed at a room temperature of 23 °C.

5 Credit authorship contribution statement

Shima Asfia & Mahsa Mohammadian: Investigation, Formal analysis, Software, Writing – original draft. **Ralf Seemann**: Conceptualization, Funding acquisition, Supervision, Writing – review and editing.

6 Declaration of competing interest

The authors declare that they have no known competing financial interests or personal relationships that could have appeared to influence the work reported in this paper.

7 Acknowledgments

We would like to thank Jean-Baptiste Fleury, who came up with the idea for this project. Financial support is acknowledged by the Deutsche Forschungsgemeinschaft (DFG), Germany, SFB1027 (project B4).

References

[1] M. Schuldiner and M. Bohnert, "A different kind of love–lipid droplet contact sites," *Biochimica et Biophysica Acta (BBA)-Molecular and Cell Biology of Lipids*, vol. 1862, no. 10, pp. 1188–1196, 2017. doi: 10.1016/j.bbalip.2017.06.005.

[2] M. F. Renne and H. Hariri, "Lipid droplet-organelle contact sites as hubs for fatty acid metabolism, trafficking, and metabolic channeling," *Frontiers in cell and developmental biology*, vol. 9, p. 726261, 2021. doi: 10.3389/fcell.2021.726261.

[3] M. Bohnert, "Tethering fat: tethers in lipid droplet contact sites," *Contact*, vol. 3, p. 2515256420908142, 2020. doi: 10.1177/2515256420908142.

[4] C. J. Stefan, W. S. Trimble, S. Grinstein, G. Drin, K. Reinisch, P. De Camilli, S. Cohen, A. M. Valm, J. Lippincott-Schwartz, T. P. Levine, *et al.*, "Membrane dynamics and organelle biogenesis—lipid pipelines and vesicular carriers," *BMC biology*, vol. 15, pp. 1–24, 2017. doi: 10.1186/s12915-017-0432-0.

[5] P.-C. Liao, E. J. Yang, T. Borgman, I. R. Boldogh, C. N. Sing, T. C. Swayne, and L. A. Pon, "Touch and go: membrane contact sites between lipid droplets and other organelles," *Frontiers in Cell and Developmental Biology*, vol. 10, p. 852021, 2022. doi: 10.3389/fcell.2022.852021.

[6] M. A. Kalutsky, T. R. Galimzyanov, and R. J. Molotkovsky, "A model of lipid monolayer–bilayer fusion of lipid droplets and peroxisomes," *Membranes*, vol. 12, no. 10, p. 992, 2022. doi: 10.3390/membranes12100992.

[7] D. Binns, T. Januszewski, Y. Chen, J. Hill, V. S. Markin, Y. Zhao, C. Gilpin, K. D. Chapman, R. G. Anderson, and J. M. Goodman, "An intimate collaboration between peroxisomes and lipid bodies," *The Journal of cell biology*, vol. 173, no. 5, p. 719, 2006. doi: 10.1083/jcb.200511125.

[8] M. Eisenberg-Bord, N. Shai, M. Schuldiner, and M. Bohnert, "A tether is a tether is a tether: tethering at membrane contact sites," *Developmental cell*, vol. 39, no. 4, pp. 395–409, 2016. doi: 10.1016/j.devcel.2016.10.022.

[9] E. Quon and C. T. Beh, "Membrane contact sites: complex zones for membrane association and lipid exchange," *Lipid Insights*, vol. 8, pp. LPI–S37190, 2015. doi: 10.4137/LPI.S37190.

[10] V. Choudhary and R. Schneiter, "A unique junctional interface at contact sites between the endoplasmic reticulum and lipid droplets," *Frontiers in cell and developmental biology*, vol. 9, p. 650186, 2021. doi: 10.3389/fcell.2021.650186.

[11] N. Jacquier, V. Choudhary, M. Mari, A. Toulmay, F. Reggiori, and R. Schneiter, "Lipid droplets are functionally connected to the endoplasmic reticulum in saccharomyces cerevisiae," *Journal of cell science*, vol. 124, no. 14, pp. 2424–2437, 2011. doi: 10.1242/jcs.076836.

[12] F. Wilfling, A. R. Thiam, M.-J. Olarte, J. Wang, R. Beck, T. J. Gould, E. S. Allgeyer, F. Pincet, J. Bewersdorf, R. V. Farese Jr, *et al.*, "Arf1/copi machinery acts directly on lipid droplets and enables their connection to the er for protein targeting," *elife*, vol. 3, p. e01607, 2014. doi: 10.7554/eLife.01607.

[13] A. R. Thiam, B. Antonny, J. Wang, J. Delacotte, F. Wilfling, T. C. Walther, R. Beck, J. E. Rothman, and F. Pincet, "Copi buds 60-nm lipid droplets from reconstituted water–phospholipid–triacylglyceride interfaces, suggesting a tension clamp function," *Proceedings of the National Academy of Sciences*, vol. 110, no. 33, pp. 13244–13249, 2013. doi: 10.1073/pnas.1307685110.

[14] K. Tauchi-Sato, S. Ozeki, T. Houjou, R. Taguchi, and T. Fujimoto, "The surface of lipid droplets is a phospholipid monolayer with a unique fatty acid composition," *Journal of Biological Chemistry*, vol. 277, no. 46, pp. 44507–44512, 2002. doi: 10.1074/jbc.M207712200.

[15] N. Kory, R. V. Farese, and T. C. Walther, "Targeting fat: mechanisms of protein localization to lipid droplets," *Trends in cell biology*, vol. 26, no. 7, pp. 535–546, 2016. doi: 10.1016/j.tcb.2016.02.007.

[16] K. Bersuker and J. A. Olzmann, "Establishing the lipid droplet proteome: Mechanisms of lipid droplet protein targeting and degradation," *Biochimica et Biophysica Acta (BBA)-Molecular and Cell Biology of Lipids*, vol. 1862, no. 10, pp. 1166–1177, 2017. doi: 10.1016/j.bbalip.2017.06.006.

[17] S. Y. Dejgaard and J. F. Presley, "Interactions of lipid droplets with the intracellular transport machinery," *International Journal of Molecular Sciences*, vol. 22, no. 5, p. 2776, 2021. doi: 10.3390/ijms22052776.

[18] H. Wang, U. Sreenivasan, H. Hu, A. Saladino, B. M. Polster, L. M. Lund, D.-w. Gong, W. C. Stanley, and C. Sztalryd, "Perilipin 5, a lipid droplet-associated protein, provides physical and metabolic linkage to mitochondria," *Journal of lipid research*, vol. 52, no. 12, pp. 2159–2168, 2011. doi: 10.1194/jlr.M017939.

[19] S. R. Bartholomew, E. H. Bell, T. Summerfield, L. C. Newman, E. L. Miller, B. Patterson, Z. P. Niday, W. E. Ackerman IV, and J. T. Tansey, "Distinct cellular pools of perilipin 5 point to roles in lipid trafficking," *Biochimica et Biophysica Acta (BBA)-Molecular and Cell Biology of Lipids*, vol. 1821, no. 2, pp. 268–278, 2012. doi: 10.1016/j.bbalip.2011.10.017.

[20] X. Zhang, W. Xu, R. Xu, Z. Wang, X. Zhang, P. Wang, K. Peng, M. Li, J. Li, Y. Tan, *et al.*, "Plin5 bidirectionally regulates lipid metabolism in oxidative tissues," *Oxidative Medicine and Cellular Longevity*, vol. 2022, no. 1, p. 4594956, 2022. doi: 10.1155/2022/4594956.

[21] J. R. Skinner, T. M. Shew, D. M. Schwartz, A. Tzekov, C. M. Lepus, N. A. Abumrad, and N. E. Wolins, "Diacylglycerol enrichment of endoplasmic reticulum or lipid droplets recruits perilipin 3/tip47 during lipid storage and mobilization," *Journal of Biological Chemistry*, vol. 284, no. 45, pp. 30941–30948, 2009. doi: 10.1074/jbc.M109.013995.

[22] V. I. Gallardo-Montejano, G. Saxena, C. M. Kusminski, C. Yang, J. L. McAfee, L. Hahner, K. Hoch, W. Dubinsky, V. A. Narkar, and P. E. Bickel, "Nuclear perilipin 5 integrates lipid droplet lipolysis with pgc-1α/sirt1-dependent transcriptional regulation of mitochondrial function," *Nature communications*, vol. 7, no. 1, p. 12723, 2016. doi: 10.1038/ncomms12723.

[23] A. R. Kimmel and C. Sztalryd, "Perilipin 5, a lipid droplet protein adapted to mitochondrial energy utilization," *Current opinion in lipidology*, vol. 25, no. 2, pp. 110–117, 2014. doi: 10.1097/MOL.0000000000000057.

[24] H. Wang, M. Bell, U. Sreenevasan, H. Hu, J. Liu, K. Dalen, C. Londos, T. Yamaguchi, M. A. Rizzo, R. Coleman, *et al.*, "Unique regulation of adipose triglyceride lipase (atgl) by perilipin 5, a lipid droplet-associated protein," *Journal of Biological Chemistry*, vol. 286, no. 18, pp. 15707–15715, 2011. doi: 10.1074/jbc.M110.207779.

[25] P. Chandrasekaran, S. Weiskirchen, and R. Weiskirchen, "Perilipins: A family of five fat-droplet storing proteins that play a significant role in fat homeostasis," *Journal of Cellular Biochemistry*, vol. 125, no. 6, p. e30579, 2024. doi: 10.1002/jcb.30579.

[26] M. Bosma, L. Sparks, G. Hooiveld, J. Jorgensen, S. Houten, P. Schrauwen, S. Kersten, and M. Hesselink, "Overexpression of plin5 in skeletal muscle promotes oxidative gene expression and intramyocellular lipid content without compromising insulin sensitivity," *Biochimica et Biophysica Acta (BBA)-Molecular and Cell Biology of Lipids*, vol. 1831, no. 4, pp. 844–852, 2013. doi: 10.1016/j.bbalip.2013.01.007.

[27] S. Gandotra, C. Le Dour, W. Bottomley, P. Cervera, P. Giral, Y. Reznik, G. Charpentier, M. Auclair, M. Delépine, I. Barroso, *et al.*, "Perilipin deficiency and autosomal dominant partial lipodystrophy," *New England Journal of Medicine*, vol. 364, no. 8, pp. 740–748, 2011. doi: 10.1056/NEJMoa1007487.

[28] E. Gianazza, G. G. Papaianni, L. Brocca, C. Banfi, and A. Mallia, "Omics approaches to study perilipins and their significant biological role in cardiometabolic disorders," *International Journal of Molecular Sciences*, vol. 26, no. 2, p. 557, 2025. doi: 10.3390/ijms26020557.

[29] C. Wang, Y. Zhao, X. Gao, L. Li, Y. Yuan, F. Liu, L. Zhang, J. Wu, P. Hu, X. Zhang, *et al.*, "Perilipin 5 improves hepatic lipotoxicity by inhibiting lipolysis," *Hepatology*, vol. 61, no. 3, pp. 870–882, 2015. doi: 10.1002/hep.27409.

[30] J. Magré, M. Delépine, E. Khallouf, T. Gedde-Dahl, L. Van Maldergem, E. Sobel, J. Papp, M. Meier, A. Mégarbané, M. Lathrop, *et al.*, "Identification of the gene altered in berardinelli–seip congenital lipodystrophy on chromosome 11q13," *Nature genetics*, vol. 28, no. 4, pp. 365–370, 2001. doi: 10.1038/ng585.

[31] S. Asfia, R. Seemann, and J.-B. Fleury, "Phospholipids diffusion on the surface of model lipid droplets," *Biochimica et Biophysica Acta (BBA)-Biomembranes*, vol. 1865, no. 1, p. 184074, 2023. doi: 10.1016/j.bbamem.2022.184074.

[32] M. Jan Akhunzada, F. D'Autilia, B. Chandramouli, N. Bhattacharjee, A. Catte, R. Di Rienzo, F. Cardarelli, and G. Brancato, "Interplay between lipid lateral diffusion, dye concentration and membrane permeability unveiled by a combined spectroscopic and computational study of a model lipid bilayer," *Scientific Reports*, vol. 9, no. 1, p. 1508, 2019. doi: 10.1038/s41598-018-37814-x.

[33] J. N. Israelachvili, *Intermolecular and surface forces*. Academic press, 2011. doi: 10.1016/C2009-0-21560-1.

Appendix (IV) Deposit of Red Blood Cells at low concentrations in evaporating droplets is dominated by a central edge growth

Authors:

Vahideh Sardari [a b], Mahsa Mohammadian [b], Shima Asfia [b], Felix Maurer [b], Dia na Örüm [b], Ralf Seemann [b], Thomas John [b], Lars Kaestner [b c], Christian Wagner [b d], Maniya Maleki [a], Alexis Darras [b]

[a] Department of Physics, Institute for Advanced Studies in Basic Sciences (IASBS), Zanjan, 45137-66731, Iran

[b] Department of Experimental Physics & Center for Biophysics, Saarland University, Saarbruecken, D-66123, Germany

[c] Department of Theoretical Medicine and Biosciences, Saarland University, Homburg, D-66421, Germany

[d] Physics and Materials Science Research Unit, University of Luxembourg, Luxembourg, L-4365, Luxembourg

https://doi.org/10.1016/j.jcis.2024.10.039

Author contributions:

V. Sardari: Writing - review & editing, Writing - original draft, Visualization, Validation, Software, Methodology, Investigation, Formal analysis, Data curation, Conceptualization. M. Mohammadian: Writing - review & editing, Investigation, Data curation. S. Asfia: Writing - review & editing, Investigation, Data curation. F. Maurer: Writing - review & editing, Software, Investigation, Formal analysis, Data curation. D. Örüm: Writing - review & editing, Investigation, Data curation. R. Seemann: Writing - review & editing, Resources. Thomas John: Writing - review & editing, Software, Formal analysis. L. Kaestner: Writing - review & editing, Resources, Methodology. C. Wagner: Writing - review & editing, Resources, Funding acquisition. M. Maleki: Writing - review & editing, Formal analysis. A. Darras: Writing - review & editing, Writing - original draft, Supervision, Project administration, Methodology, Investigation, Funding acquisition, Formal analysis, Data curation, Conceptualization.

Abstract:

Evaporation of blood droplets and diluted blood samples is a topic of intensive research, as it is considered a potential low-cost diagnostic tool. So far, samples with a volume fraction down to a few percent of red blood cells have been studied, and these were reportedly dominated by a “coffee-ring” deposit. In this study, samples with lower volume fractions were used to investigate the growth of the evaporative deposit from sessile droplets in more detail. We observed that blood samples and salt solutions with less than 1% volume fraction of red blood cells are dominated by a central deposit. We characterized the growth process of this central deposit by evaporating elongated drops and determined that it is consistent with the Kardar-Parisi-Zhang process in the presence of quenched disorder. Our results showed a sensitivity of the deposit size to fibrinogen concentration and the shape of red blood cells, suggesting that this parameter could be developed into a new and cost-effective clinical marker for inflammation and red blood cell deformation.

Journal of Colloid and Interface Science 679 (2025) 939–946

Contents lists available at ScienceDirect

Journal of Colloid And Interface Science

journal homepage: www.elsevier.com/locate/jcis

Regular Article

Deposit of Red Blood Cells at low concentrations in evaporating droplets is dominated by a central edge growth

Vahideh Sardari [a,b], Mahsa Mohammadian [b], Shima Asfia [b], Felix Maurer [b], Diana Örüm [b], Ralf Seemann [b], Thomas John [b], Lars Kaestner [b,c], Christian Wagner [b,d], Maniya Maleki [a], Alexis Darras [b,*]

[a] Department of Physics, Institute for Advanced Studies in Basic Sciences (IASBS), Zanjan, 45137-66731, Iran
[b] Department of Experimental Physics & Center for Biophysics, Saarland University, Saarbruecken, D-66123, Germany
[c] Department of Theoretical Medicine and Biosciences, Saarland University, Homburg, D-66421, Germany
[d] Physics and Materials Science Research Unit, University of Luxembourg, Luxembourg, L-4365, Luxembourg

GRAPHICAL ABSTRACT

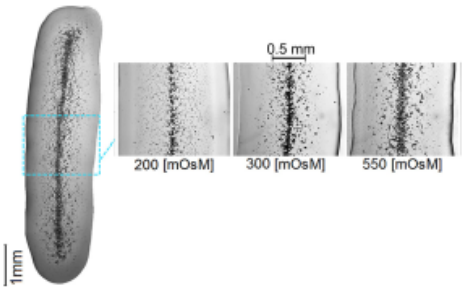

ABSTRACT

Evaporation of blood droplets and diluted blood samples is a topic of intensive research, as it is considered a potential low-cost diagnostic tool. So far, samples with a volume fraction down to a few percent of red blood cells have been studied, and these were reportedly dominated by a "coffee-ring" deposit. In this study, samples with lower volume fractions were used to investigate the growth of the evaporative deposit from sessile droplets in more detail. We observed that blood samples and salt solutions with less than 1% volume fraction of red blood cells are dominated by a central deposit. We characterized the growth process of this central deposit by evaporating elongated drops and determined that it is consistent with the Kardar-Parisi-Zhang process in the presence of quenched disorder. Our results showed a sensitivity of the deposit size to fibrinogen concentration and the shape of red blood cells, suggesting that this parameter could be developed into a new and cost-effective clinical marker for inflammation and red blood cell deformation.

* Corresponding author.
E-mail addresses: alexis.darras@uni-saarland.de, alexis.charles.darras@gmail.com (A. Darras).

https://doi.org/10.1016/j.jcis.2024.10.039
Received 1 July 2024; Received in revised form 26 September 2024; Accepted 7 October 2024
Available online 10 October 2024

1. Introduction

The formation of a dried blood stain is a phenomenon that has garnered significant research interest, with applications ranging from low-cost diagnostic methods, e.g., for tuberculosis, thalassemia, and neonatal jaundice [1,2], to forensic investigations [3,4]. In the soft matter community, the evaporation of colloidal droplets resting on a substrate, i.e., a sessile droplet, has been an area of intensive research in recent decades, following the seminal work of Deegan et al. [5]. Various mechanisms have been highlighted as fundamentally important for the final structure of the deposits, with the coffee-ring effect being omnipresent. The coffee-ring effect refers to the fact that, for a small sessile droplet of a wetting liquid with a pinned contact line, an outward flow near the contact line typically drags the particles toward the pinned edge of the droplet due to the inhomogeneous evaporation rate along the droplet's surface [5]. However, when a sufficiently high salt concentration is considered, the dominant mechanism becomes solutal Marangoni recirculation due to the gradient of salt concentration. Indeed, a significant increase in salt concentration also leads to an increase in surface tension, and concentration gradients can therefore induce a substantial gradient in surface tension, which can create a central deposit of the particles [6–8].

In the case of blood evaporative deposits, the roles of temperature [9], ambient humidity [10], the substrate's nature, and the ions and proteins present in the plasma [11,12] on the final structure have been extensively studied. Moreover, seminal studies have shown the effects of red blood cell (RBC) properties by comparing rigidified cells or spheres with healthy RBCs [13], while others have highlighted the effect of dilution by studying patterns obtained from diluted whole blood in distilled water and Phosphate Buffered Saline (PBS), down to blood concentrations of around 10% [14]. However, the detailed influence of RBC properties, such as shape and aggregability, on the deposit growth and final state remains unclear. This is particularly relevant, as previous studies have demonstrated that, in the case of solid particles, the anisotropy of colloids can modify particle aggregation regimes, reverse the deposit pattern [15], and dictate their growth dynamics [16].

As RBCs aggregate into mostly linear structures called rouleaux in the presence of certain proteins [17–19], one can hypothesize that the length of these rouleaux acts as an effective particle eccentricity, influencing the structure of the evaporative deposit. The aggregability of RBCs, i.e., their tendency to form longer rouleaux and networks with wider gaps, is known to be heavily influenced by cell rigidity and fibrinogen concentration [18,20,21].

Thus, the main objective of this study is to determine whether evaporative deposits of dilute RBC suspensions show sensitivity to RBC aggregability and shape, which could be leveraged to develop low-cost screening methods for pathological changes in RBC aggregability and shape. We focus on droplets with volume fractions $\phi < 1\%$ of RBCs (compared to the physiological level of $\phi \approx 45\%$) in plasma- and PBS-based solutions. We observed a central deposit for the various suspending liquids with isotonic osmolarities. Building on this result, we created line-shaped droplets and studied how cell shape and aggregation modify the growth and final central linear deposit. We mixed plasma with serum to modify RBC aggregation [20], while varying the osmolarity of the PBS-based suspensions to alter RBC shape. All conditions led to growth consistent with the Kardar-Parisi-Zhang process in the presence of quenched disorder (KPZQ) [16,22]. However, the final sizes of the deposits varied as a function of cell shape, volume, and aggregability, indicating that studying these patterns could potentially serve as low-cost screening indicators for deformed RBCs or abnormal aggregation levels.

2. Methods

2.1. Ethics statement

Human blood withdrawal from healthy volunteers was performed after explicitly obtaining their informed consent. Blood withdrawal and handling were conducted in accordance with the Declaration of Helsinki and approved by the ethics committee "Aerztekammer des Saarlandes" (reference No. 176/21)

2.2. Experimental protocol

Fresh blood was drawn from healthy donors via venous blood sampling into tubes containing Ethylenediamine tetraacetic acid (EDTA) and a tube for serum (S-Monovette, Sarstedt, Nümbrecht, Germany). Cells were separated from the plasma by centrifuging the EDTA tubes for 7 minutes at 3000 rcf using a fixed-angle centrifuge (Hermle Z 36 HK, Hermle, Wehingen, Germany). The unit rcf stands for Relative Centrifugal Field, expressing the centrifugal acceleration as a multiple of gravitational acceleration g. Plasma was then obtained as the supernatant and was transferred immediately after centrifugation into a clean 1.5 mL Eppendorf tube using a micropipette. Serum was collected in a similar fashion, except that the blood was allowed to clot by leaving the collection tube undisturbed at room temperature for 30 minutes, according to the serum-tube manufacturer's guidelines (S-Monovette, Sarstedt, Nümbrecht, Germany). Clotted components were then removed by centrifuging with the same protocol as for the plasma. Serum was obtained as the supernatant. Afterwards, 1 mL samples with volume fraction $\phi = 3 \times 10^{-3}$ of RBCs were prepared by suspending the packed cells in PBS ($Gibco, USA$), plasma and/or serum. Samples were kept at room temperature for the duration of the experiments (less than 6 h).

In order to investigate whether changes in RBC shapes can lead to a different growth class of the edges obtained in the deposits, we also suspended RBCs in solutions of various osmolarities. In healthy individuals, RBCs at rest typically possess a biconcave disk shape. However, the osmolarity of the surrounding medium can change the shape of the RBCs according to the stomatocyte-discocyte-echinocyte (SDE) sequence [23–25]. To that end, solutions with osmolarities of (130, 200, 300, 550, 800 mOsmol/L), with 5 mg/mL of fibrinogen to ensure aggregation between RBCs, were prepared according to the protocols described in the next paragraphs. Washed RBCs were then resuspended in each solution with the same volume fraction $\phi = 3 \times 10^{-3}$ as earlier. Representative shapes of RBCs as observed under the confocal microscope are shown in Fig. A.6.

To prepare the RBC suspensions with osmolarity lower than physiological and PBS values (≈ 300 mOsmol/L), we first diluted fibrinogen from human plasma (Product code F3879-5G, 50-70% protein, (≥ 80% of protein is clottable) Sigma Aldrich, Burlington, Massachusetts, United States) in a solution of physiological osmolarity. For stability reasons, human plasma fibrinogen is typically stored as a powder containing around 60% protein by mass, stabilized with 15% sodium citrate and 25% NaCl. We experimentally determined that an iso-osmotic solution of fibrinogen in PBS can be reproduced by using 5% distilled water for each 1 mg/mL of fibrinogen (i.e., for each $1/0.6 \approx 1.67$ mg/mL of the powder). However, due to possible heterogeneity in the powder, the osmolarity of this solution was always checked with a freezing-point osmometer (Osmomat 3000basic, Gonotec, Berlin, Germany). Since this first step may require repetition to achieve the desired concentration of fibrinogen at the correct osmolarity, and because fibrinogen dissolves faster at 300 mOsmol/Lthan in solutions of lower osmolarity, we always first prepared an iso-osmotic solution with a fibrinogen concentration of $F_i * Osm_{iso}/Osm_t$. Here, $F_t = 5$ mg/mL is the target fibrinogen concentration, $Osm_{iso} = 300$ mOsmol/L is the osmolarity of the isotonic solution, and $Osm_t < Osm_{iso}$ is the target osmolarity. The isotonic solution was then diluted with distilled water, using proportions of Osm_t/Osm_{iso} of the isotonic fibrinogen solution and $1 - Osm_t/Osm_{iso}$ of distilled water. Finally, 45 ± 5 mg/mL of Bovine Serum Albumin (BSA) (≥ 96%, Sigma Aldrich, Burlington, Massachusetts, United States) were added to the solution, both to prevent deformation of RBCs due to the glass effect and to limit salt crystallization at the end of the evaporation process. Red blood cells were then suspended in each solution following the previously described protocol.

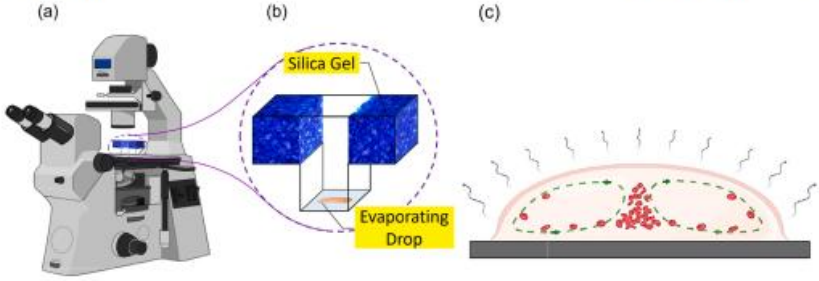

Fig. 1. Experimental setup: (a) Schematic of the inverted transmission microscope, and (b) the T-shaped drying chamber where the sample drop is placed on a microscopic slide. The slide's contact with the chamber is sealed with petroleum jelly. (c) Schematic of the solutal Marangoni flow inside the evaporating droplet, which transports the cells and gathers them in the center of the droplet. Such a flow pattern is observed in solutions with high salt concentration [6,26].

To prepare the RBC suspensions with osmolarity higher than physiological (and PBS) values (550, 800 mOsmol/L), isotonic solutions with 5 mg/mL of fibrinogen and 45 mg/mL of BSA were prepared as described previously. Afterwards, a mass $m = \Delta C\, V\, M/2$ of NaCl (> 99.5, VWR, Radnor, Pennsylvania, USA) was added to the solution, where ΔC is the required increase in osmolarity, V is the volume of the solution, and $M = 58.44$ g/mol is the molar mass of NaCl.

The final osmolarity of the solutions was always checked with a freezing-point osmometer and only used if the deviation was lower than 10% from the target value.

To create the deposits, a 5 μL pendant drop of the sample was formed at the tip of an adjustable 2-20 μL volume micropipette (Eppendorf, Hamburg, Germany). The pendant droplet was then placed on a glass slide (Microscope cover glass, ECN 631-1586, VWR, Radnor, Pennsylvania, USA), which had been previously cleaned with isopropanol and dried with compressed air (contact angle at rest of PBS was measured to be $52 \pm 3°$). To start an experiment with an elongated droplet, the 5 μL-drop was spread along 7 mm on the glass slide, using the same adjustable micropipette and a marked distance below the glass slide. To suppress the airflow and control the humidity of the environment in which the drop was placed for drying, a T-shaped hood was used. Both top sides of the hood were filled with completely dry blue silica gels to absorb humidity, as described in earlier works [7,8,27] (see Fig. 1). The glass slide with the droplet was placed under the microscope, and the T-shaped hood was adjusted on top of the glass slide with petroleum jelly (KORASILON-Paste, Kurt Obermeier GmbH, Bad Berleburg, Germany) on its base. The petroleum jelly ensured firm cohesion between the chamber and the glass slide and prevented the passage of airflow into the chamber. The drop was observed under an inverted transmission microscope (Nikon Eclipse $TE200$, Nikon, Tokyo, Japan) using a 4× objective. White light was sent through a short-pass filter with a cut-off wavelength of 450 nm (FESH0450, Thorlabs, Newton, New Jersey, USA). The filter was used to increase the contrast between the RBCs, whose absorption peak is at 415 nm due to hemoglobin, and the surrounding environment. Images of the evaporating drop were taken at intervals of 1 s using a CMOS camera (DMK 37BUX250, The Imaging Source, Charlotte, North Carolina, USA) attached to the microscope. Images were recorded until the droplet was completely dried and cracks appeared (see Appendix Fig. A.1), i.e., around 40 minutes. Examples of the obtained pictures are depicted in Fig. 2.

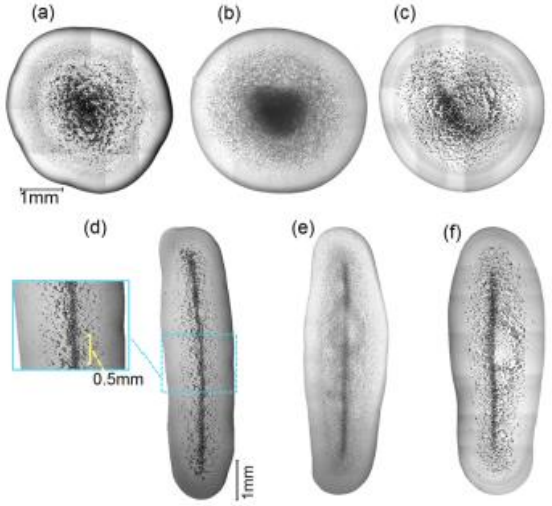

Fig. 2. Pictures of droplets from various suspensions of RBCs ($\phi = 3\,10^{-3}$), shortly before complete evaporation and the appearance of cracks (see Supp Fig. A.1 for completely dried deposits). (a-f) Whole drops were reconstructed by stitching series of pictures at higher zoom levels. (a-c) Spherical cap droplets of 5 μL; (d-f) Elongated droplets of 5 μL spread along 7 mm on the glass slide. (d) The inset shows the area of a single picture, where the deposition of red blood cells was investigated over time. Supernatants were (a and d) autologous plasma, (b and e) 4.5 mg/mL BSA solution in PBS, and (c and f) 5 mg/mL fibrinogen solution in PBS with 4.5 mg/mL BSA. The images were stitched together using ImageJ.

2.3. Image analysis

Using a homemade MATLAB code, the images of elongated droplets (see Fig. 2 (d-f)) were processed to binarize and isolate the central particle deposit. For each image, the code first averages the intensity perpendicularly to the main axis of the droplet, i.e., along y, and assesses the central position of the droplet as the y-coordinate with the minimal averaged intensity (since the RBCs have an absorption maximum at 420 nm, i.e., for blue light). The central deposit is then divided into two parts, splitting the picture at this central position, i.e., defining $y = 0$, as illustrated in Fig. 3(a). This effectively converts the central deposit into two growing edges. Analyzing both sides independently made it possible to monitor possible asymmetry in the droplet and/or deposit shape, which was used to reject data when significant differences were observed. The pictures were then binarized using an Otsu threshold on pixel intensity. Afterwards, only the connected components in contact with the central edge at $y = 0$ are considered as the growing edge, while other cells are discarded in further analysis. Furthermore, to ensure that only stable parts of the edge are considered, only pixels preserved in at least 9 out of 10 consecutive images are kept in the final picture. These final pictures, exemplified in Fig. 3(a), were analyzed to extract the properties of the deposit.

Deposits are characterized by their spatial extension, conventionally called profile height $h(x,t)$ measured as the distance between the center

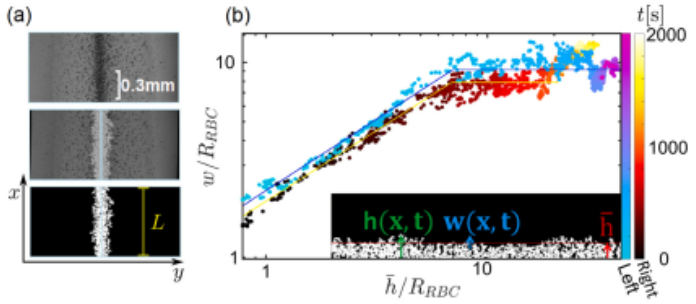

Fig. 3. Illustration of the image analysis process. (a) Snapshot of the central deposit with the raw experimental picture split at the detected center (for the resulting pattern of 0.3% volume suspension of RBCs in a 50-50 mixture of autologous serum and plasma), with overlaid final edges and the final binarized edges. This picture was taken 35 minutes after placing the drop on the slide. The x, y axes and the length of the system L are also indicated for further reference. (b) Scaling of the interface roughness width with average profile height for the superposition of the left side of the pattern and the right side of the pattern. Distances are normalized by the characteristic cell radius $R_{RBC} = 4.48\,\mu m$, in order to compare samples with possible radius changes (when various osmolarities are used). Solid lines are the fits used to obtain the parameter from Eq. (3). The slope of the first linear part, before saturation is reached, is the beta value. Color bars indicate the elapsed time based on the frame number after placing the drop on the surface of the microscope slide. (For interpretation of the colors in the figure(s), the reader is referred to the web version of this article.)

line and the farthest white pixel along y, at a given x (see Fig. 3(b)). The profile height is initially computed independently on the left and right sides of the center line. The growth of the central edge is then described through the relationship between $\bar{h}(t)$, the average of $h(x,t)$ along x, and $w(t)|_L$, the standard deviation of $h(x,t)$ evaluated on a system of size L along x, conventionally called the (roughness) width of the deposit (see Fig. 3(b) for graphical definitions).

2.4. Edge growth statistics

Usually, in order to describe the deposit growth quantitatively, both its mean profile height $\bar{h}(t)$ and roughness width $w(t)|_L$, which is the standard deviation of surface fluctuations around its mean value, are studied. For a discrete system, as our experimental pictures made of pixels, these two quantities are defined as [28,29]:

$$\bar{h}(t) = \frac{1}{L}\sum_{i=1}^{L} h(i,t) \tag{1}$$

where $h(i,t)$ indicates the profile height of the deposit at the i-th pixel along x at the time t, and L is the size of the system in pixels (see Fig. 3(a)). If the deposition rate (the number of particles reaching the surface per unit of time) is constant, the mean profile height increases linearly with time ($\bar{h} \sim t$). To quantify the growth process, the roughness width is investigated as a function of time

$$w(t)|_L = \sqrt{\frac{1}{L}\sum_{i=1}^{L}\left[h(i,t) - \bar{h}(t)\right]^2}. \tag{2}$$

For many phenomena [30–37], the roughness width w increases as a power of time

$$w(t)|_L \propto t^{\beta}, \tag{3}$$

where β is called the growth exponent and determines the time-dependent dynamics of the growth process. In experimental contexts, since defining the time zero is often difficult or arbitrary to some extent, a common approach consists in assuming that the scaling between w and t also translates between w and $\bar{h}$: $w(\bar{h})|_L \sim L^{\alpha} f(\frac{\bar{h}}{L^z})$. In our experiments, this beta coefficient was then obtained by fitting an piece-wise function, defined as an arbitrary straight line, continuously connected to a horizontal line (see Fig. 3(b)). The slope of the first line was considered to be the β parameter. The final horizontal line was used in the fit, because the roughness width eventually saturates at a value that increases as a power law of the system size:

$$w_{sat} \propto L^{\alpha} \tag{4}$$

The exponent α is the roughness exponent of the saturated surface. The above relations are often expressed in the relation introduced by Family–Vicsek [38]:

$$w(t)|_L \propto L^{\alpha} f\left(\frac{t}{L^z}\right), \tag{5}$$

where $z = \frac{\alpha}{\beta}$ is the dynamical exponent, and $f(u) \propto u^{\beta}$ if $u \ll 1$ and approaches a constant when $u \gg 1$ [29,38].

In order to measure the roughness coefficient α from Eq. (4), we calculate the local roughness width by dividing the pictures into windows of length l along the deposit axis, and average the results obtained from all the windows [39],

$$w^2(t)\Big|_l = \left\langle \frac{1}{l}\sum_{x=x_0}^{x_0+l}\left[h(x,t) - \bar{h}_l(t)\right]^2 \right\rangle_{x_0} \tag{6}$$

where $\bar{h}_l(t)$ is the average profile height of the selected window and <> indicates the ensemble averaging. According to Eq. (4), the local roughness width increases as a power law when the window size increases. Experimentally, it has already been shown that this exponent can follow various regimes, with transitions at given system sizes L [36]. The roughness exponent was then obtained by fitting the data obtained after $w(t)|_L$ saturated with a continuous piece-wise function, with two successive lines having positive slopes, followed by a constant value. The first line's slope was considered as the roughness exponent at short-length scales α_s. The slope of the second line is the roughness exponent at long length scales α_l (see Appendix Fig. A.2 for an example of the fitting process).

The previous scaling relationships can be used to define universality classes. In the context of evaporating droplets, it has been previously shown that the exponent β is sensitive to the shape of the particles, which can modify the growth regime of the edge formed by the coffee ring process. In particular, spheres have been shown to follow a Poisson process, characterized by $\beta = 0.5$ and $\alpha \approx 0$, while anisotropic particles, with anisotropic interactions, exhibited a growth belonging to the Kardar-Parisi-Zhang process with quenched disorder (KPZQ) with $\beta = 0.68$ and $\alpha = 0.63$ [16]. Given that the RBC shape can be altered by physio-chemical stresses or genetic diseases, one of the objectives of this work is to determine if the growth of the observed central edges can belong to various growth mechanisms. In particular, we tested if artificial changes in RBC shapes and aggregability can lead to a different growth class of the central Marangoni edge. To that end, we analyzed

the growth of the central edge obtained with various suspensions, using the image analysis described previously.

3. Results and discussion

In the beginning, dried deposits were obtained from spherical cap droplets with different suspending liquids (see Fig. 2(a-c)): autologous plasma, 4.5 mg/mL BSA solution in PBS, and in 1 mL of fibrinogen solutions (concentrations upto 5 mg/mL were used for fibrinogen in PBS, 4.5 mg/mL of BSA was also added in order to prevent the glass effect and the formation of slat crystals in the final dried deposits). As schematized in Fig. 1(c) and displayed in Fig. 2(a-c), RBCs migrate and accumulate towards the center of the drop due to a dominating solutal Marangoni flow. Hence, the pattern of all the dried drops in the conducted experiments includes central deposits of RBCs due to a solutal Marangoni recirculation loop. In order to study the growth of this central deposit, linear droplets were placed on a glass slide, as illustrated in Fig. 2(d-f). This setup allowed the use of classical 2D edge growth descriptions, previously used to model coffee rings [16] and described in Section 2.4. The dynamics of deposition were recorded at one frame per second with a 4X objective, around the middle of the droplet's line. A typical picture is displayed in the insert of Fig. 2(d). Interestingly, most of the droplet evaporation we observed occurred while the triple-phase line was pinned; the contact angle of the droplet decreased during the formation of the central edge, without influencing the exponents (α and β) describing the formation process of the central edge (see further results). It is therefore also likely that changing the initial contact angle without altering the liquid or the substrate (e.g., by using other deposition protocols that take advantage of the possible hysteresis observed in the formation of this contact angle) would only have a marginal influence on the parameters we measured.

As stated before, the main objective of this study is to determine whether evaporative deposits of dilute RBC suspensions present some sensitivity to RBC aggregability and shapes, which could be used to develop low-cost screening methods for pathological modifications. To determine whether the aggregability of the RBCs modifies the growth of the central deposit, we performed experiments by suspending 0.3% volume of RBCs in plasma, serum, and a 50-50 mixture of autologous serum and plasma.

Indeed, serum can basically be described as fibrinogen-free plasma, and fibrinogen is one of the main molecules promoting aggregation in blood samples. Using autologous serum offers a practical way to modify the RBCs' aggregability while maintaining other parameters as close as possible to their physiological conditions, as already employed in different studies [20,40,41]. The parameters obtained for three fibrinogen levels are displayed in Fig. 4, for fresh blood samples from 3 healthy donors and a repetition of 10 droplets. Although all suspensions demonstrated growth with an exponent close to that of a KPZQ process ($\beta \approx 0.68$ for KPZQ; our experimental values lie within $\beta \approx 0.64 \pm 0.04$), it is interesting to note that there is a significant difference in the distribution of the maximal roughness $w(t)|_L$ and maximal average profile height $\bar{h}(t)$ reached by the deposits over the course of the experiment. These maximal values are typically reached at the end of the experiment, but noise and minor perturbations (such as irregularities in the shape of the droplet) can slightly shift the observation time of these values. The significance of these variations is summarized by the range of p-values obtained from two-sample Kolmogorov-Smirnov tests. The p-values are the probabilities that the differences observed between the experimental measurements of two populations are due to random fluctuations from the same intrinsic continuous Probability Density Function. These tests have been performed using the function kstest2 in MATLAB. The ranges of p-values are abbreviated as ns (not significant) for $p > 0.1$, while the number n of stars $*$ refers to a significance level of $p < 10^{-n}$. Interestingly, changes in h_{max} and w_{max} seem to be more sensitive to an increase in fibrinogen levels, meaning that one could potentially detect inflammation with a method based on this observation, as fibrinogen is

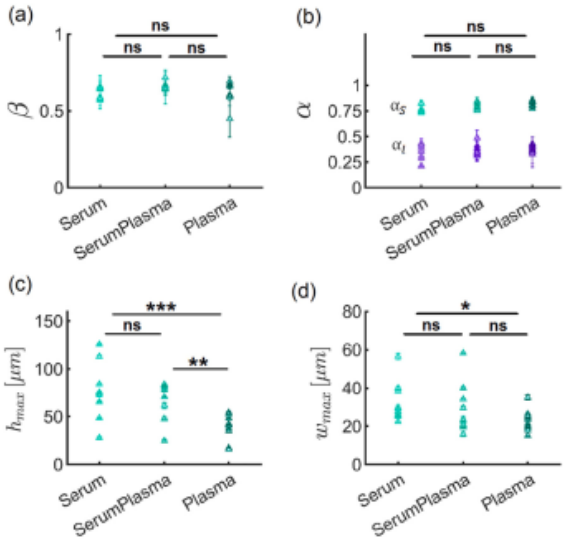

Fig. 4. Experimental results: (a) Average growth exponents, (b) Average roughness exponent, (c) Maximum profile height, and (d) Maximum roughness width, obtained for 0.3% red blood cell suspension formed in 1 mL of Serum, Plasma, and a 50-50 mixture of autologous serum and plasma (SerumPlasma). Measurements were repeated ten times for all three colloidal suspensions. The significance of the differences in the distributions is abbreviated as ns (not significant) for $p > 0.1$, while the number n of stars $*$ refers to a significance level of $p < 10^{-n}$.

a well-known inflammation marker [42]. Despite the fact that the internal convective movement is driven by Marangoni flow, there is no evidence that this systematic trend is due to a systematic change in the intensity of the solutal Marangoni flow, because there is no significant or systematic variation in the surface tension between serum, plasma, and the serum-plasma mixture (see Appendix Fig. A.3 for measurements with the pendant drop method). The most reasonable assumption is that the modification of the RBC aggregation is the parameter responsible for this change [18].

Since RBCs are one of the most deformable cell types, whose shape can be altered in pathologies, we also performed experiments to investigate whether artificial changes in RBC shapes and aggregation can lead to variations in the growth of the central Marangoni edge. More accurately, we tested if shapes from the Stomatocyte-Discocyte-Echinocyte (SDE) sequence, obtained via a change in osmolarity, would lead to any difference in the dynamics of the deposit formation. Although the osmolarity of the suspending phase should increase during evaporation of the droplet and possibly alter the shape of the RBCs during the experiments, we noticed that the significant part of the central deposit growth occurs within ten minutes of the evaporation process, while the overall evaporation process took around 40 minutes. The overall increase in osmolarity over the formation of the central deposit is therefore around $1/0.75 - 1$, i.e., an increase of approximately 33%, assuming a constant evaporation rate. This overall increase is too small to significantly alter the shape of the RBCs. Moreover, the osmolarity is probably inhomogeneous in the droplet, and the increase in osmolarity is likely limited to the edge of the droplet, since strong Marangoni recirculation is linked to a salt concentration gradient towards the edge of the droplet [26,43,44]. Finally, a closer inspection of the dried patterns shows that discocytes are still forming rouleaux in the case of an initial osmolarity of 300 mOsmol/L and that spherocytic or echinocytic shapes are still conserved in the dried deposit. Changes in RBC shapes during the formation of the deposit are therefore negligible.

Growth, roughness exponent, maximum profile height, and maximum roughness width obtained for various osmolarity levels are dis-

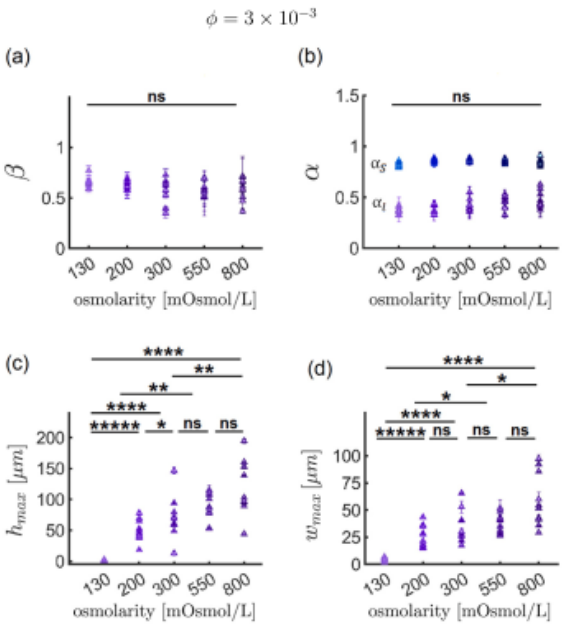

Fig. 5. Experimental results: (a) Average growth exponents, (b) Average roughness exponent, (c) Maximum profile height, and (d) Maximum roughness width, obtained for 0.3% red blood cell suspension were formed in 1 mL solutions of varying osmolarity. Measurements have been repeated ten times for all three colloidal suspensions. The abbreviation ns stands for not significant. The significance of p-values is defined as ns for $p > 0.1$, while the number n of stars $*$ refers to a significance level of $p < 10^{-n}$.

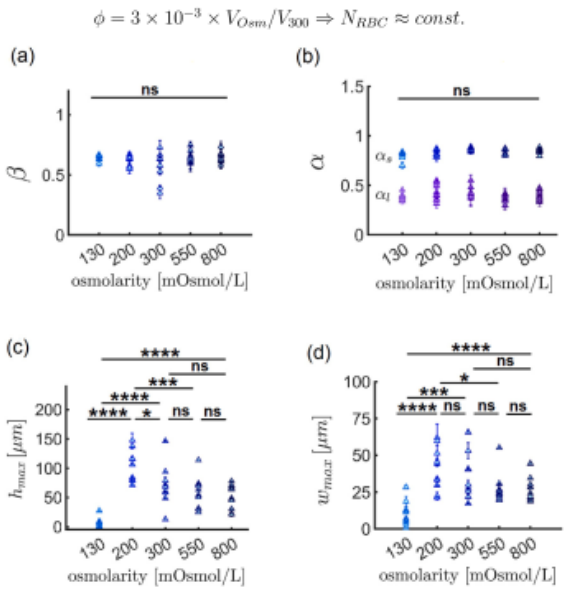

Fig. 6. Experimental results: (a) Average growth exponents, (b) Average roughness exponent, (c) Maximum profile height, and (d) Maximum roughness width, obtained for red blood cell suspensions with a volume fraction $\phi = 3 \times 10^{-3} \times V_{Osm}/V_{300}$, keeping the number of blood cells per milliliter constant. Measurements have been repeated ten times for all three colloidal suspensions. The abbreviation ns stands for not significant. The significance of p-values is defined as ns for $p > 0.1$, while the number n of stars $*$ refers to a significance level of $p < 10^{-n}$.

played in Fig. 5. According to previous results with inorganic particles, we expected some changes in the growth regime of the central deposit for various particle shapes, especially when moving from isotropic to anisotropic shapes [15,16]. The change in cell shape did not significantly impact the overall morphology or the universal class of growth. All samples were consistent with the KPZQ universality class, regardless of cell shape alterations. However, we also observed a significant increase in the maximal profile height of the central deposit, which was particularly sensitive to changes in osmolarity in the lower range, i.e., in the spherocyte-discocyte part of the SDE sequence. It is important to note that the volume of each blood cell also exhibits a clear dependence on osmolarity [45,46] (see Appendix Fig. A.4). Consequently, it was not clear at this stage whether this dependency is based on the shape of the erythrocytes or their volume in droplets of various initial osmolarities. However, we could rule out a change in the intensity of the Marangoni flow, as there was no significant difference in the surface tension of the various suspensions (see Appendix Fig. A.3).

As long as the volume fraction is kept below 1%, we noticed that increasing the volume fraction increases the maximum height and width but does not modify the formation dynamics. We therefore performed an additional set of experiments, maintaining a constant number of blood cells, instead of maintaining a constant volume fraction of $\phi = 3 \times 10^{-3}$ across all osmolarities. To that end, we estimated the average volume of RBCs at various osmolarities, V_{Osm}, through statistics from 3D scans performed with a confocal microscope (see Appendix Fig. A.4 for values), and suspended the RBCs with a volume fraction computed as $\phi = 3 \times 10^{-3} \times V_{Osm}/V_{300mOsmol/L}$, where $V_{300mOsmol/L} = 90\,\mu m^3$ is the standard volume of discocytes at a physiological osmolarity of 300 mOsmol/L (compatible with our measurements) [47]. With this change, we maintained a comparable number of RBCs in all samples, rather than a similar volume. Results with this protocol are depicted in Fig. 6. Interestingly, a significant increase in the maximal profile height is still observed from 130 mOsmol/L to 200 mOsmol/L, but the maximal roughness width decreases or remains constant at higher osmolarities. We can rule out that the osmolarity of the sample alone is responsible for the observed trend, as it is not reproduced when changing another parameter. Normalizing the dimensions of the central deposit by the length size of the cells (i.e., the cubic root of the average volume $V_{Osm}^{1/3}$ measured for a specific osmolarity) does not significantly alter the observed trends. Therefore, the volume of the cells alone does not explain the trends observed at low osmolarity in Figs. 6 and 5, although the trend observed in Fig. 6 at high osmolarity might be related to this change in volume, as correcting for the number of cells shows that there are no significant differences in the profile height of the deposit beyond 300 mOsmol/L in Fig. 5 (see Appendix, Fig. A.5 for the graph with normalization by the characteristic radius).

4. Conclusion

Our results showed that suspensions of red blood cells at low volume fractions ($\phi = 3 \times 10^{-3}$) form a central deposit, which contradicts the common assumption that blood evaporation is dominated by the classical coffee-ring effect [1–4,9–12,14,48]. These results suggest that Marangoni stresses should be incorporated into models used to explain the formation of cracks and patterns in dried blood deposits [48,49]. We demonstrated that the growth of this central deposit follows dynamics close to the predictions of the Kardar-Parisi-Zhang process with quenched disorder (KPZQ) scaling. This KPZQ scaling is robust enough to be observed in all osmolarities where the Spherocyte-Discocyte-Echinocyte transition can be seen, regardless of the shape adopted by the RBCs during the growth of the Marangoni edge. Our investigations also showed that the maximal profile height (in terms of average spatial extension of the 2D deposit) of this edge depends on

the properties of the red blood cells. In particular, higher aggregation of red blood cells results in a smaller deposit, while spherocytes tend to create smaller deposits, with the highest degree of significance. These results suggest that characterizing the size of this central deposit has potential applications as a clinical tool to detect changes in cell volume and/or geometry, which have not been considered before. However, our results also indicate that this size has a smaller sensitivity to changes corresponding to higher osmolarity levels. This suggests that developing automatic and highly reproducible elongated droplet shapes or exploring the effects of other control parameters, such as volume fraction, surrounding humidity, and temperature, might be an important step toward developing practical applications. Future work will focus on two aspects: (i) understanding the fundamental mechanisms of the transition between a central deposit and the accumulation of particles at the contact line as the volume fraction of cells increases, and (ii) quantifying how actual pathological modifications of RBC properties can be identified via patterns of blood evaporative deposits.

CRediT authorship contribution statement

Vahideh Sardari: Writing – review & editing, Writing – original draft, Visualization, Validation, Software, Methodology, Investigation, Formal analysis, Data curation, Conceptualization. **Mahsa Mohammadian:** Writing – review & editing, Investigation, Data curation. **Shima Asfia:** Writing – review & editing, Investigation, Data curation. **Felix Maurer:** Writing – review & editing, Software, Investigation, Formal analysis, Data curation. **Diana Örüm:** Writing – review & editing, Investigation, Data curation. **Ralf Seemann:** Writing – review & editing, Resources. **Thomas John:** Writing – review & editing, Software, Formal analysis. **Lars Kaestner:** Writing – review & editing, Resources, Methodology. **Christian Wagner:** Writing – review & editing, Resources, Funding acquisition. **Maniya Maleki:** Writing – review & editing, Formal analysis. **Alexis Darras:** Writing – review & editing, Writing – original draft, Supervision, Project administration, Methodology, Investigation, Funding acquisition, Formal analysis, Data curation, Conceptualization.

Declaration of competing interest

The authors declare that they have no known competing financial interests or personal relationships that could have appeared to influence the work reported in this paper.

Acknowledgements

V.S. acknowledges funding from a Visiting Research Scholar Grant of the Ministry of Science, Research and Technology of Iran for her research stay in Germany. A.D. acknowledges funding by the Young Investigator Grant of the Saarland University.

Appendix A. Supplementary material

Supplementary material related to this article can be found online at https://doi.org/10.1016/j.jcis.2024.10.039.

Data availability

Data will be made available on request.

References

[1] B.S. Sikarwar, M. Roy, P. Ranjan, A. Goyal, Automatic disease screening method using image processing for dried blood microfluidic drop stain pattern recognition, J. Med. Eng. Technol. 40 (5) (2016) 245–254.
[2] L. Bahmani, M. Neysari, M. Maleki, The study of drying and pattern formation of whole human blood drops and the effect of thalassaemia and neonatal jaundice on the patterns, Colloids Surf. A, Physicochem. Eng. Asp. 513 (2017) 66–75.
[3] Y. Liu, D. Attinger, K. De Brabanter, Automatic classification of bloodstain patterns caused by gunshot and blunt impact at various distances, J. Forensic Sci. 65 (3) (2020) 729–743.
[4] D. Attinger, K. De Brabanter, C. Champod, Using the likelihood ratio in bloodstain pattern analysis, J. Forensic Sci. 67 (1) (2022) 33–43.
[5] R.D. Deegan, O. Bakajin, T.F. Dupont, G. Huber, S.R. Nagel, T.A. Witten, Capillary flow as the cause of ring stains from dried liquid drops, Nature 389 (6653) (1997) 827–829.
[6] M. Rossi, A. Marin, C.J. Kähler, Interfacial flows in sessile evaporating droplets of mineral water, Phys. Rev. E 100 (3) (2019) 033103.
[7] A. Darras, N. Vandewalle, G. Lumay, Transitional bulk-solutal Marangoni instability in sessile drops, Phys. Rev. E 98 (6) (2018) 062609.
[8] A. Darras, N. Vandewalle, G. Lumay, Combined effects of Marangoni, sedimentation and coffee-ring flows on evaporative deposits of superparamagnetic colloids, Colloid Interface Sci. Commun. 32 (2019) 100198.
[9] A. Pal, A. Gope, G. Iannacchione, Temperature and concentration dependence of human whole blood and protein drying droplets, Biomolecules 11 (2) (2021) 231.
[10] W.B. Zeid, D. Brutin, Influence of relative humidity on spreading, pattern formation and adhesion of a drying drop of whole blood, Colloids Surf. A, Physicochem. Eng. Asp. 430 (2013) 1–7.
[11] R. Chen, L. Zhang, D. Zang, W. Shen, Blood drop patterns: formation and applications, Adv. Colloid Interface Sci. 231 (2016) 1–14.
[12] A. Pal, A. Gope, A. Sengupta, Drying of bio-colloidal sessile droplets: advances, applications, and perspectives, Adv. Colloid Interface Sci. 314 (2023) 102870.
[13] L. Lanotte, D. Laux, B. Charlot, M. Abkarian, Role of red cells and plasma composition on blood sessile droplet evaporation, Phys. Rev. E 96 (5) (2017) 053114.
[14] A. Pal, A. Gope, J.D. Obayemi, G.S. Iannacchione, Concentration-driven phase transition and self-assembly in drying droplets of diluting whole blood, Sci. Rep. 10 (1) (2020) 18908.
[15] P.J. Yunker, T. Still, M.A. Lohr, A. Yodh, Suppression of the coffee-ring effect by shape-dependent capillary interactions, Nature 476 (7360) (2011) 308–311.
[16] P.J. Yunker, M.A. Lohr, T. Still, A. Borodin, D.J. Durian, A.G. Yodh, Effects of particle shape on growth dynamics at edges of evaporating drops of colloidal suspensions, Phys. Rev. Lett. 110 (3) (2013) 035501.
[17] C. Wagner, P. Steffen, S. Svetina, Aggregation of red blood cells: from rouleaux to clot formation, C. R. Phys. 14 (6) (2013) 459–469.
[18] M. Brust, O. Aouane, M. Thiébaud, D. Flormann, C. Verdier, L. Kaestner, M. Laschke, H. Selmi, A. Benyoussef, T. Podgorski, et al., The plasma protein fibrinogen stabilizes clusters of red blood cells in microcapillary flows, Sci. Rep. 4 (1) (2014) 4348.
[19] P. Steffen, C. Verdier, C. Wagner, Quantification of depletion-induced adhesion of red blood cells, Phys. Rev. Lett. 110 (1) (2013) 018102.
[20] A.K. Dasanna, A. Darras, T. John, G. Gompper, L. Kaestner, C. Wagner, D.A. Fedosov, Erythrocyte sedimentation: effect of aggregation energy on gel structure during collapse, Phys. Rev. E 105 (2) (2022) 024610.
[21] A. Darras, K. Peikert, A. Rabe, F. Yaya, G. Simionato, T. John, A.K. Dasanna, S. Buvalyy, J. Geisel, A. Hermann, et al., Acanthocyte sedimentation rate as a diagnostic biomarker for neuroacanthocytosis syndromes: experimental evidence and physical justification, Cells 10 (4) (2021) 788.
[22] Z. Csahók, K. Honda, E. Somfai, M. Vicsek, T. Vicsek, Dynamics of surface roughening in disordered media, Phys. A, Stat. Mech. Appl. 200 (1–4) (1993) 136–154.
[23] G. Brecher, M. Bessis, Present status of spiculed red cells and their relationship to the discocyte-echinocyte transformation: a critical review, Blood 40 (3) (1972) 333–344.
[24] N.M. Geekiyanage, M.A. Balanant, E. Sauret, S. Saha, R. Flower, C.T. Lim, Y. Gu, A coarse-grained red blood cell membrane model to study stomatocyte-discocyte-echinocyte morphologies, PLoS ONE 14 (4) (2019) e0215447.
[25] G. Simionato, K. Hinkelmann, R. Chachanidze, P. Bianchi, E. Fermo, R. van Wijk, M. Leonetti, C. Wagner, L. Kaestner, S. Quint, Red blood cell phenotyping from 3d confocal images using artificial neural networks, PLoS Comput. Biol. 17 (5) (2021) e1008934.
[26] A. Marin, S. Karpitschka, D. Noguera-Marín, M.A. Cabrerizo-Vílchez, M. Rossi, C.J. Kähler, M.A. Rodríguez Valverde, Solutal Marangoni flow as the cause of ring stains from drying salty colloidal drops, Phys. Rev. Fluids 4 (4) (2019) 041601.
[27] A. Darras, F. Mignolet, N. Vandewalle, G. Lumay, Remote-controlled deposit of superparamagnetic colloidal droplets, Phys. Rev. E 98 (6) (2018) 062608.
[28] A.-L. Barabási, H.E. Stanley, Fractal Concepts in Surface Growth, Cambridge University Press, 1995.
[29] F. Family, Dynamic scaling and phase transitions in interface growth, Phys. A, Stat. Mech. Appl. 168 (1) (1990) 561–580.
[30] P. Meakin, R. Jullien, Restructuring effects in the rain model for random deposition, J. Phys. 48 (10) (1987) 1651–1662.
[31] Z. Csahók, T. Vicsek, Kinetic roughening in a model of sedimentation of granular materials, Phys. Rev. A 46 (8) (1992) 4577.
[32] M. Kurnaz, K. McCloud, J. Maher, Sedimentation of glass beads under the influence of gravity, Fractals 1 (04) (1993) 1008–1021.
[33] M. Kurnaz, J. Maher, Sedimentation to form rough, quasi-one-dimensional interfaces, Phys. Rev. E 53 (1) (1996) 978.
[34] T.J. Oliveira, F. Aarão Reis, Roughness exponents and grain shapes, Phys. Rev. E, Stat. Nonlinear Soft Matter Phys. 83 (4) (2011) 041608.
[35] K.V. McCloud, M.L. Kurnaz, J.V. Maher, Deposition-rate effects on rough surfaces formed by sedimenting particles, Phys. Rev. E 56 (5) (1997) 5768.

[36] K. McCloud, M. Kurnaz, The effect of the third dimension on rough surfaces formed by sedimenting particles in quasi-two-dimensions, Int. J. Mod. Phys. B 16 (08) (2002) 1217–1223.
[37] U. Cardak, K. McCloud, M. Kurnaz, Experimental and computational study of the effect of the system size on rough surfaces formed by sedimenting particles in quasi-two-dimensions, Granul. Matter 8 (2006) 81–86.
[38] F. Family, T. Vicsek, Scaling of the active zone in the eden process on percolation networks and the ballistic deposition model, J. Phys. A, Math. Gen. 18 (2) (1985) L75.
[39] V. Sardari, F. Safari, M. Maleki, Dynamics of the surface growth resulted from sedimentation of spheres in a Hele-Shaw cell containing a low-viscosity fluid, Phys. Fluids 36 (5) (2024) 053303, https://doi.org/10.1063/5.0200886.
[40] A. Darras, T. John, C. Wagner, L. Kaestner, Erythrocyte sedimentation rate: a physics-driven characterization in a medical context, J. Vis. Exp. 193 (2023) e64502.
[41] T. John, L. Kaestner, C. Wagner, A. Darras, Early stage of erythrocyte sedimentation rate test: fracture of a high-volume-fraction gel, PNAS Nexus 3 (1) (2024) pgad416.
[42] D.R. Germolec, K.A. Shipkowski, R.P. Frawley, E. Evans, Markers of inflammation, in: Immunotoxicity Testing: Methods and Protocols, 2018, pp. 57–79.
[43] N. Shahidzadeh-Bonn, S. Rafaı, D. Bonn, G. Wegdam, Salt crystallization during evaporation: impact of interfacial properties, Langmuir 24 (16) (2008) 8599–8605.
[44] N. Shahidzadeh, M.F. Schut, J. Desarnaud, M. Prat, D. Bonn, Salt stains from evaporating droplets, Sci. Rep. 5 (1) (2015) 10335.
[45] M. Friebel, J. Helfmann, M.C. Meinke, Influence of osmolarity on the optical properties of human erythrocytes, J. Biomed. Opt. 15 (5) (2010) 055005.
[46] P. Heubusch, C.Y. Jung, F.A. Green, The osmotic response of human erythrocytes and the membrane cytoskeleton, J. Cell. Physiol. 122 (2) (1985) 266–272.
[47] C. Brugnara, D.C. Tosteson, Cell volume, k transport, and cell density in human erythrocytes, Am. J. Physiol., Cell Physiol. 252 (3) (1987) C269–C276.
[48] D. Roy, K.K. Dewangan, A. Rasheed, S. Jain, A. Singh, D. Chakravortty, S. Basu, et al., Insights into the mechanics of sessile whole blood droplet evaporation, arXiv preprint, arXiv:2402.12334, 2024.
[49] M.G. Hennessy, R.V. Craster, O.K. Matar, Drying-induced stresses in poroelastic drops on rigid substrates, Phys. Rev. E 105 (5) (2022) 054602.